Application Opportunities with Multispectral Remote Sensing Data

Satellite Remote Sensing
Energy Balance
VIS, IR, and MW Radiative Transfer
EOS Terra & Aqua MODIS
Multispectral Applications
(Ocean Color, Snow/Ice, Vegetation, Aerosols, Fires, Volcanic Ash, Clouds, Moisture)
Detecting Climate Trends

Satellite remote sensing of the Earth-atmosphere

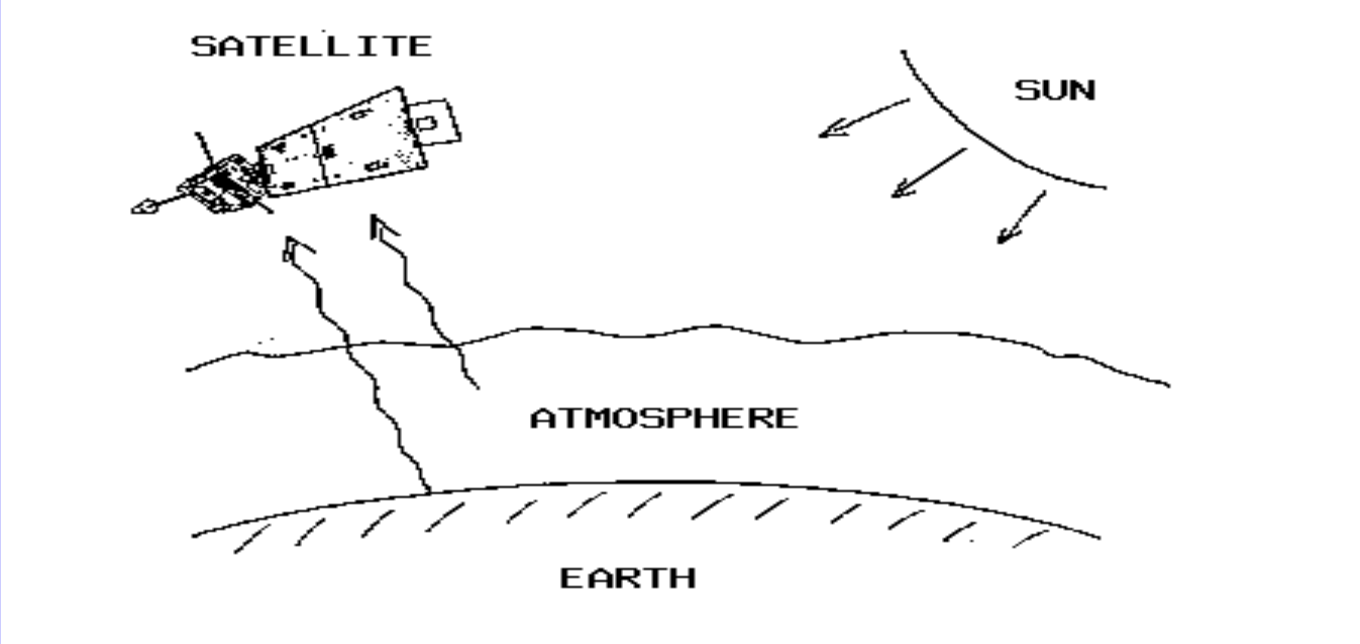

Observations depend on

telescope characteristics (resolving power, diffraction)
detector characteristics (signal to noise)
communications bandwidth (bit depth)
spectral intervals (window, absorption band)
time of day (daylight visible)
atmospheric state (T, Q, clouds)
earth surface (Ts, vegetation cover)

Remote Sensing Advantages

* provides a regional view

* enables one to observe & measure the causes & effects of climate & environmental changes (both natural & human-induced)

* provides repetitive geo-referenced looks at the same area

* covers a broader portion of the spectrum than the human eye

* can focus in on a very specific bandwidth in an image

* can also look at a number of bandwidths simultaneously

* operates in all seasons, at night, and in bad weather

Solar (visible) and Earth emitted (infrared) energy

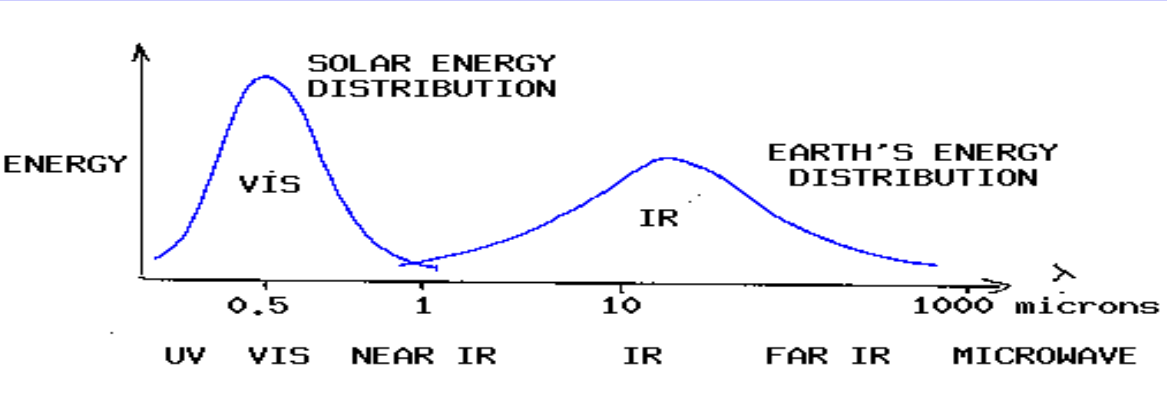

Incoming solar radiation (mostly visible) drives the earth-atmosphere (which emits infrared).

Over the annual cycle, the incoming solar energy that makes it to the earth surface (about 50 %) is balanced by the outgoing thermal infrared energy emitted through the atmosphere.

The atmosphere transmits, absorbs (by H2O, O2, O3, dust) reflects (by clouds), and scatters (by aerosols) incoming visible; the earth surface absorbs and reflects the transmitted visible. Atmospheric H2O, CO2, and O3 selectively transmit or absorb the outgoing infrared radiation. The outgoing microwave is primarily affected by H2O and O2.

Key Areas of Uncertainty in Understanding Climate & Global Change

* Earth's radiation balance and the influence of clouds on radiation and the hydrologic cycle

* Oceanic productivity, circulation and air-sea exchange

* Transformation of greenhouse gases in the lower atmosphere, with emphasis on the carbon cycle

* Changes in land use, land cover and primary productivity, including deforestation

* Sea level variability and impacts of ice sheet volume

* Chemistry of the middle and upper stratosphere, including sources and sinks of stratospheric ozone

* Volcanic eruptions and their role in climate change

Radiative Energy Balance

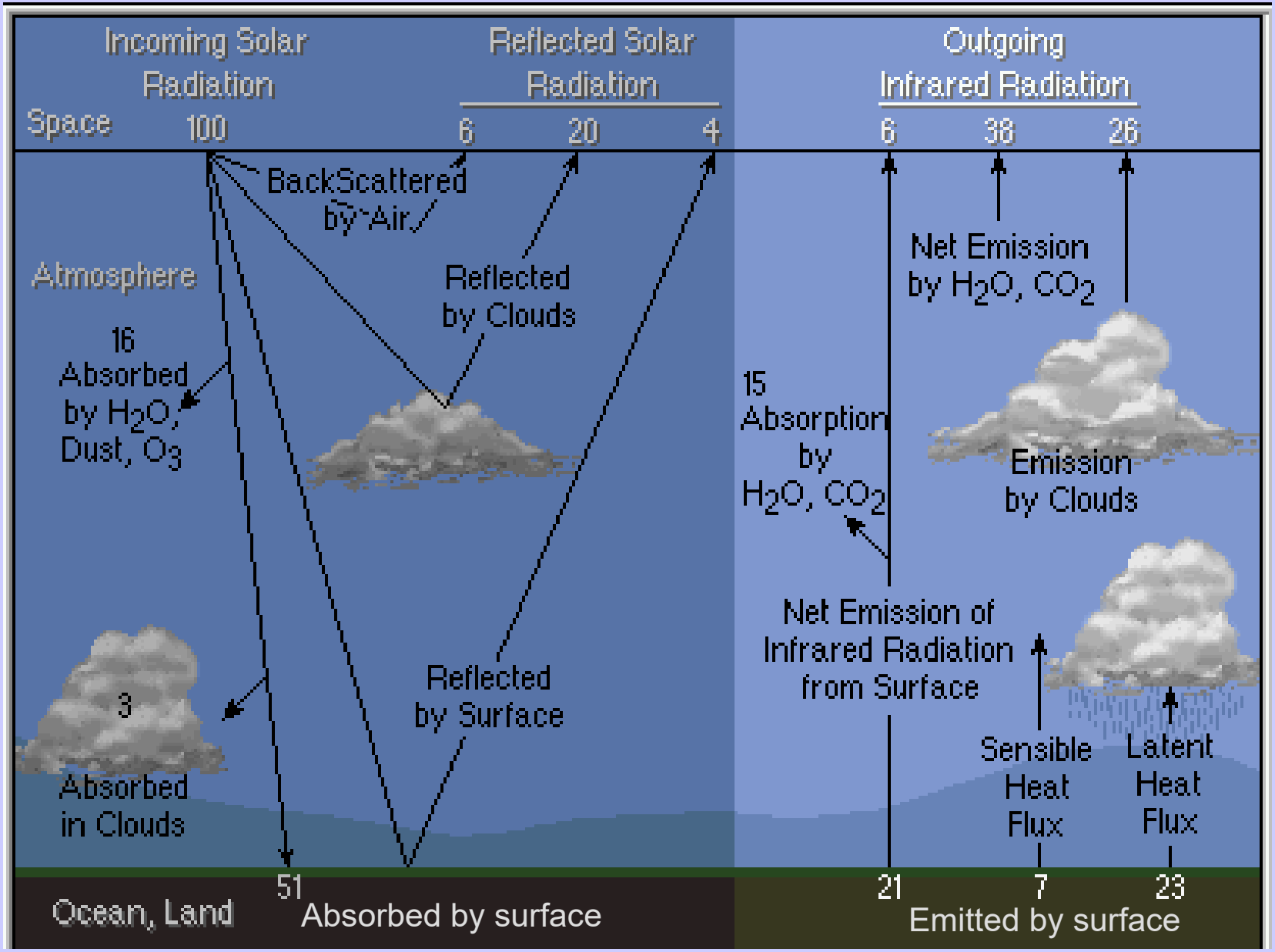

Solar Spectrum

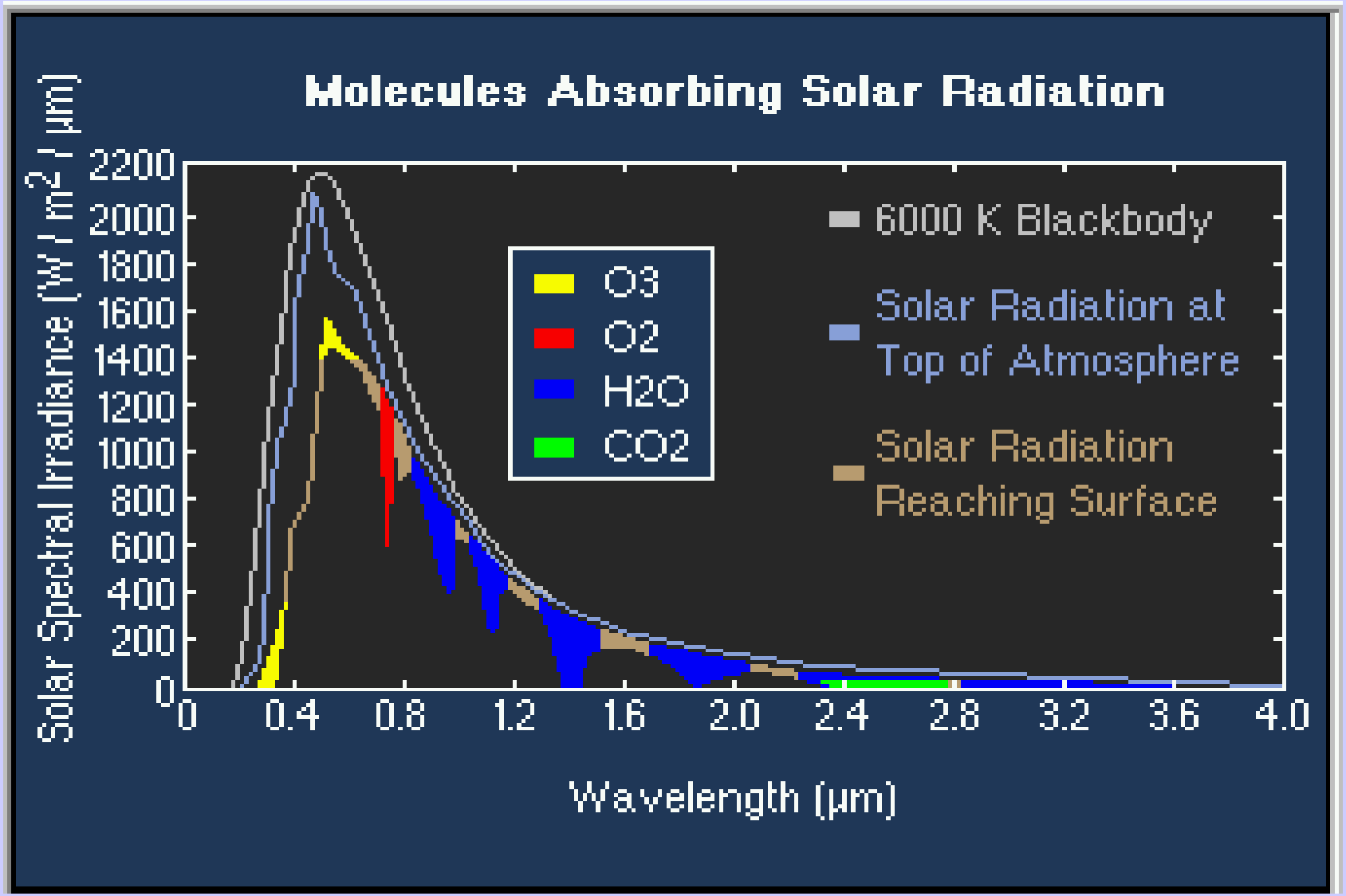

Earth emitted spectra overlaid on Planck function envelopes

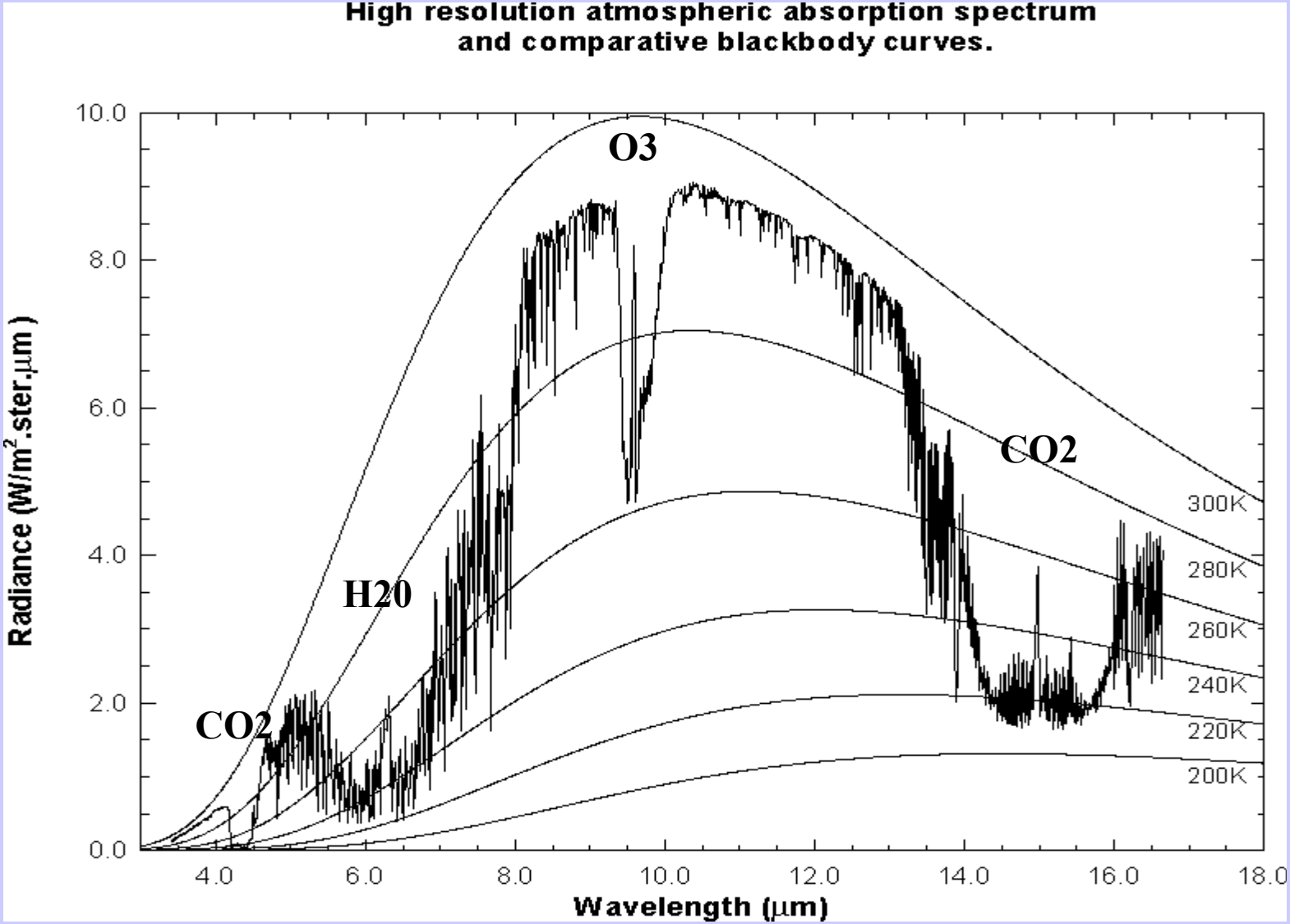

Radiative Transfer through the Atmosphere

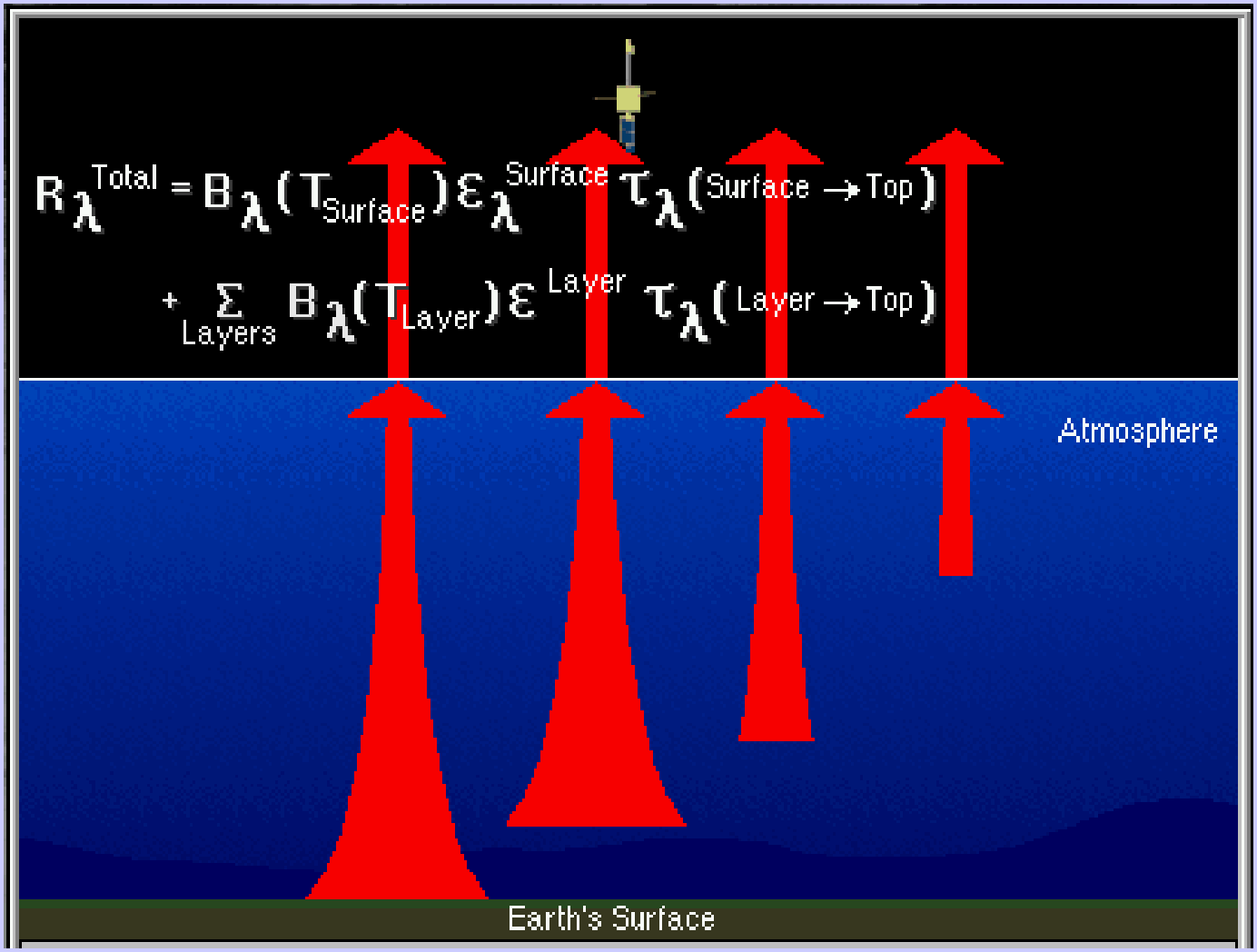

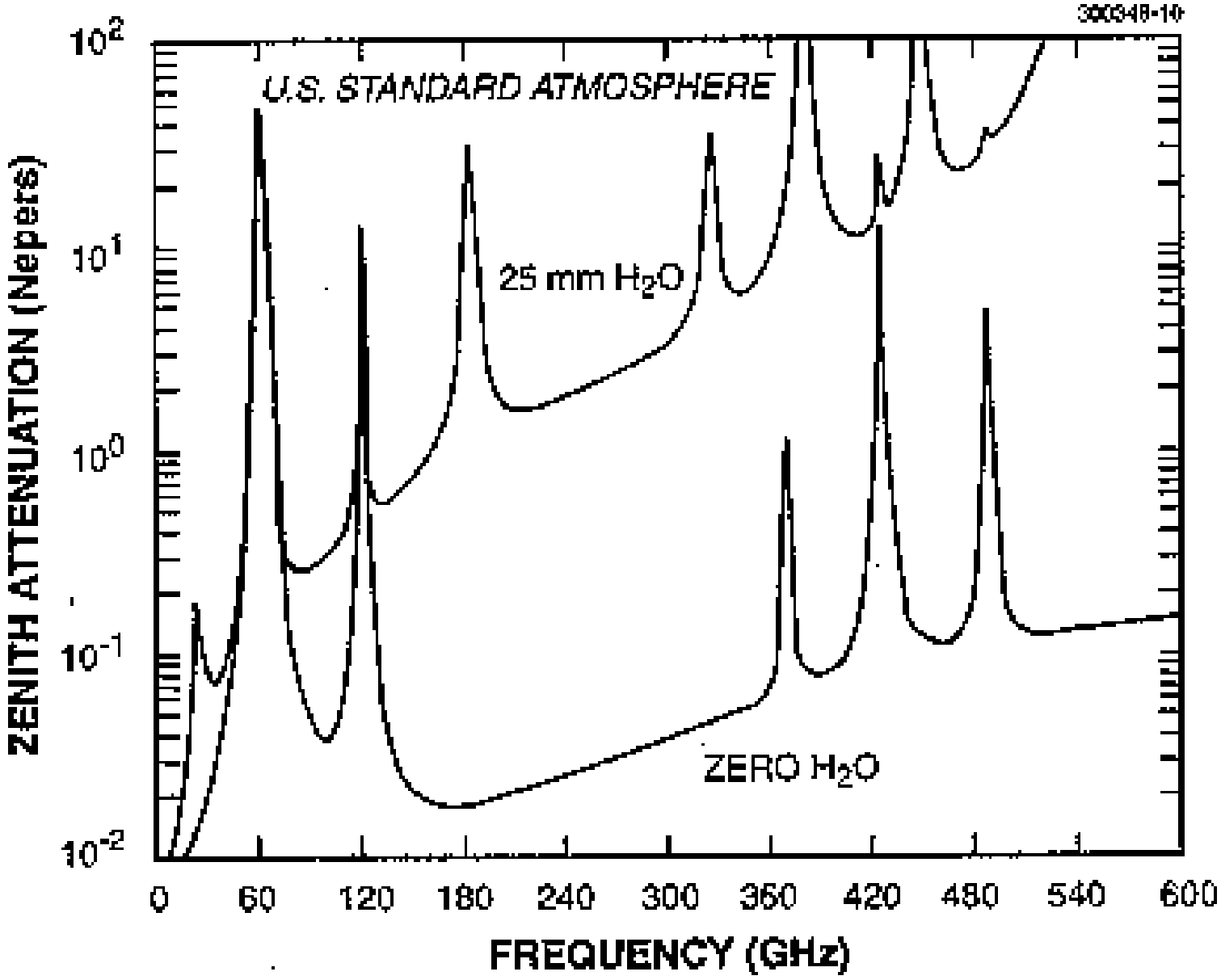
U.S. STANDARD ATMOSPHERE
25 mm H_2O
ZERO H_2O
ZENITH ATTENUATION (Nepers)
10^2
10^1
10^0
10^{-1}
10^{-2}
0
60
120
180
240
300
360
420
480
540
600
FREQUENCY (GHz)

Clouds viewed from polar orbiting TIROS launched 1 Apr 1960

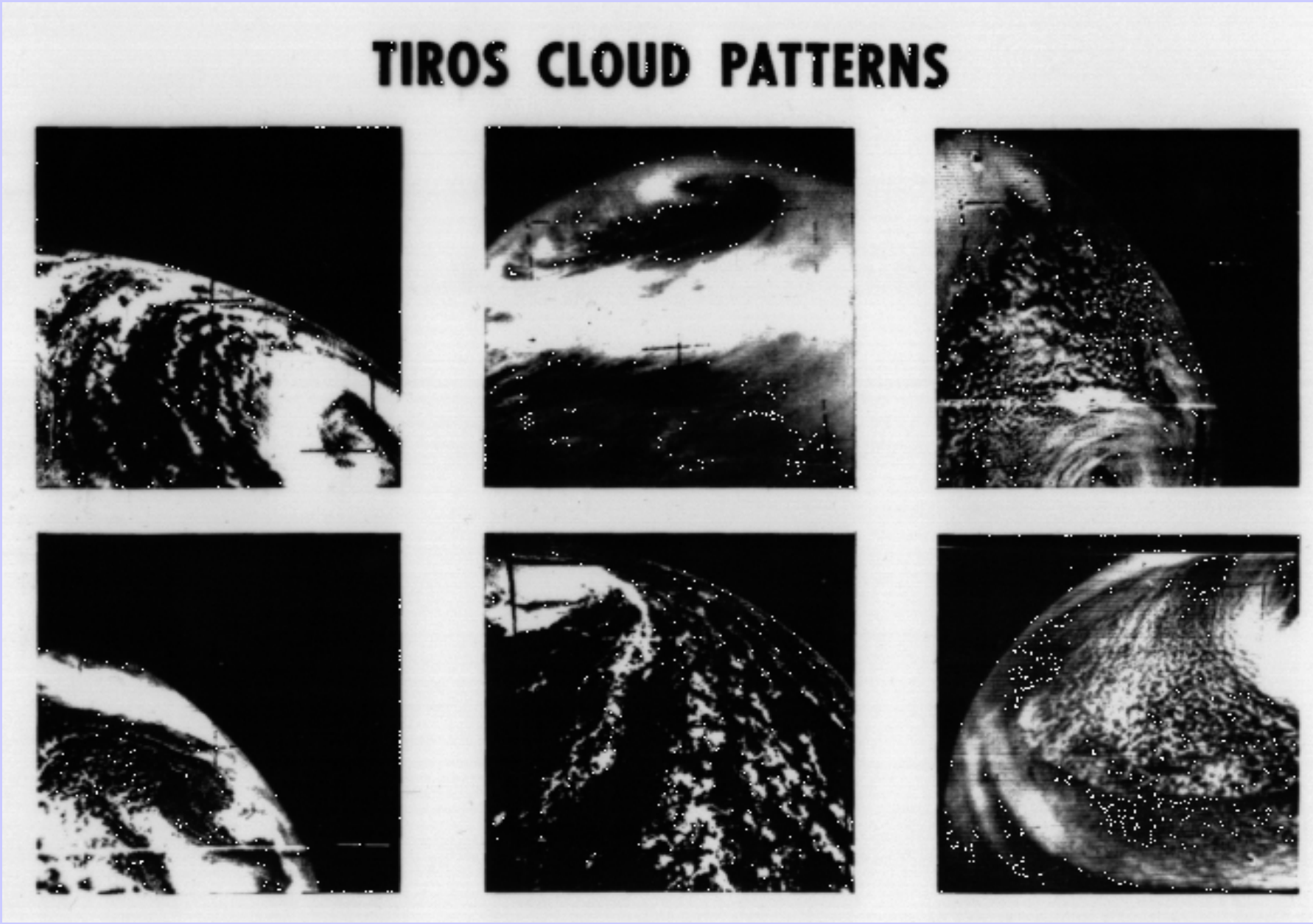

Evolution of Leo Obs

Terra was launched in 1999 and the EOS Era began

MODIS, CERES, MOPITT, ASTER, and MISR reach polar orbit

Aqua and ENVISAT followed in 2002

MODIS and MERIS leading to VIIRS
AIRS leading to IASI and CrIS
AMSU leading to ATMS

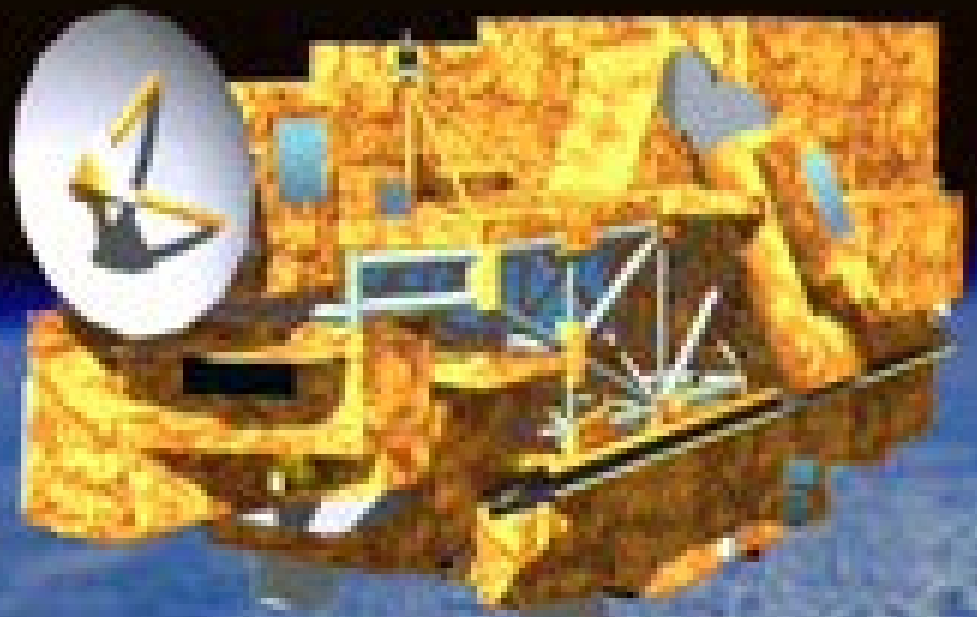

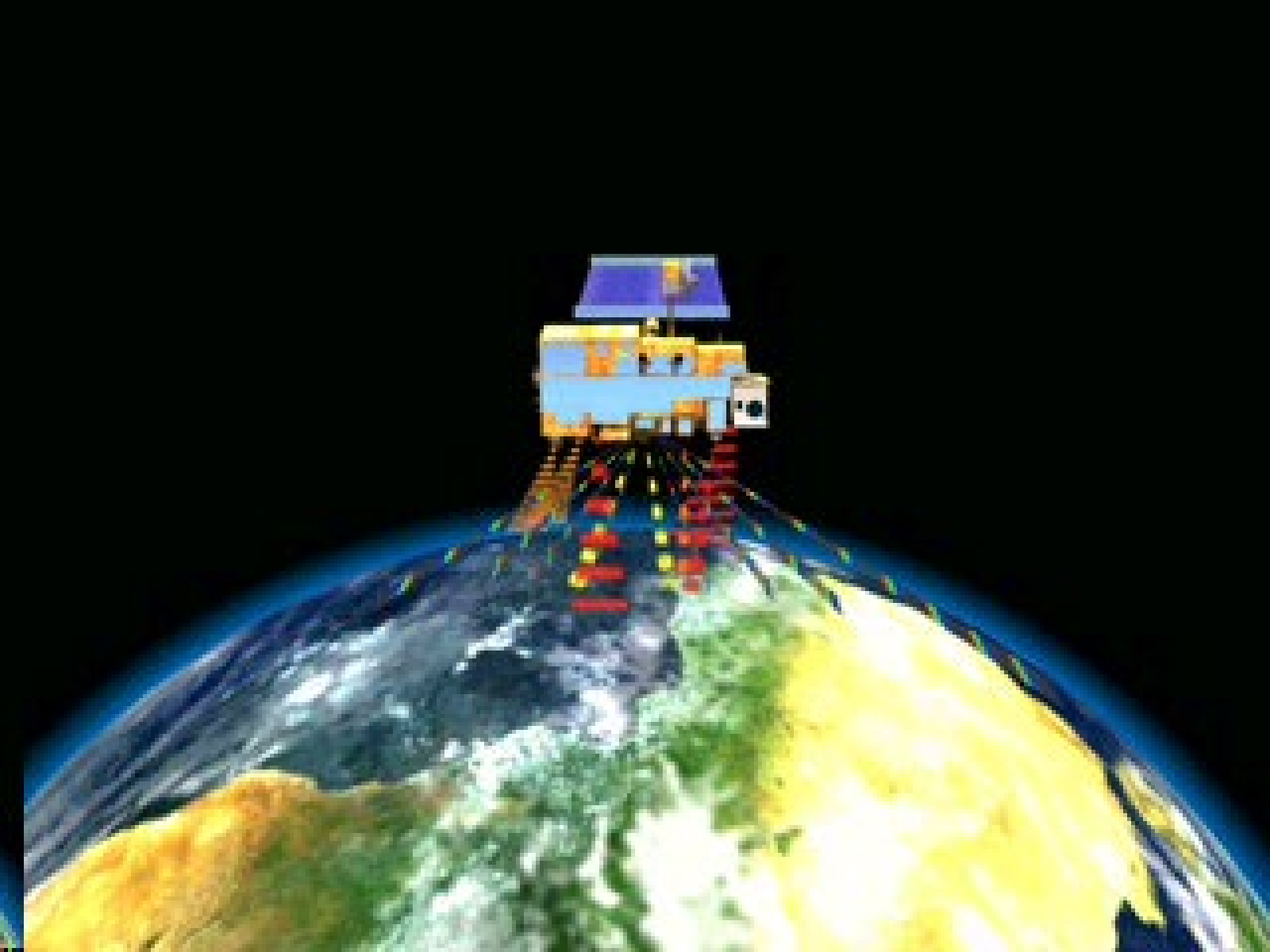

Launch of EOS-Terra (EOS-AM) Satellite - A New Era Begins

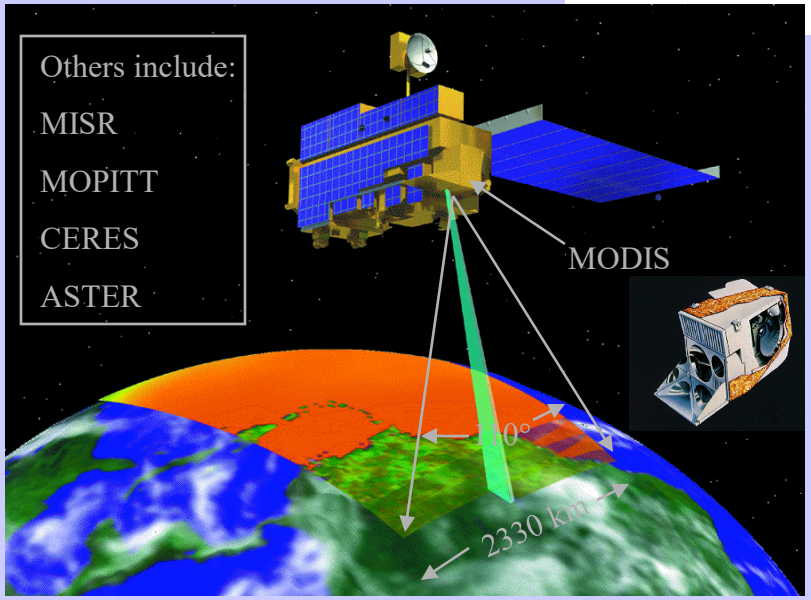

MODIS instrument Specifications:

Bands 1-2 (0.66,0.86 μm): 250 m

Bands 3-7 (0.47, 0.55, 1.24, 1.64, 2.13 μm): 500 m

Bands 8-36: 1 km

Launch date: December 18, 1999, 1:57 PT
Earth viewdoor open date: February 24, 2001

Allen Chu/NASA GSFC

Followed by the launch of EOS-Aqua (EOS-PM) Satellite

“ ”

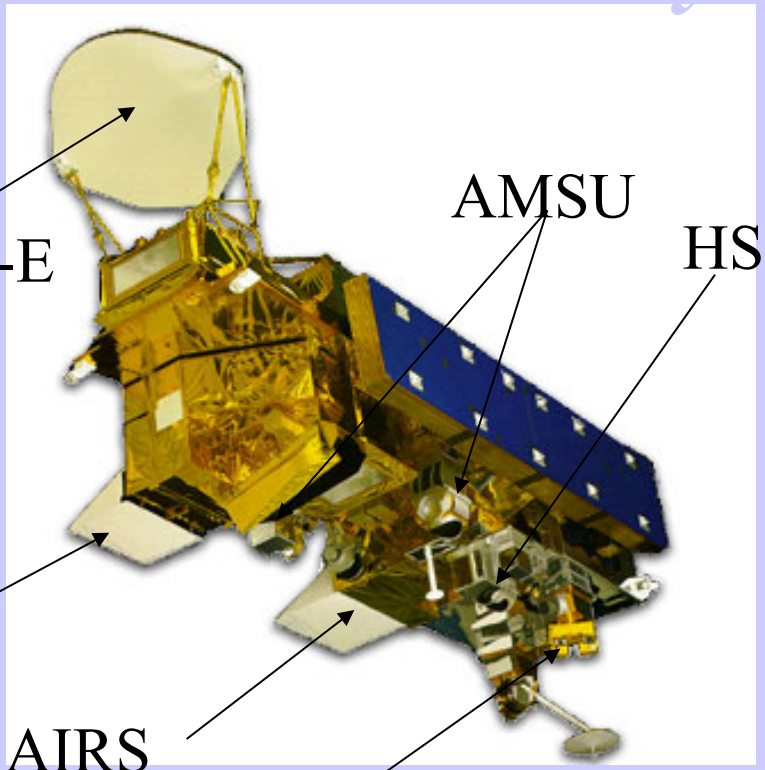

Launch date: May 4, 2002, 2:55 PDT
Earth view door open date: June 25, 2002

VIIRS, MODIS, FY-1C, AVHRR

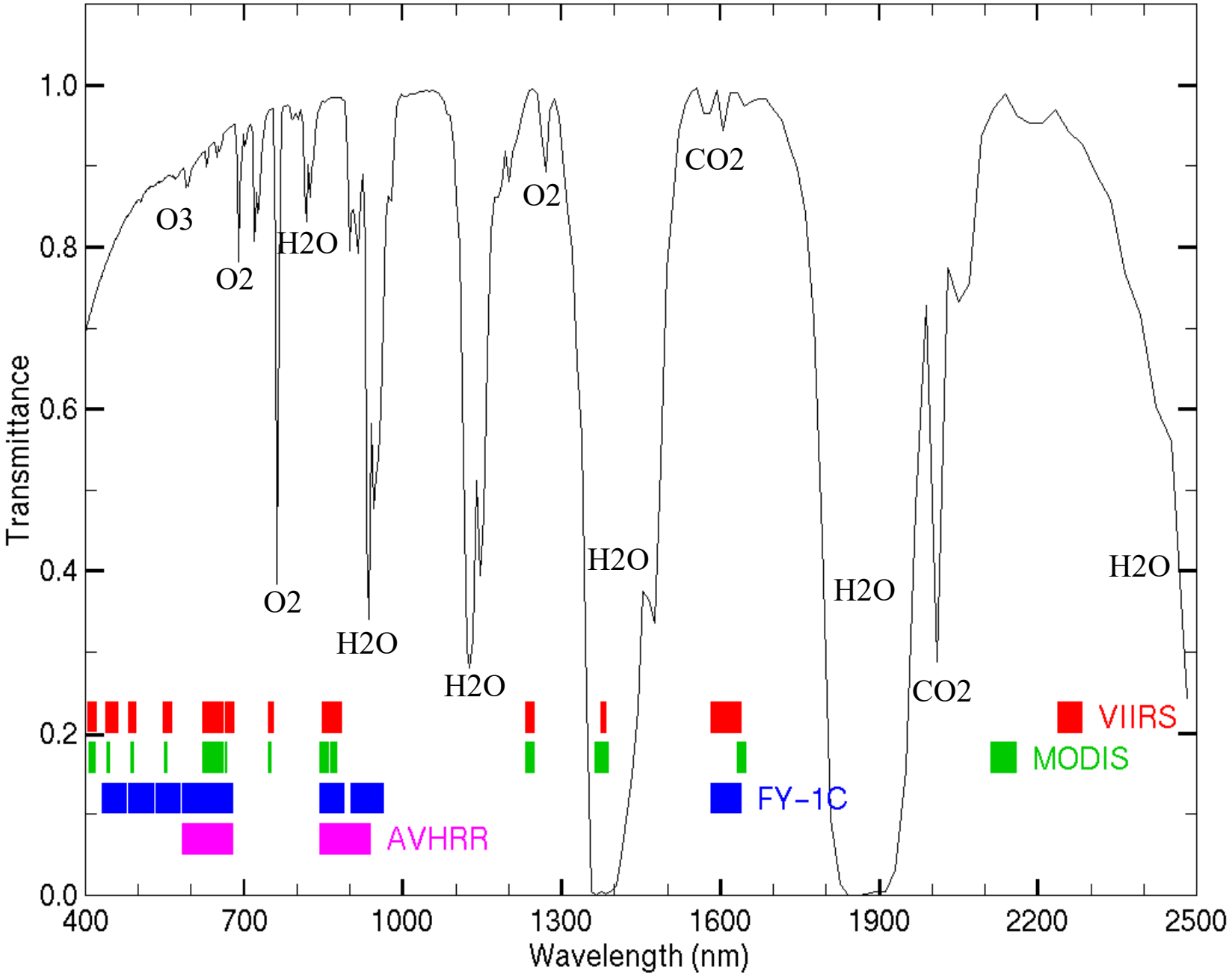

MODIS IR Spectral Bands

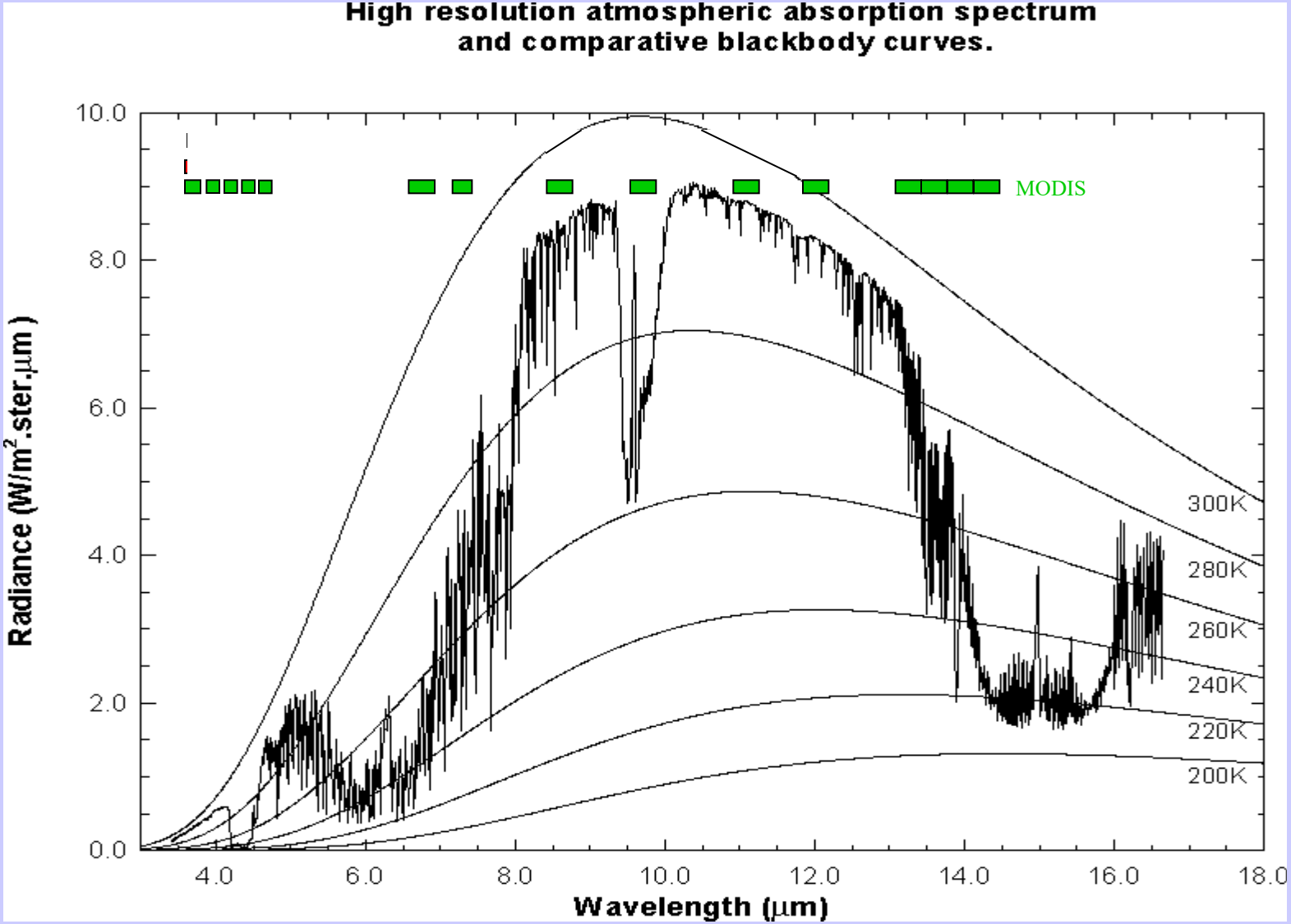

Application Opportunities with Multispectral Remote Sensing Data

Satellite Remote Sensing

Energy Balance

VIS, IR, and MW Radiative Transfer

EOS Terra & Aqua MODIS

Multispectral Applications

(Ocean Color, Snow/Ice, Vegetation, Aerosols, Fires, Volcanic Ash, Clouds)

Detecting Climate Trends

OCEAN-SOLAR RADIATION

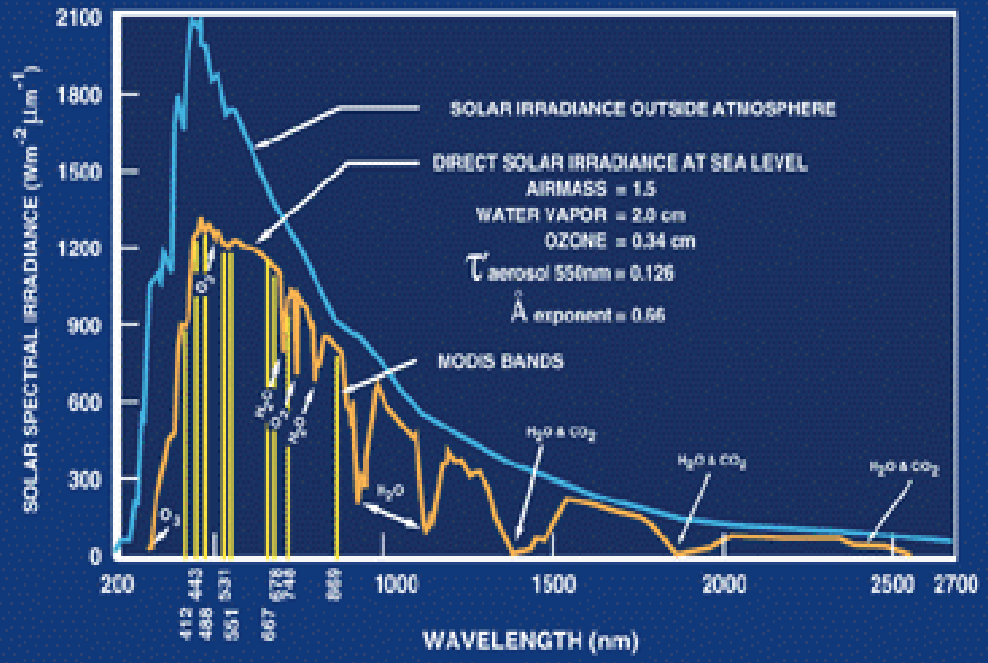

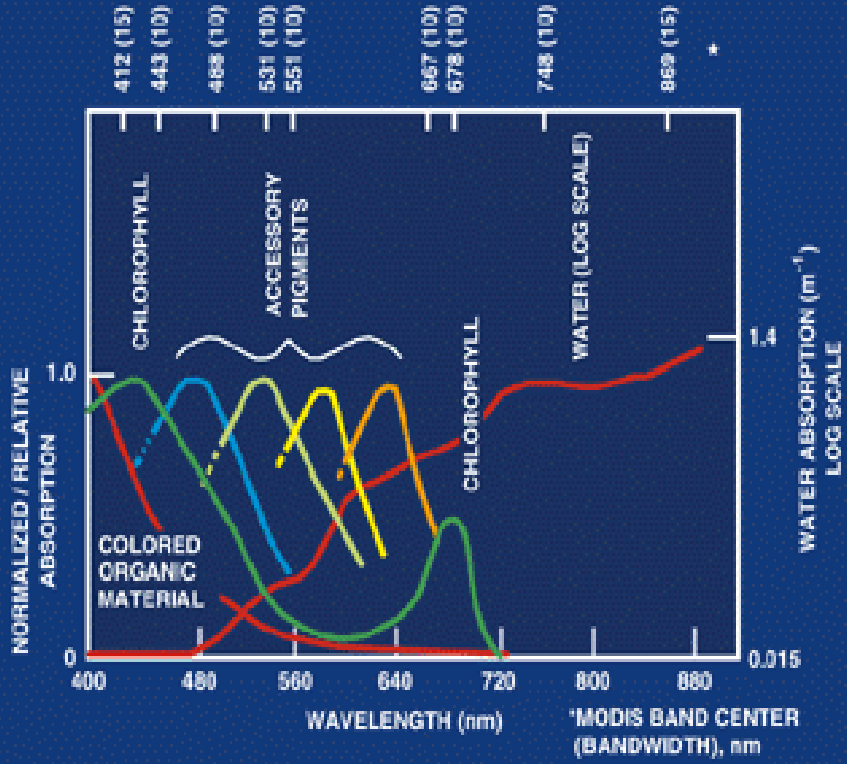


MODIS views the Mississippi

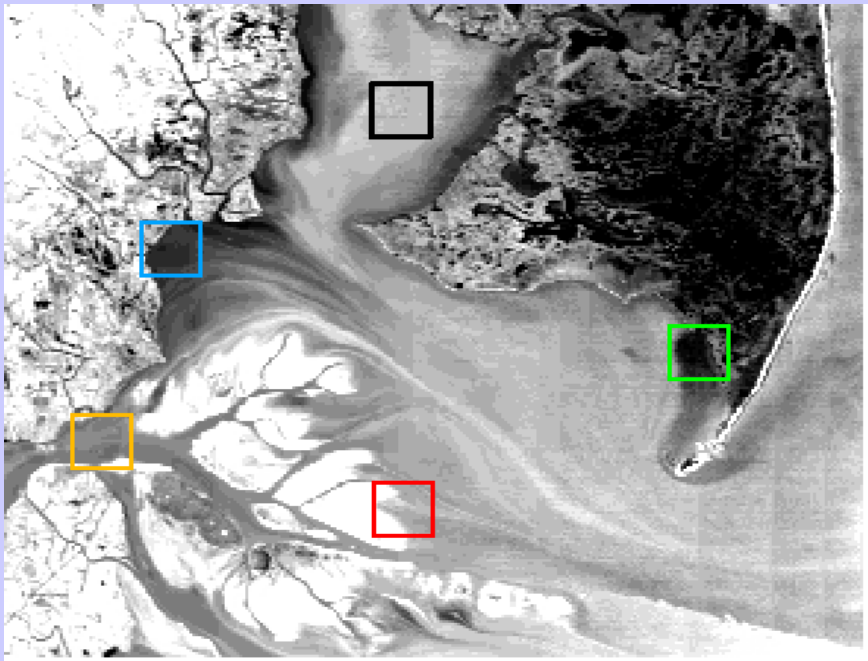

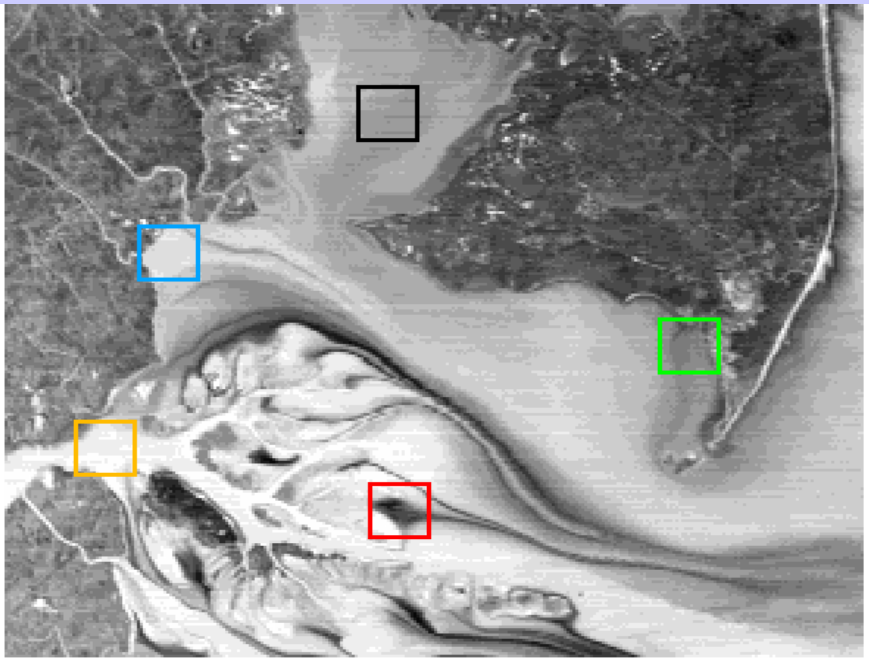

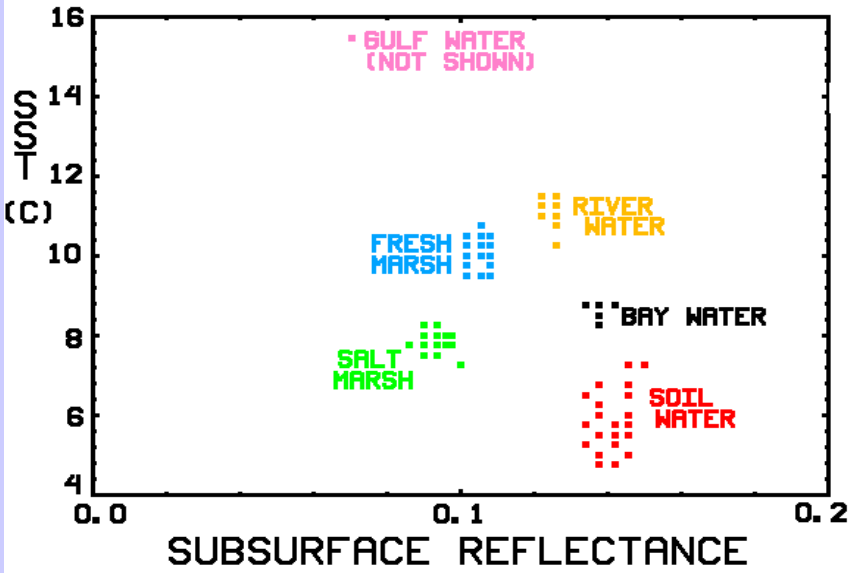

MAMS WATER TYPE ANALYSIS
DEC 4 1990

SHOWN:

* .66um REFLECTANCE (LEFT)
* SPLIT WINDOW SST (RIGHT)

Coastal Oceanography Northern Gulf of Mexico

Numerical Models and Satellite Ocean Color

NCOM 1/24 Degree IASNFS

MODIS Chlorophyll

Naval Research Laboratory

Stennis Space Center MS

August 14, 2003

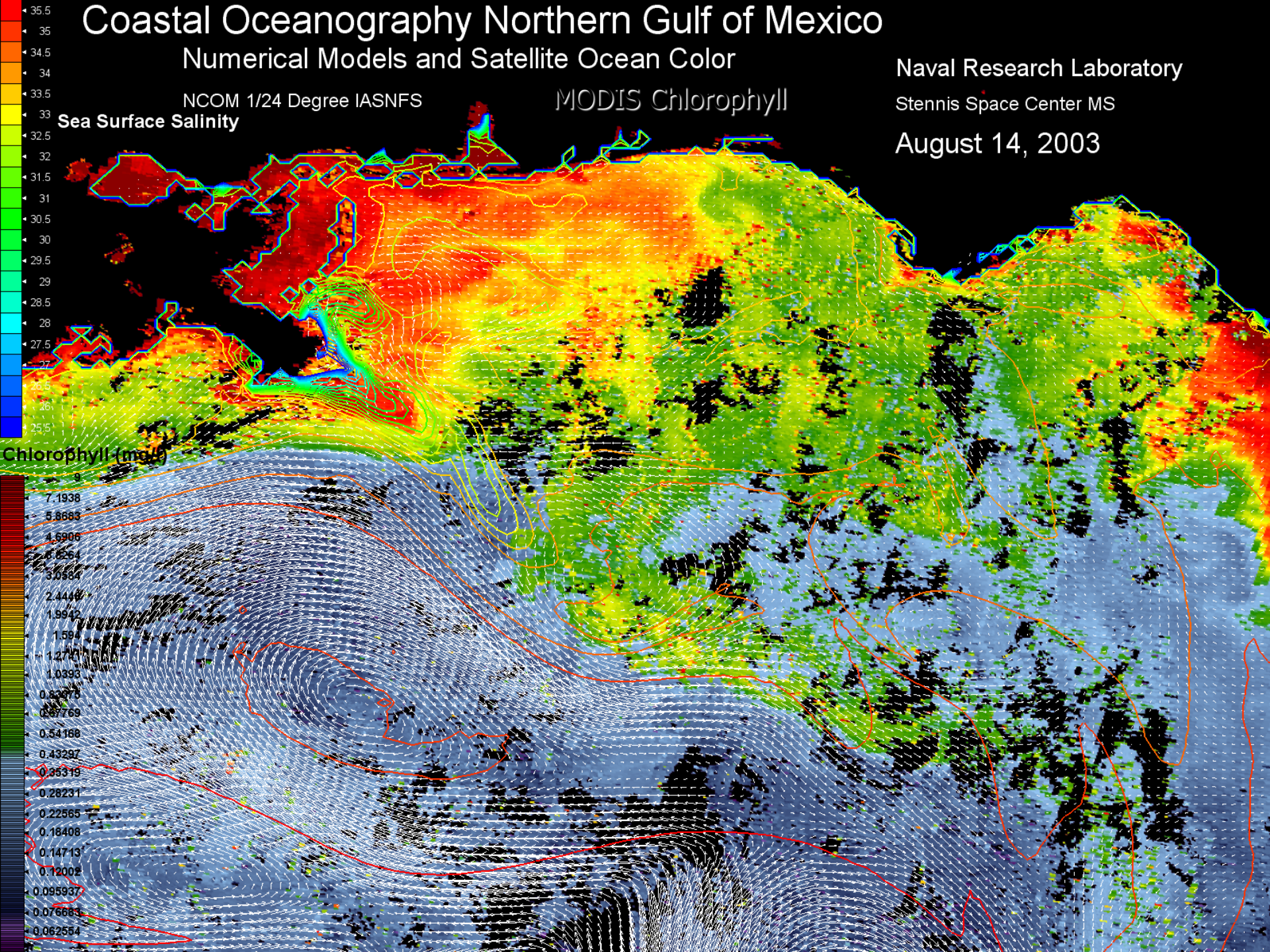

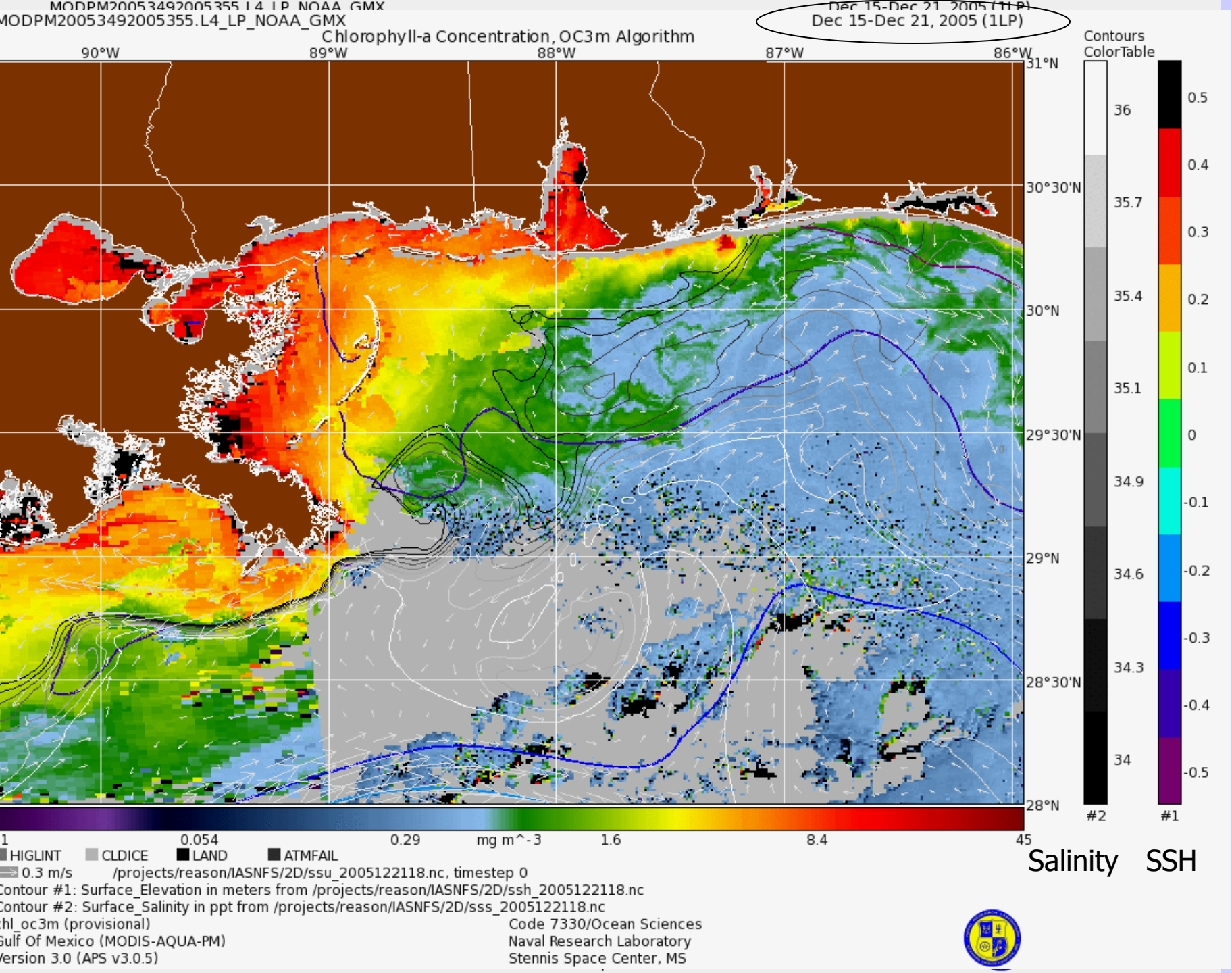
MODPM20053492005355.L4_LP_NOAA_GMX
Chlorophyll-a Concentration, OC3m Algorithm
Dec 15-Dec 21, 2005 (1LP)
90°W
89°W
88°W
87°W
86°W
31°N
30°30'N
30°N
29°30'N
29°N
28°30'N
28°N
Contours
ColorTable
36
35.7
35.4
35.1
34.9
34.6
34.3
34
#2
0.5
0.4
0.3
0.2
0.1
0
-0.1
-0.2
-0.3
-0.4
-0.5
#1
1
0.054
0.29
mg m^-3
1.6
8.4
45
HIGLINT
CLDICE
LAND
ATMFAIL
0.3 m/s
/projects/reason/IASNFS/2D/ssu_2005122118.nc, timestep 0
Contour #1: Surface_Elevation in meters from /projects/reason/IASNFS/2D/ssh_2005122118.nc
Contour #2: Surface_Salinity in ppt from /projects/reason/IASNFS/2D/sss_2005122118.nc
chl_oc3m (provisional)
Gulf Of Mexico (MODIS-AQUA-PM)
Version 3.0 (APS v3.0.5)
Code 7330/Ocean Sciences
Naval Research Laboratory
Stennis Space Center, MS
Salinity
SSH

Comparison of Spatial resolutions Chesapeake Bay March 13, 2004 Monitoring the Estuarine and Riverine Environment

New Capabilities for Managing Coastal Resources

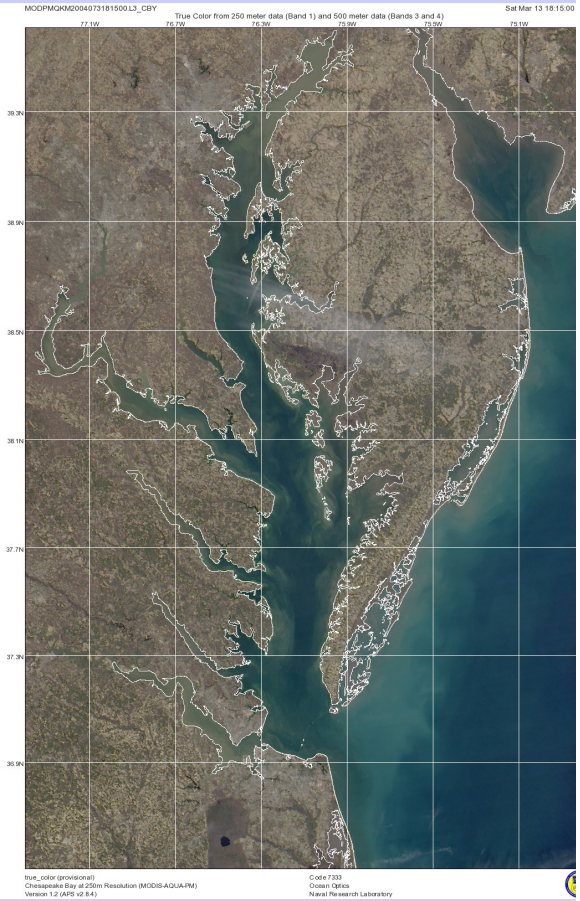

(Franz, McClain, Martinolich, Casey)

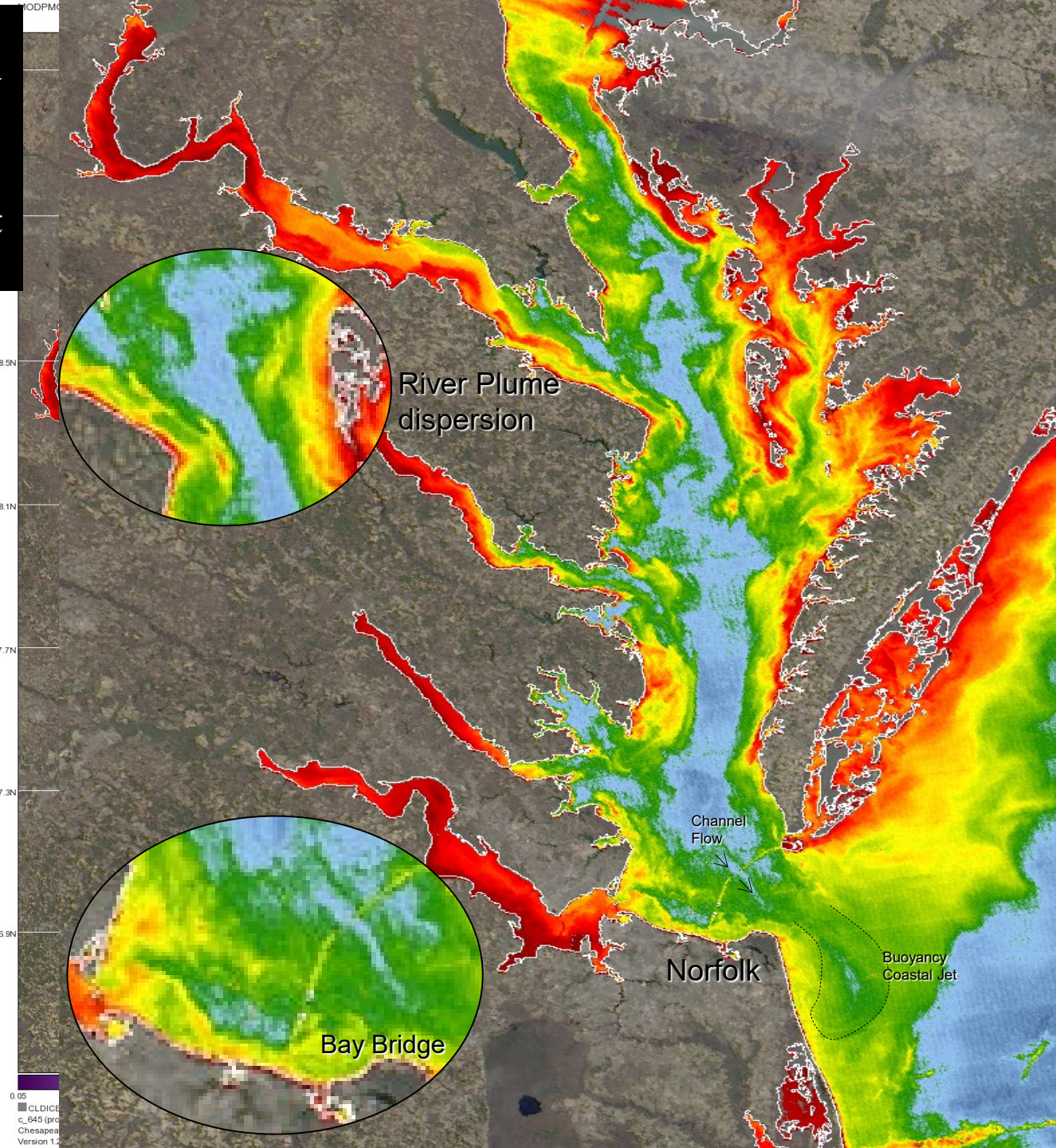

MODIS SEA SURFACE TEMPERATURE

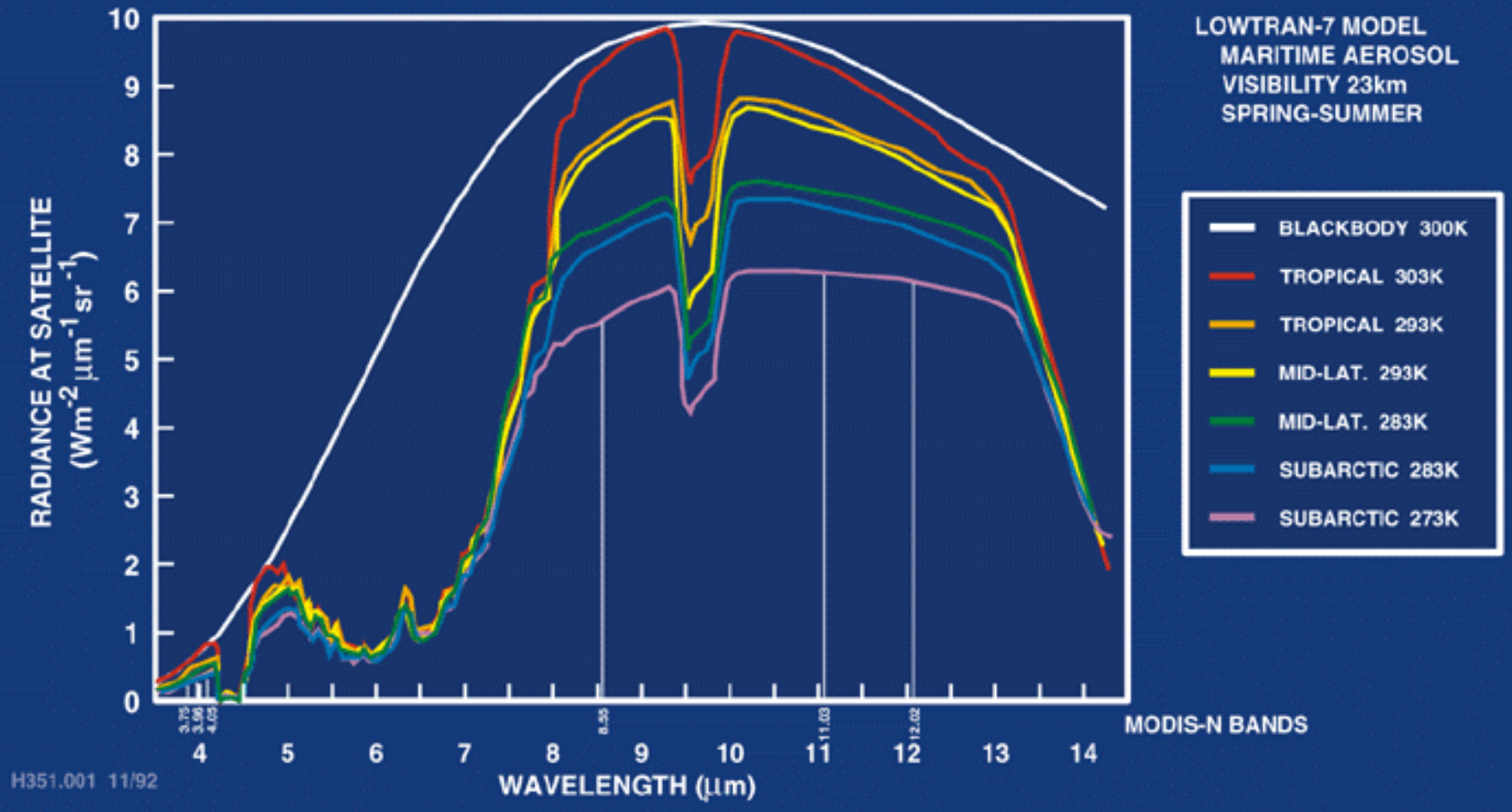

SST - MODIS and AVHRR

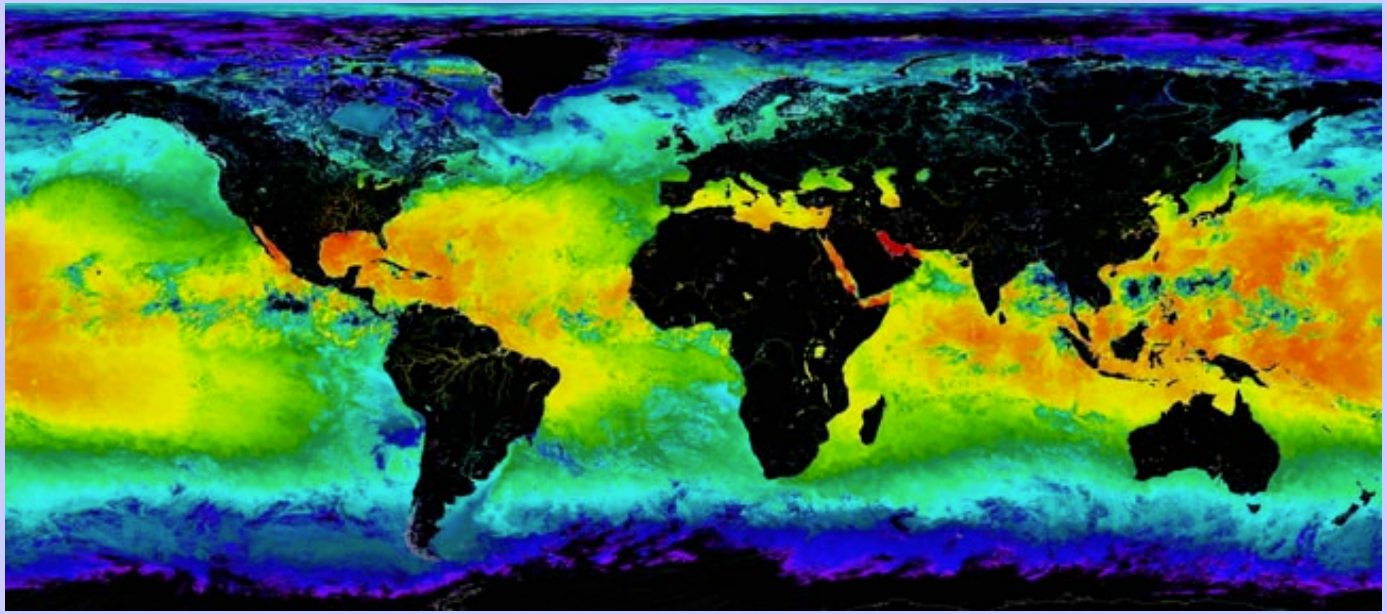

MODIS 4 µm Night SST

Improved coverage in tropical regions. Color scales are not identical, cloud mask is not applied.

AVHRR Night SST

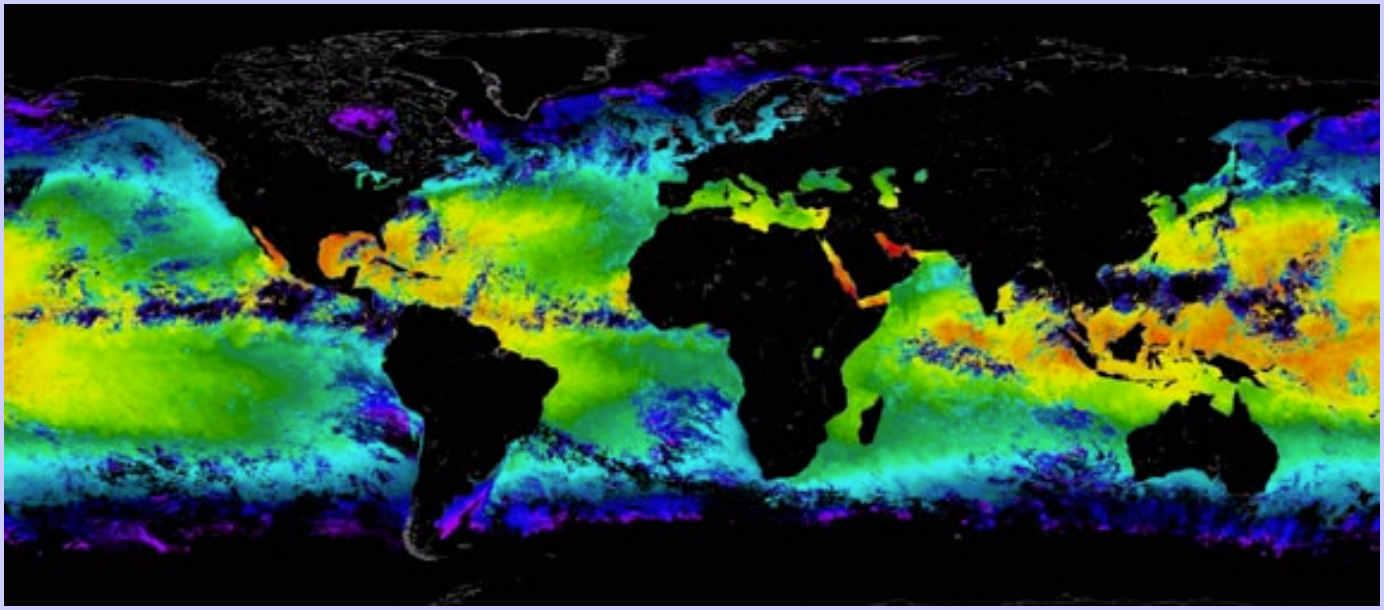

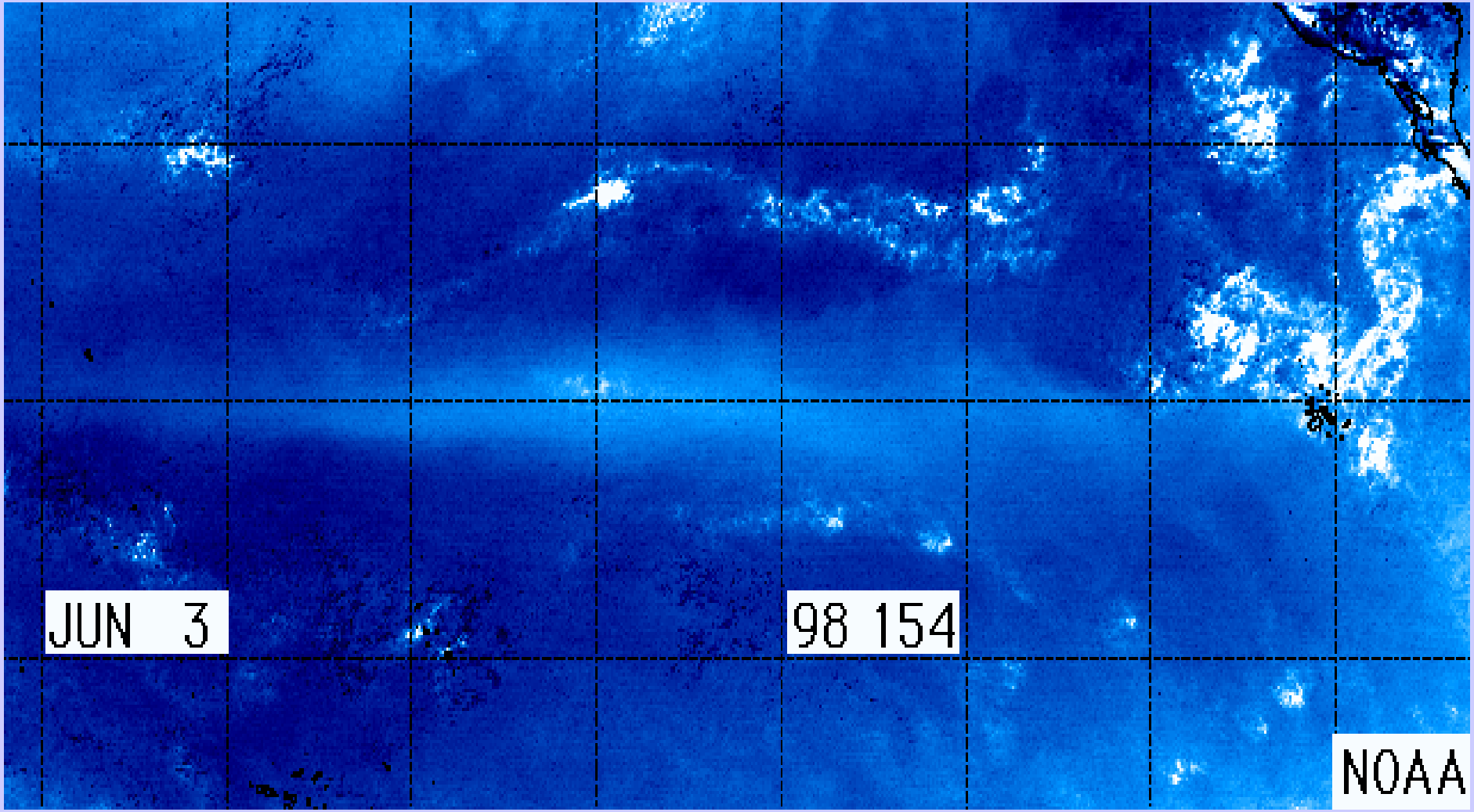

SST Waves from Legeckis

LAND-SOLAR RADIATION

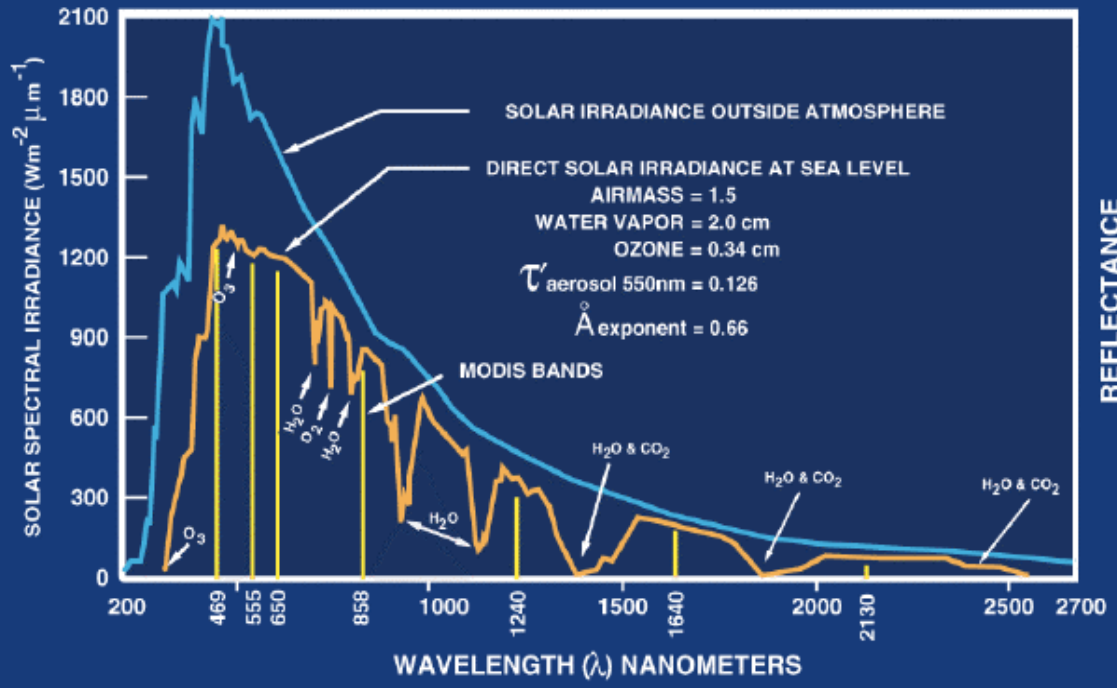

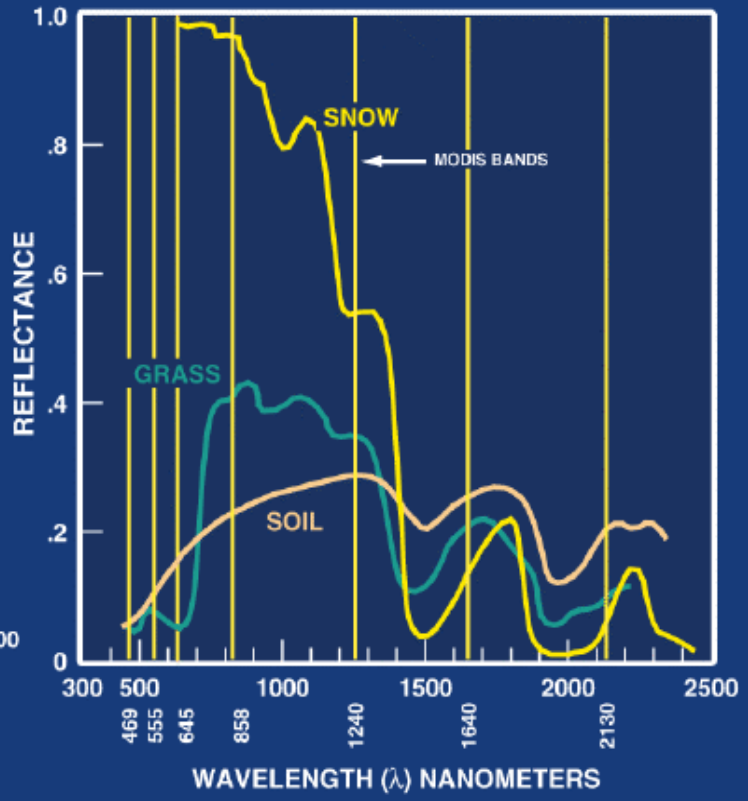

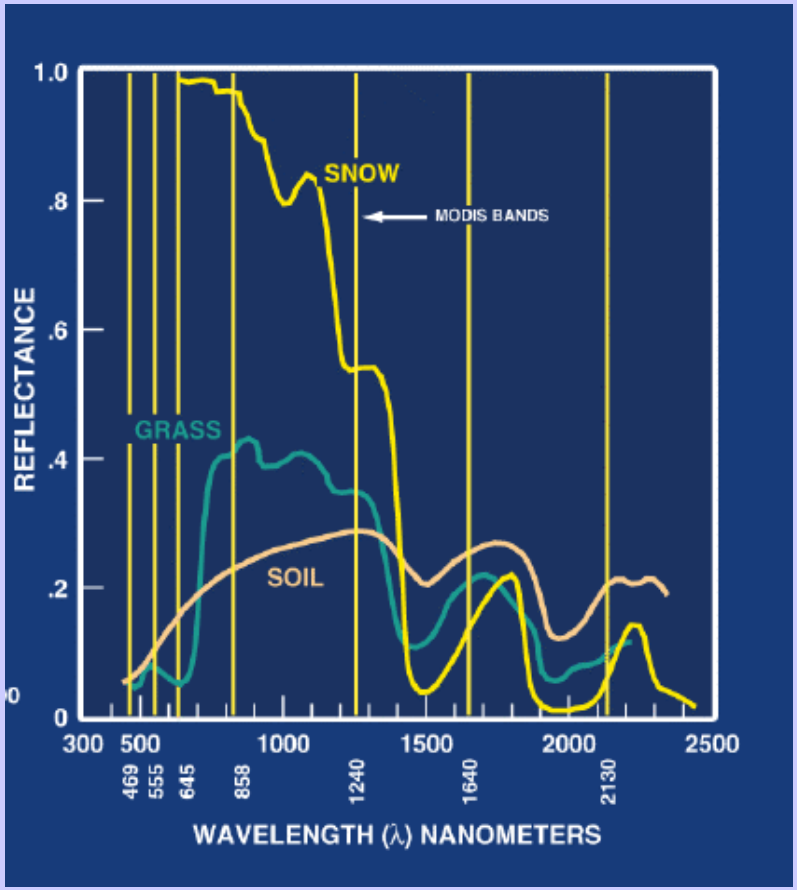

Investigating with Multi-spectral Combinations

Given the spectral response of a surface or atmospheric feature

Select a part of the spectrum where the reflectance or absorption changes with wavelength

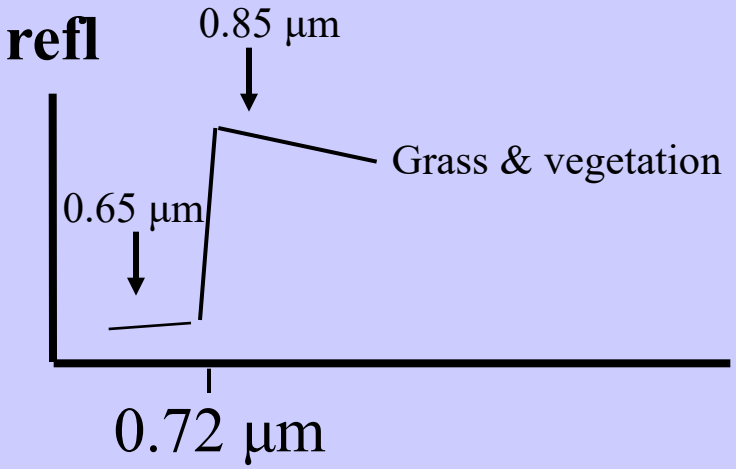

e.g. reflection from grass

If 0.65 μm and 0.85 μm channels see the same reflectance than surface viewed is not grass;
if 0.85 μm sees considerably higher reflectance than 0.65 μm then surface might be grass

LAND - THERMAL RADIATION

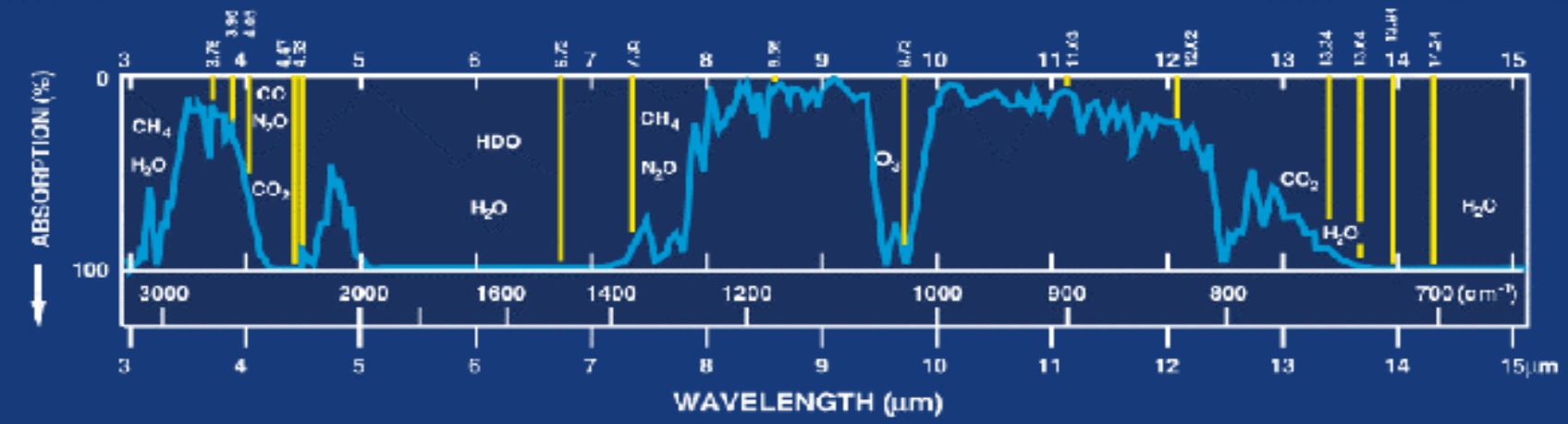

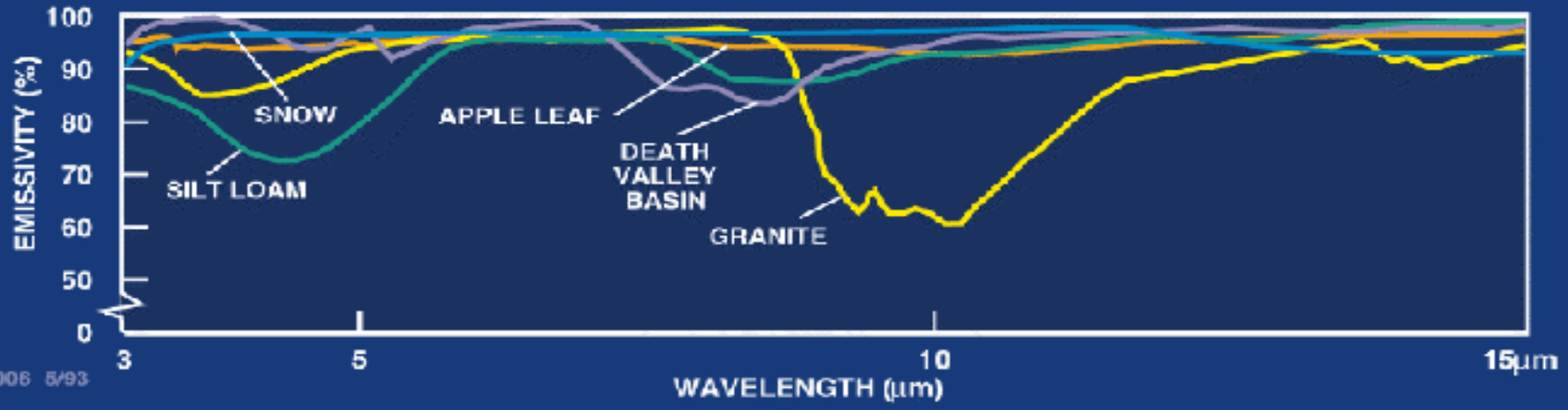

C351.006 5/93

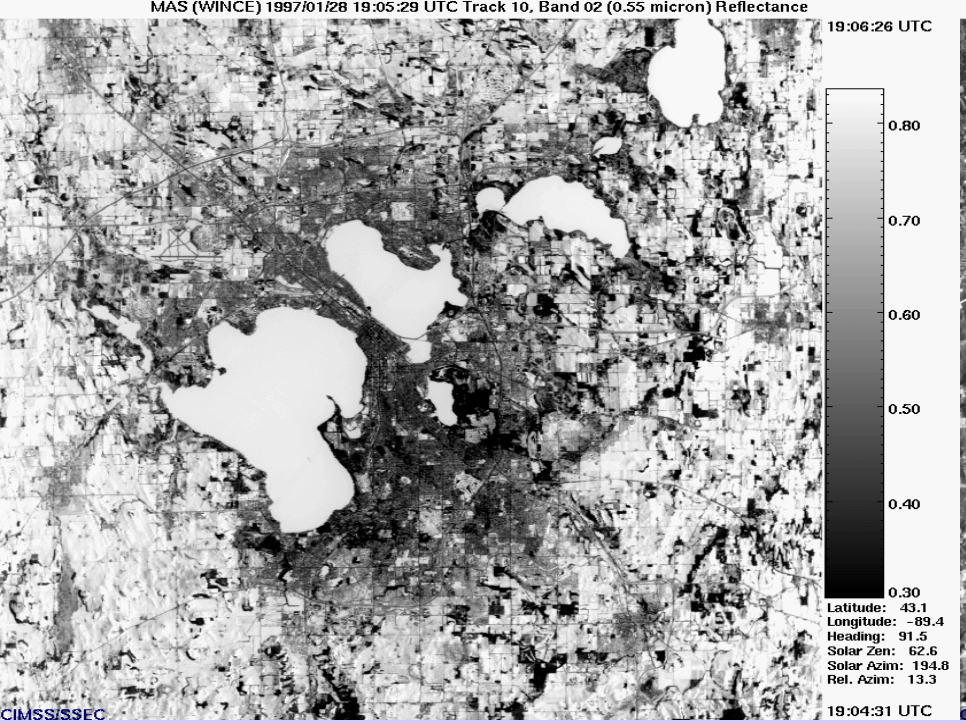

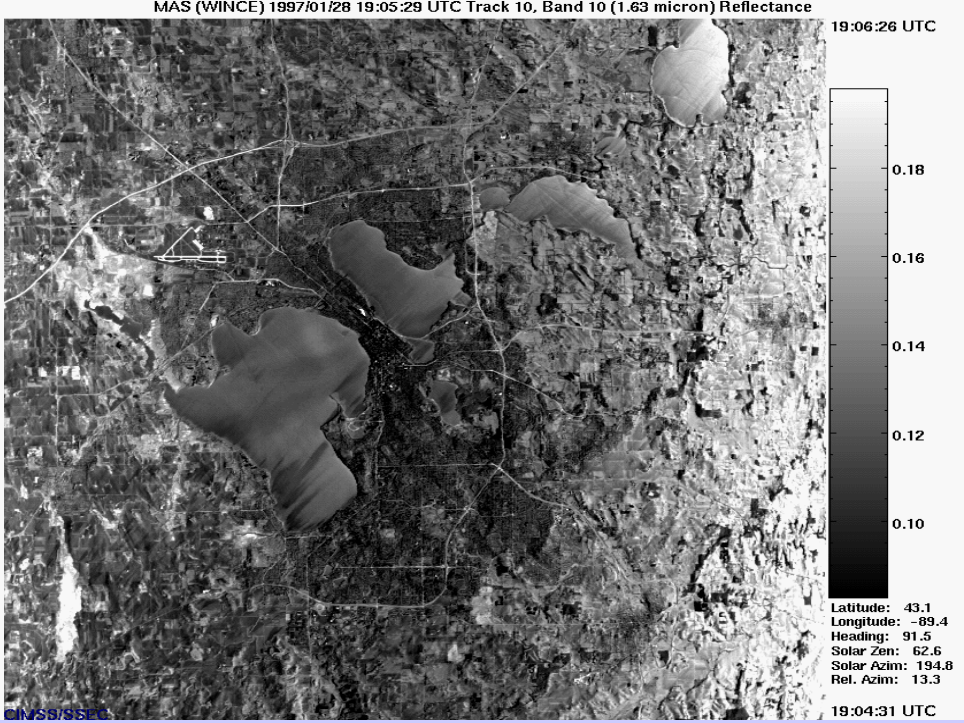

MODIS Airborne Simulator (MAS)
0.6, 1.6, & 11.0 um data over Madison in Jan 97

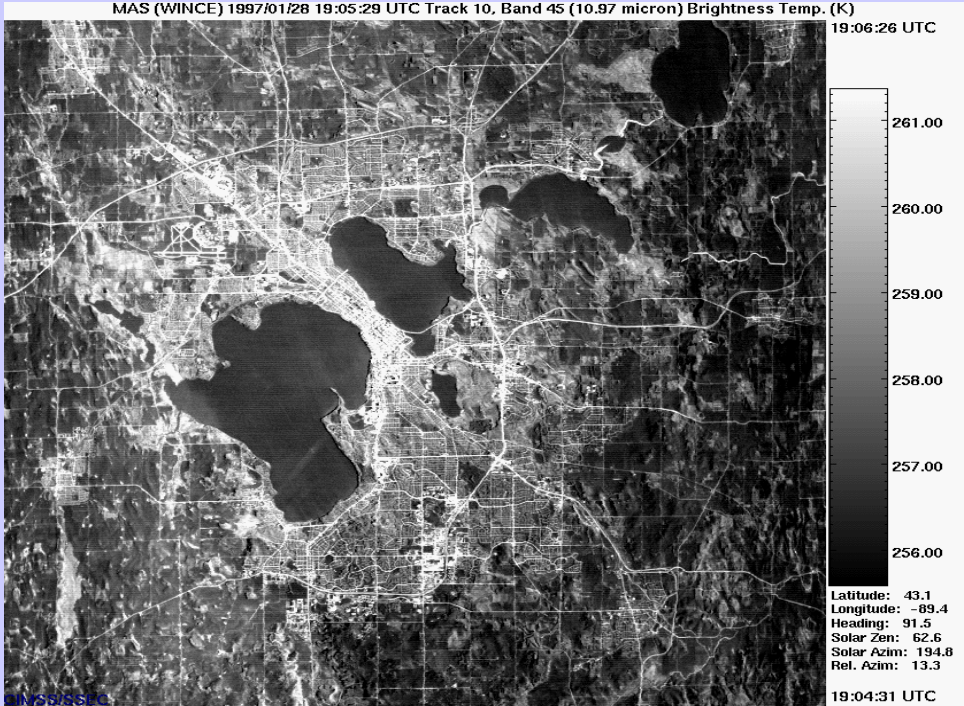

Example with MODIS

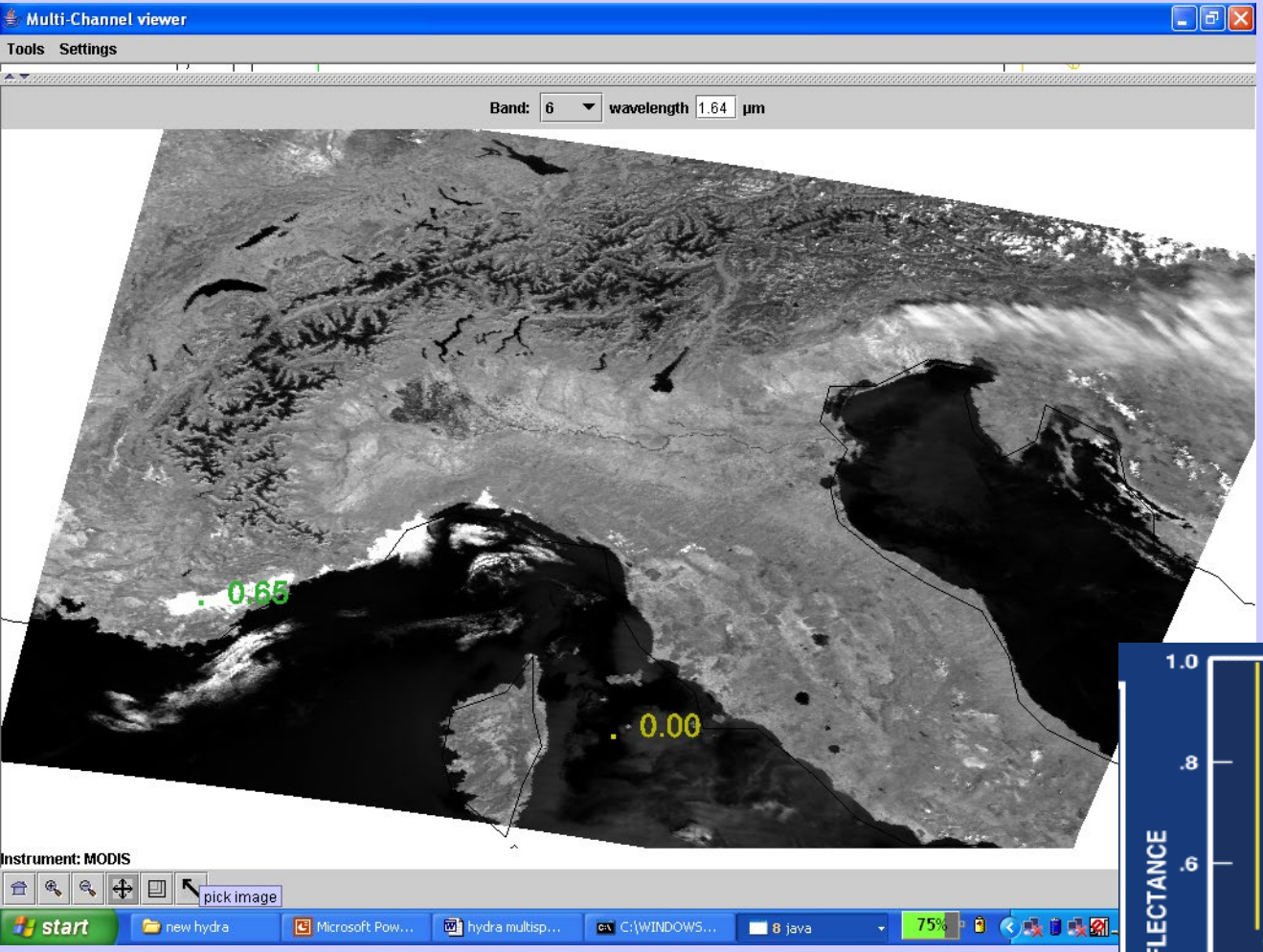

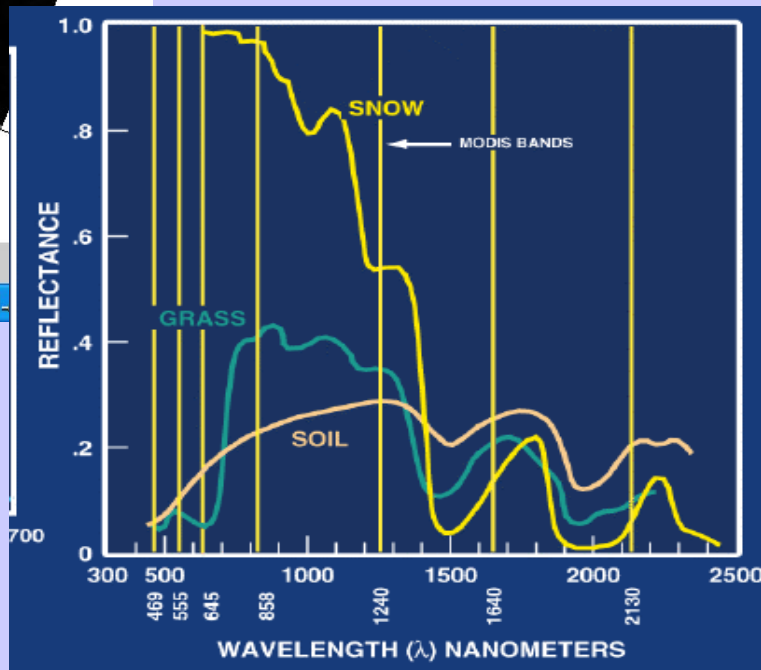

low refl at 1.6 um from snow in mountains

MODIS scatterplot of r1.6 (y-axis) and BT11 (x-axis)

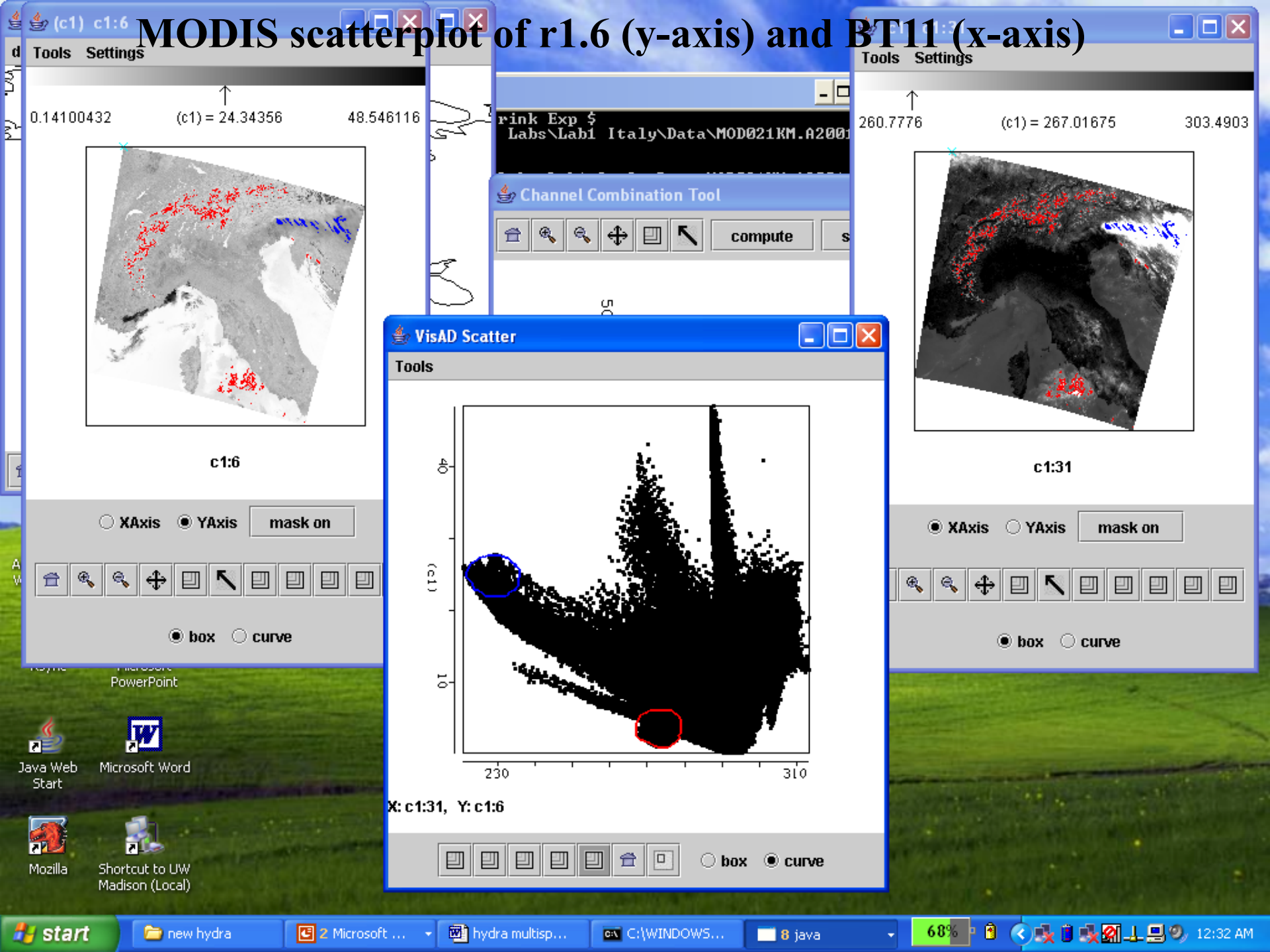

Observing Sea Ice Leads With MODIS

MODIS Band 1 Image of Western Arctic, 1 km (subsampled)

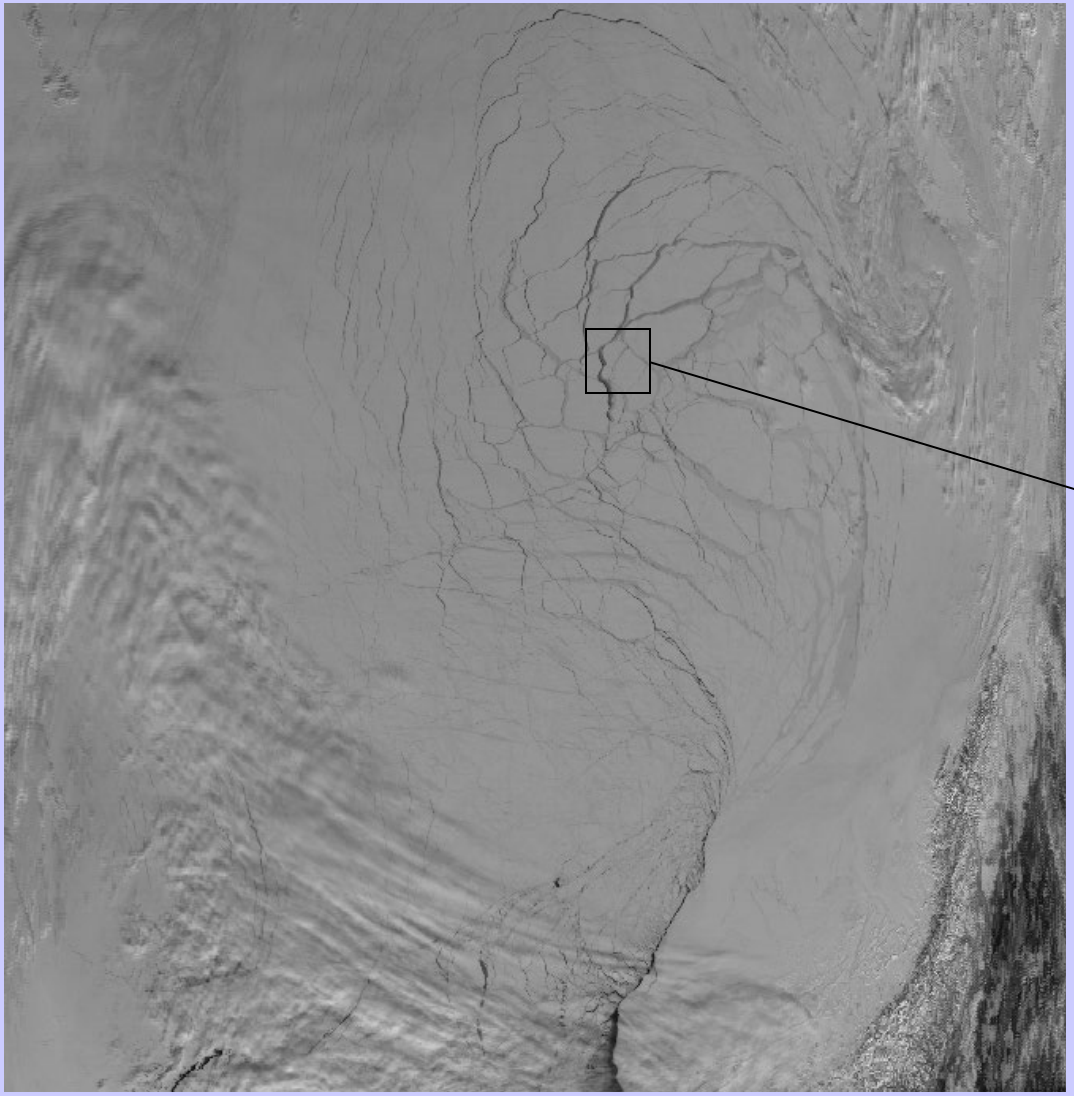

MODIS Full Resolution, 250 m Pixels

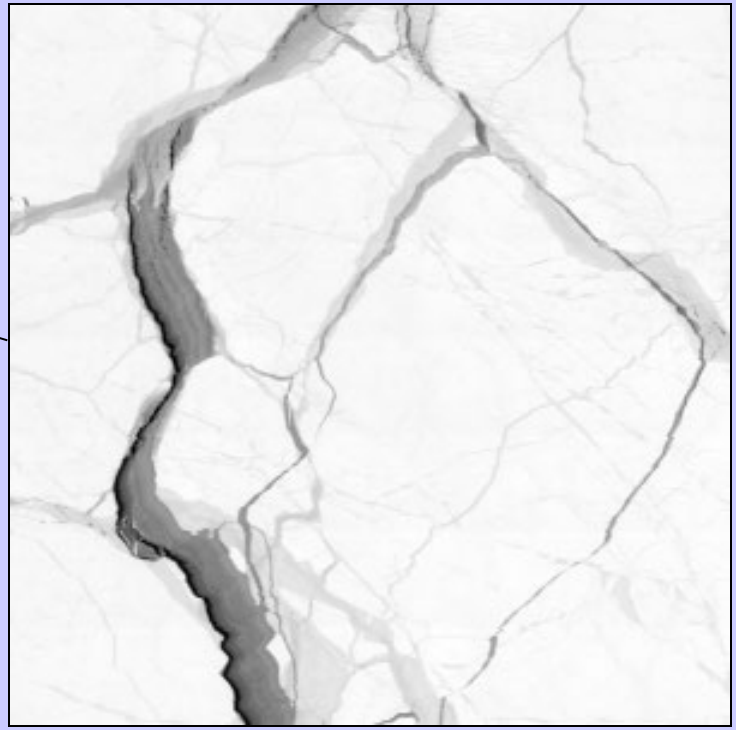

MODIS Image and snow map - November 3, 2000

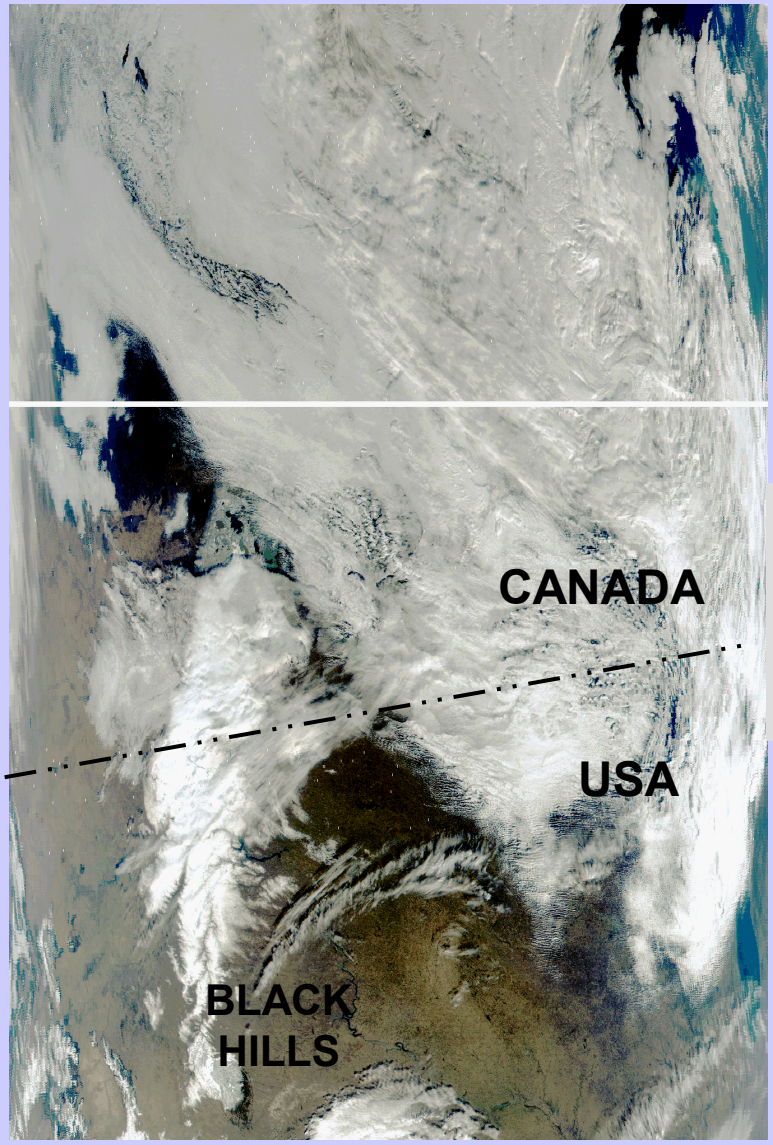

MODIS bands 1, 4, 3

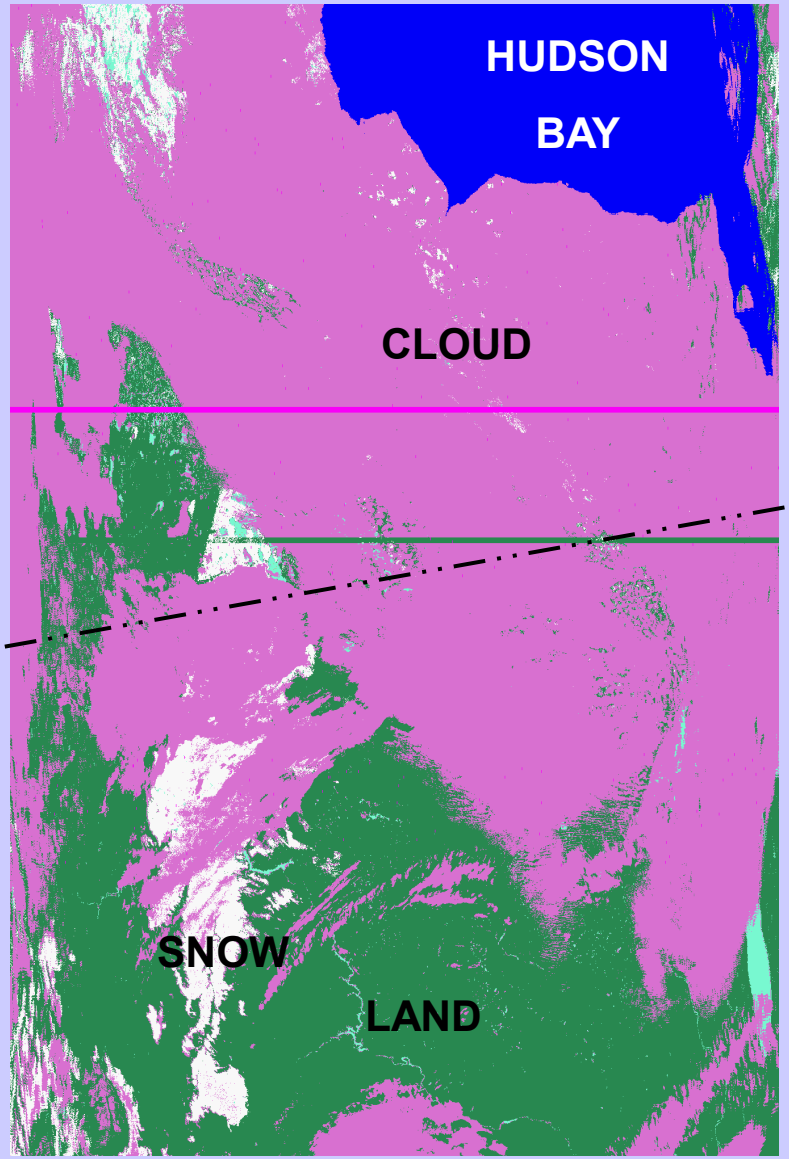

9.0 million sq. km of snow cover

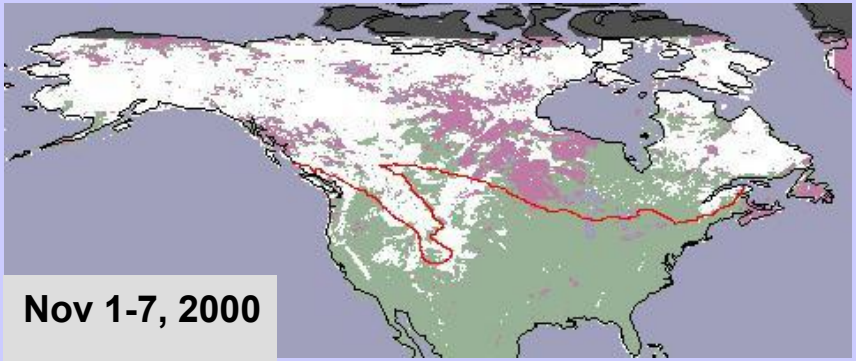

10.8 million sq. km of snow cover

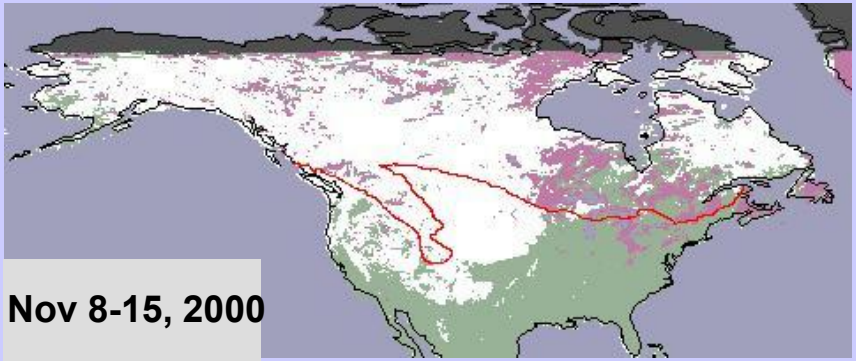

Change in maximum snow extent between two composite periods seen above (1.8 million sq. km)

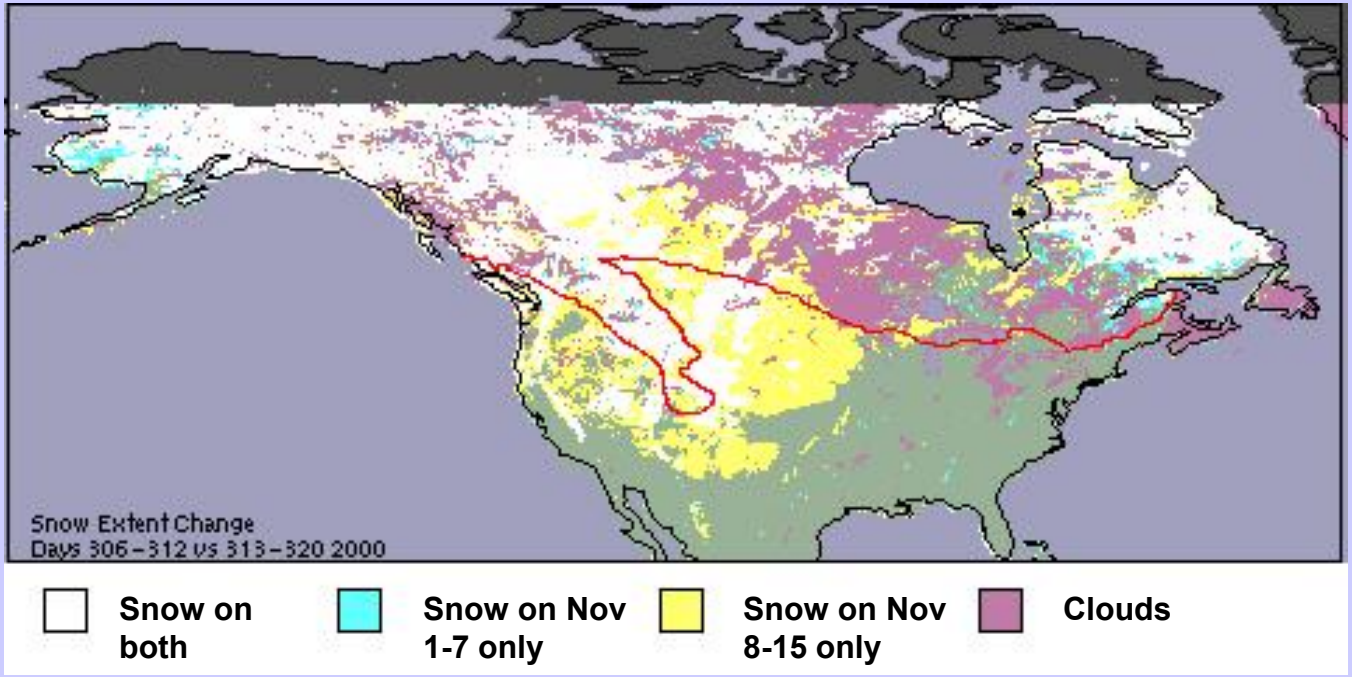

Spatially Complete Spectral Albedo Maps
(E. G. Moody, M. D. King, S. Platnick, C. B. Schaaf, F. Gao – GSFC)

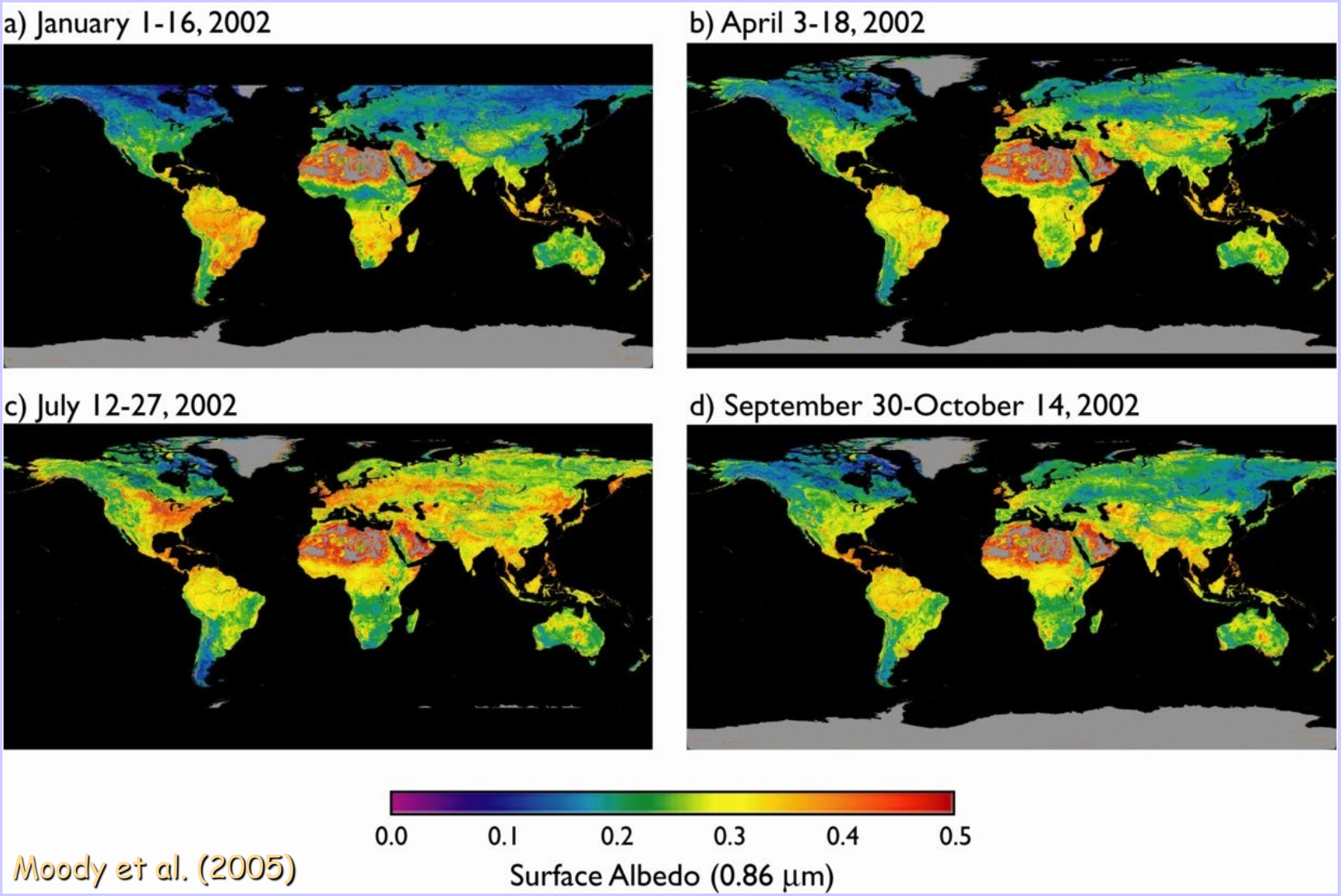

Moody et al. (2005)

NDVI versus EVI

EVI is a useful proxy for 'greenness' or photosynthetically active vegetation in optically dense canopies, as found throughout the Amazon (LAI= 4 -7), by relying on the more sensitive NIR canopy reflectance which is less prone to saturate

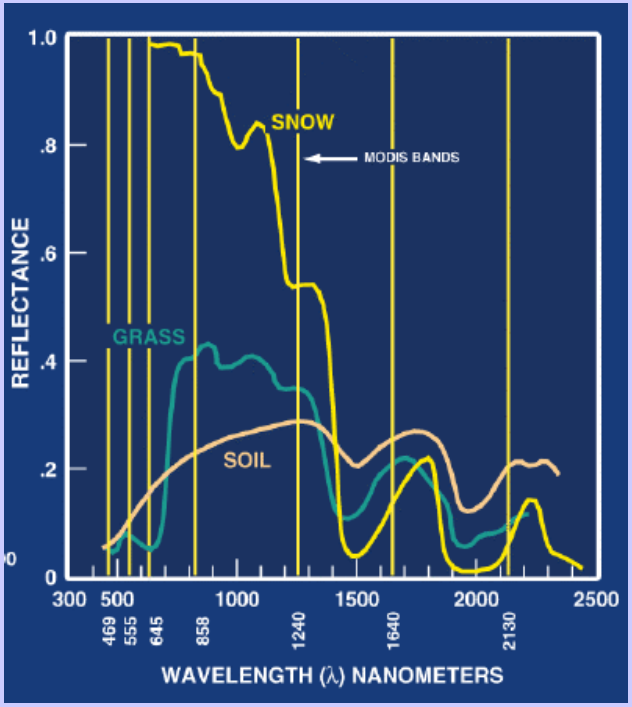

$$NDVI = (\rho 0.8 - \rho 0.6) / (\rho 0.8 + \rho 0.6)$$

$$EVI = 2.5 \times \frac{\rho_{NIR} - \rho_{red}}{1 + \rho_{NIR} + (6 \times \rho_{red} - 7.5 \times \rho_{blue})}$$

Basin-wide greening in dry season

October EVI (dry) minus June EVI (wet season) CMG

from Huete et al

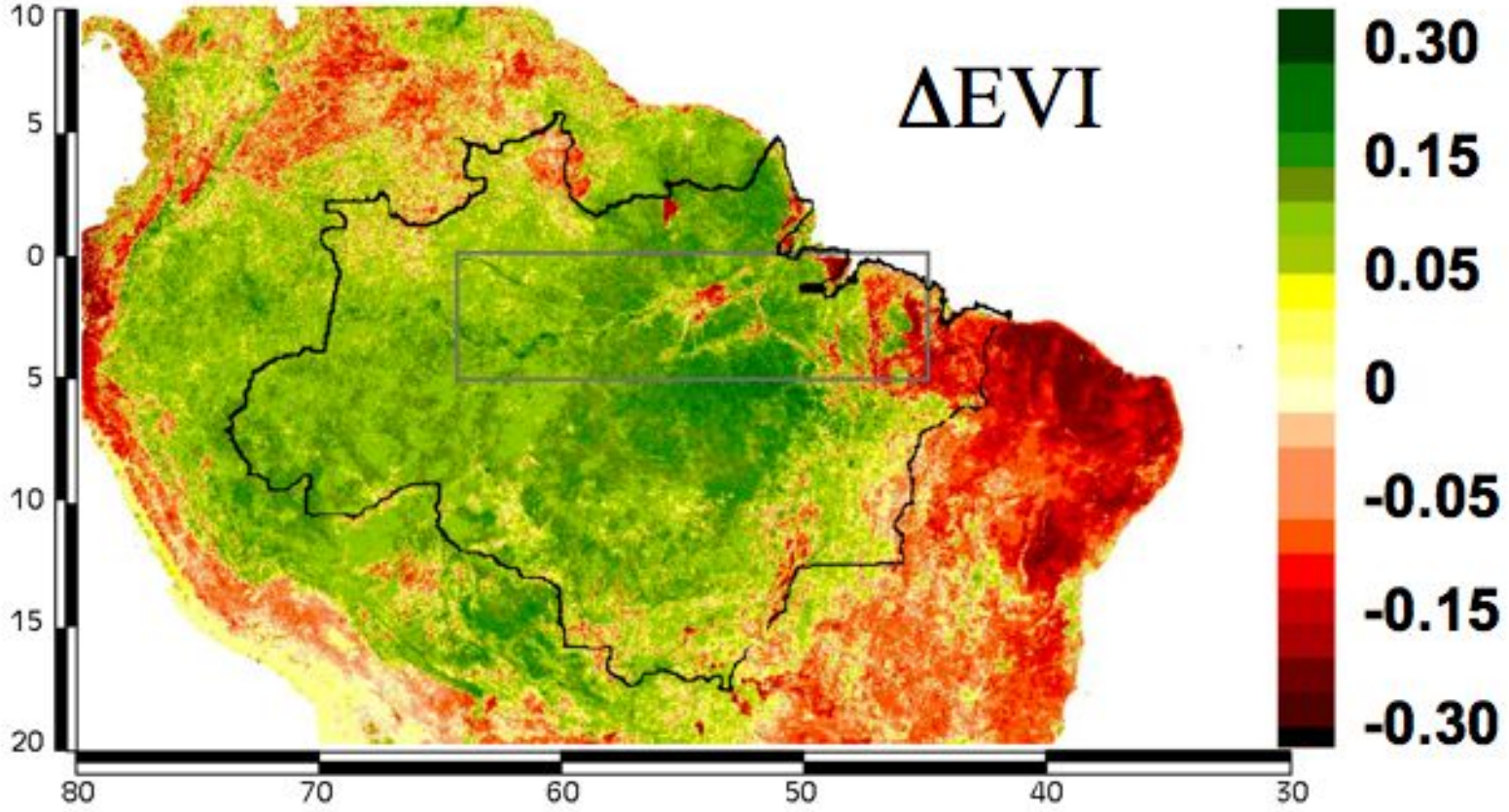

- green colors depict 'greening' and red colors depict 'browning' in the dry season

Spatially Explicit Behavior: Pattern

a

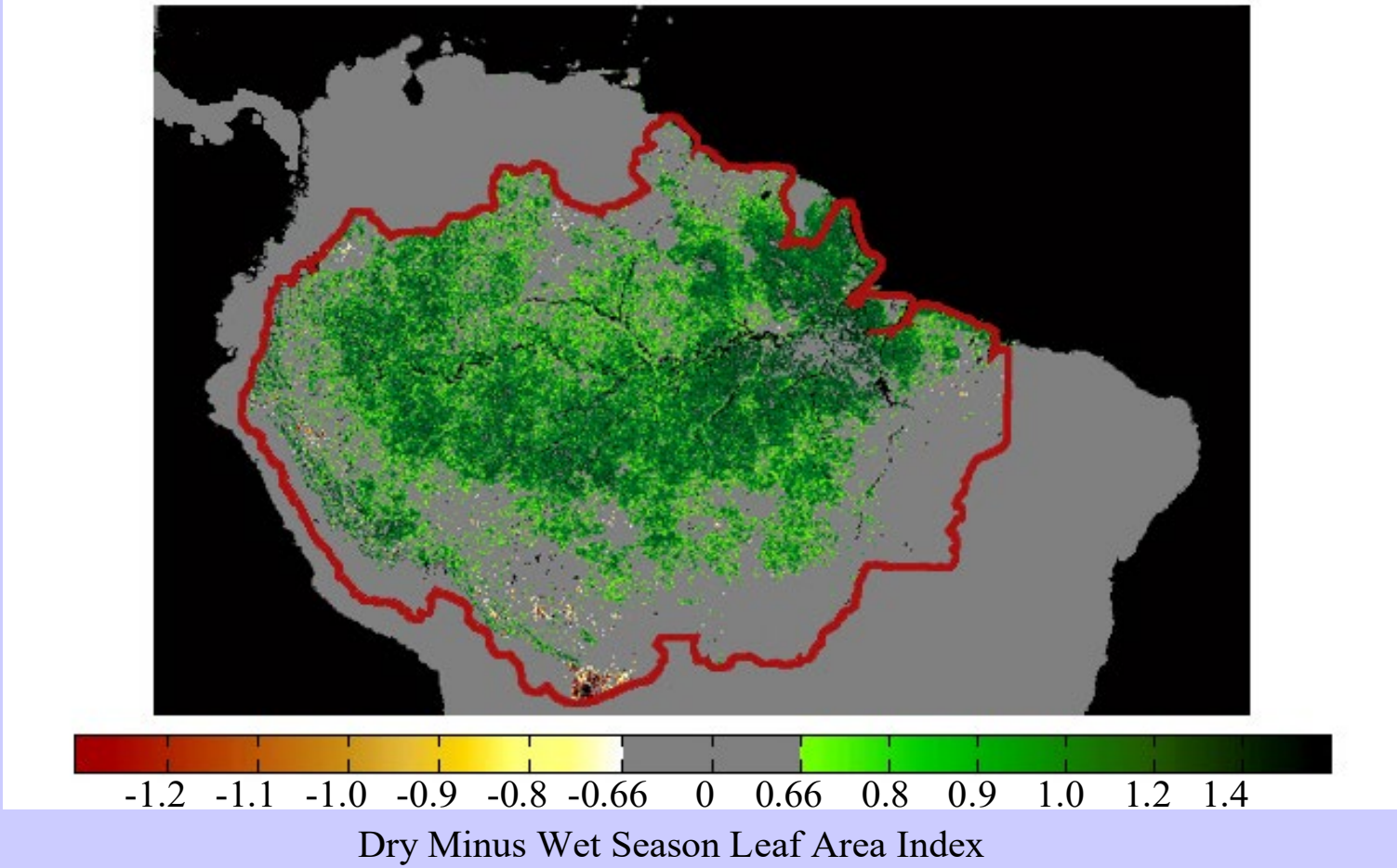

The derived spatial pattern of seasonal LAI amplitude reveals a heretofore unknown picture of phenology over a broad contiguous swath of land, anchored to the Amazon river, from its mouth in the east to its western-most reaches in Peru, in the heart of the basin.

Spatially Averaged Behavior: LAI Amplitude

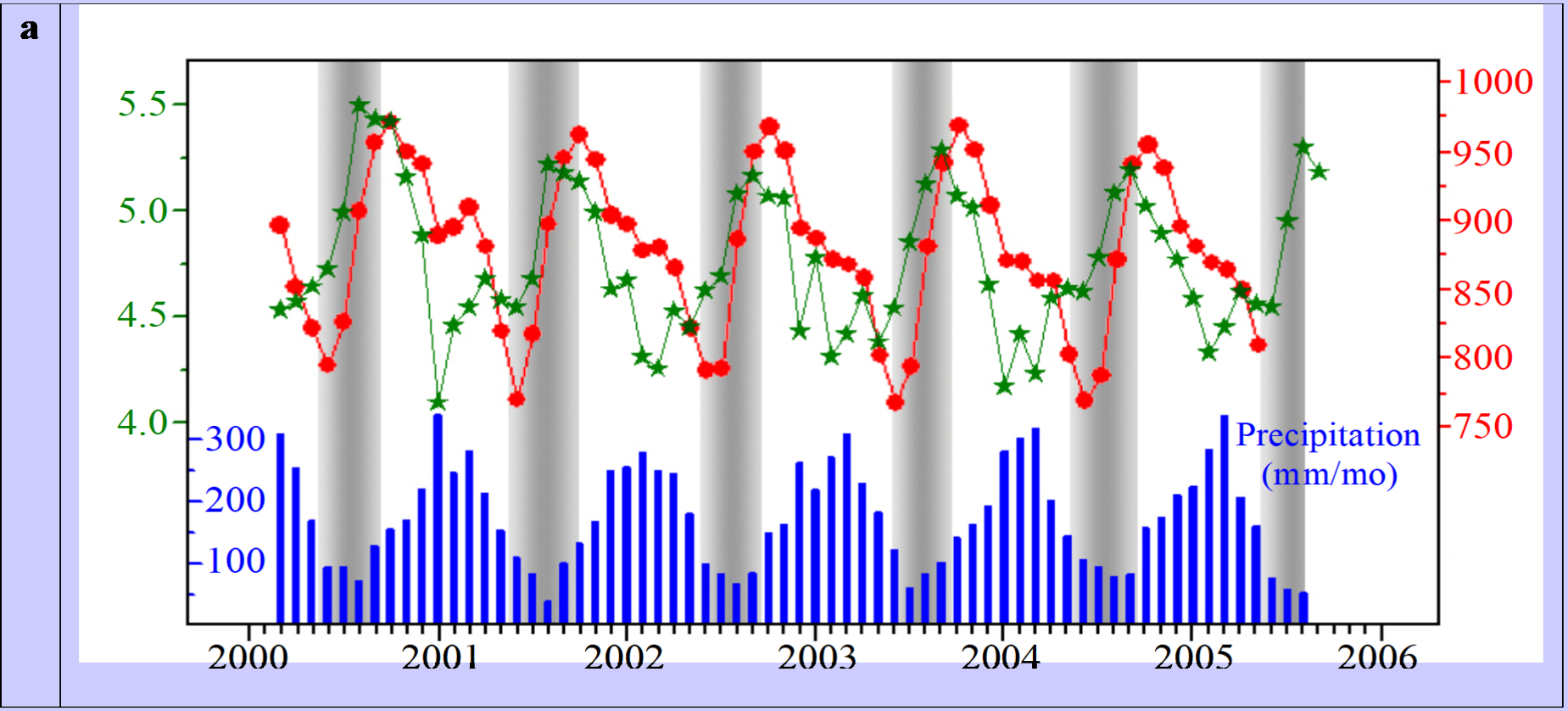

- **Leaf area data of the Amazon rainforests exhibit *notable seasonality*, with an amplitude (peak to trough difference) that is about 25% of the average annual LAI of 4.7, over the entire course of the data record. (from Myneni et al.)**

Aerosol Types and Origin

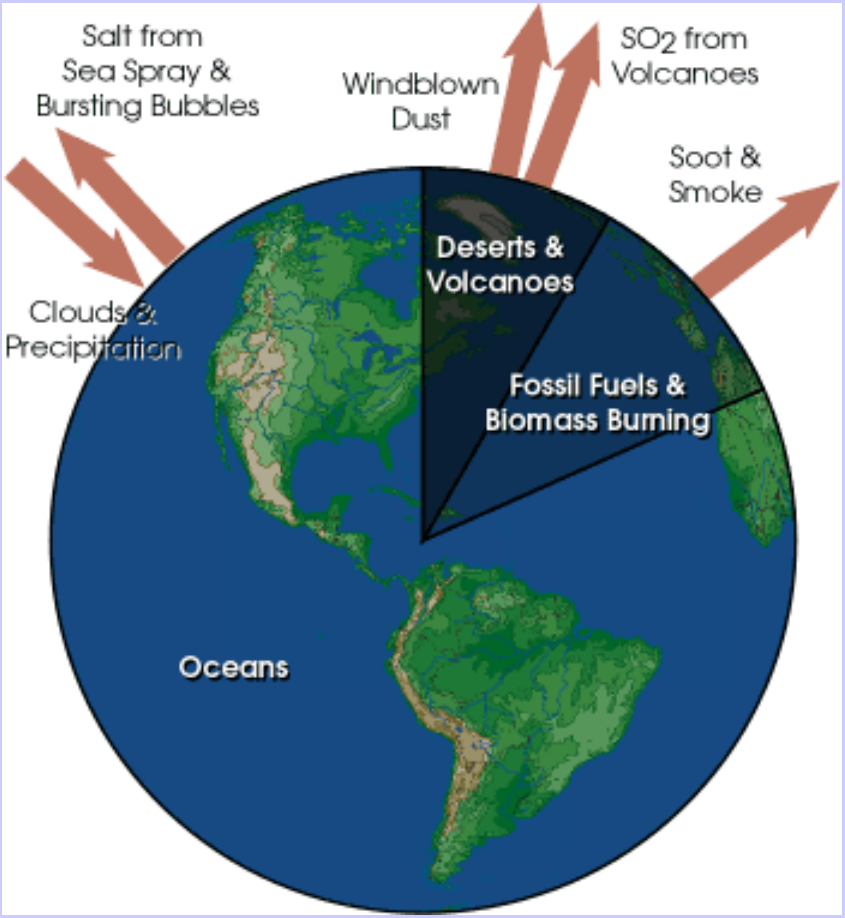

- Aerosol particles larger than about 1 μm in size are produced by windblown dust and sea salt from sea spray and bursting bubbles
- Aerosols smaller than 1 μm are mostly formed by condensation processes such as conversion of sulfur dioxide (SO2) gas (released from volcanic eruptions) to sulfate particles and by formation of soot and smoke during burning processes.
- After formation, aerosols are mixed and transported by atmospheric motions and are primarily removed by clouds and precipitation.

Aerosol Size Distribution

There are 3 modes :

- « **nucleation** »: radius is between 0.002 and 0.05 µm. They result from combustion processes, photo-chemical reactions, etc.

- « **accumulation** »: radius is between 0.05 µm and 0.5 µm. Coagulation processes.

- « **coarse** »: larger than 1 µm. From mechanical processes like aeolian erosion.

« fine » particles (nucleation and accumulation) result from anthropogenic activities, coarse particles come from natural processes.

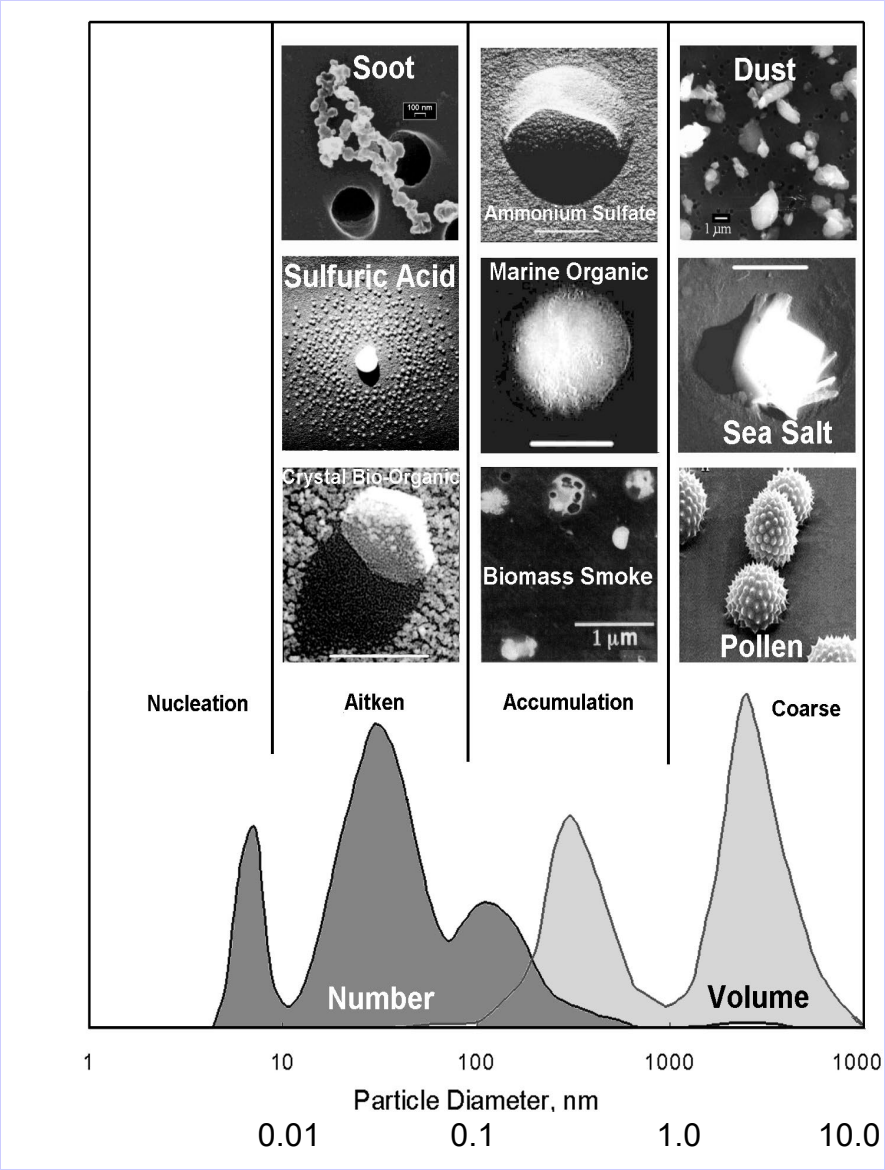

Measurements in the Solar Reflected Spectrum across the region covered by AVIRIS

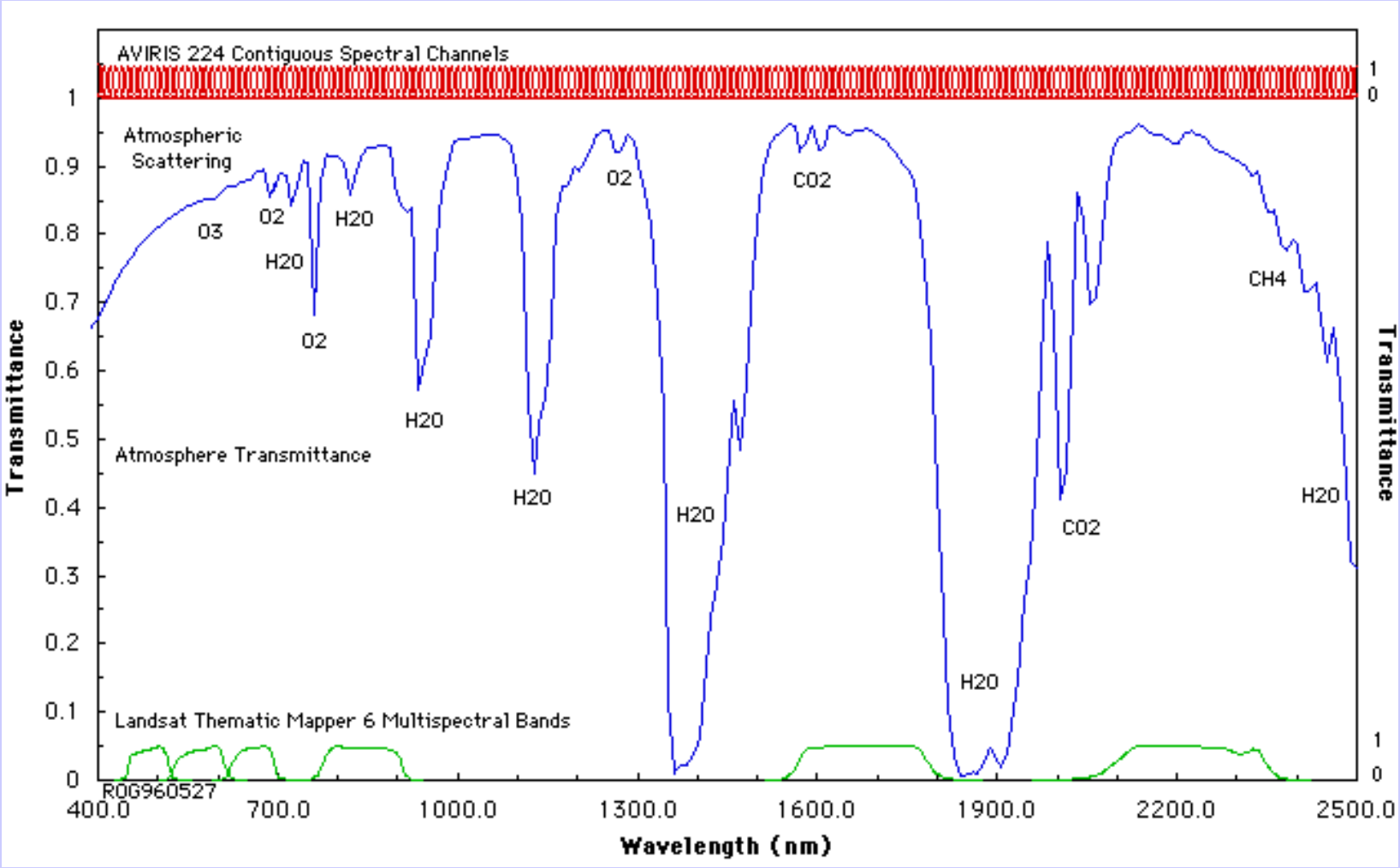

AVIRIS Movie #1

AVIRIS Image - Linden CA 20-Aug-1992
224 Spectral Bands: 0.4 - 2.5 μm
Pixel: 20m x 20m Scene: 10km x 10km

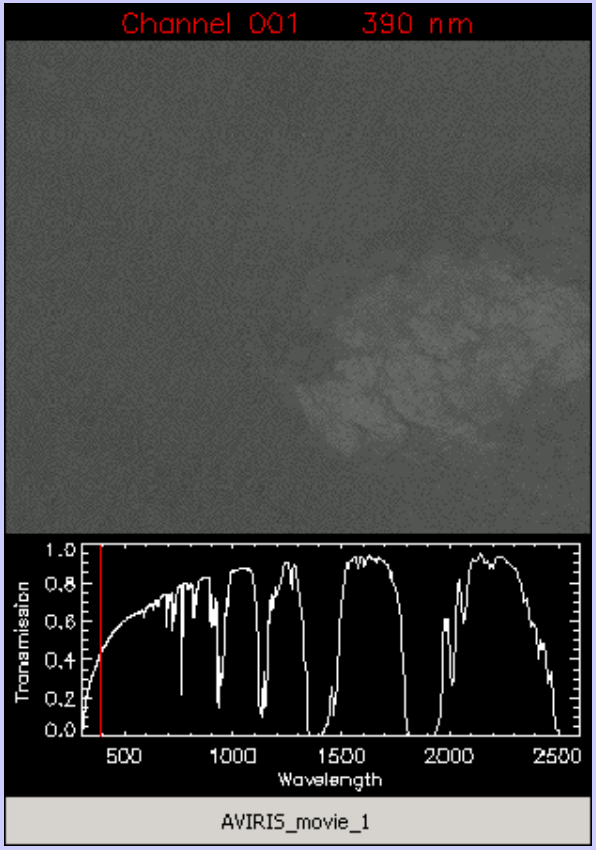

Cuiaba Brazil mosaic on 25 August 1995 shows a forest clearing fire. True color image, and single band images in black and white.

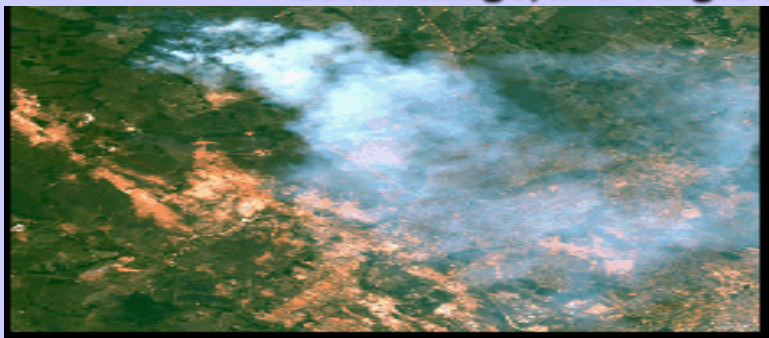

True color

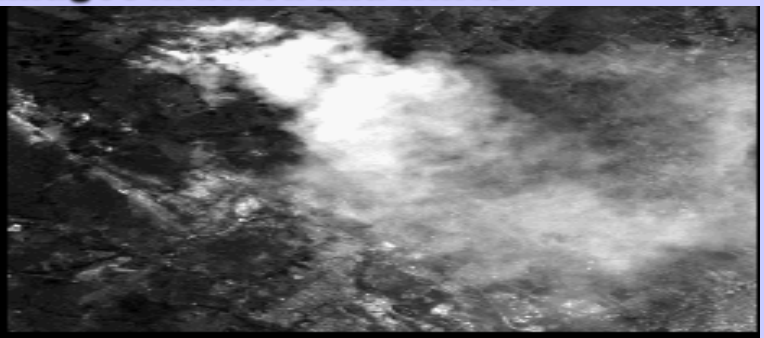

500.5 nm

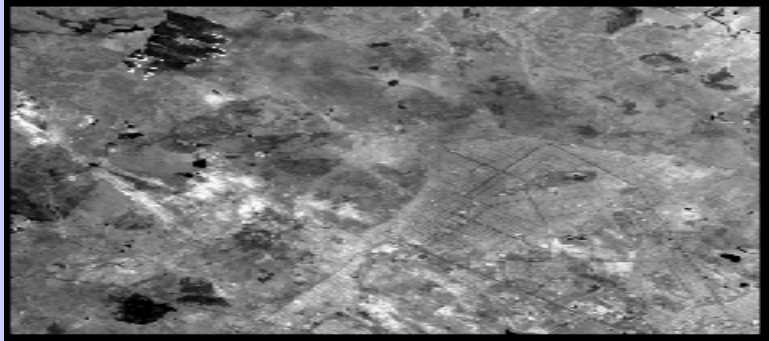

1000.2 nm

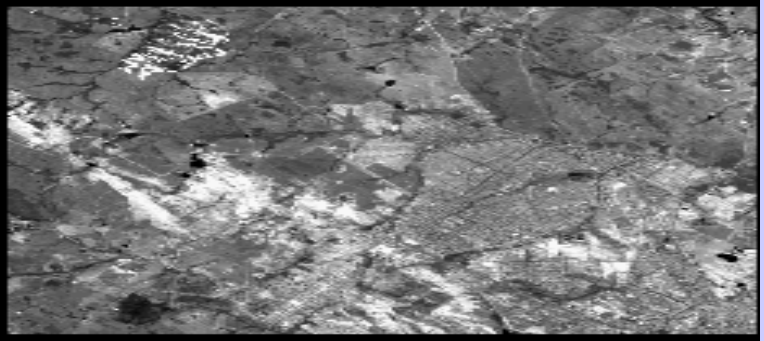

1501.4 nm

2000.5 nm

2508.5 nm

Pollution off Northeast United States (08/14/02)

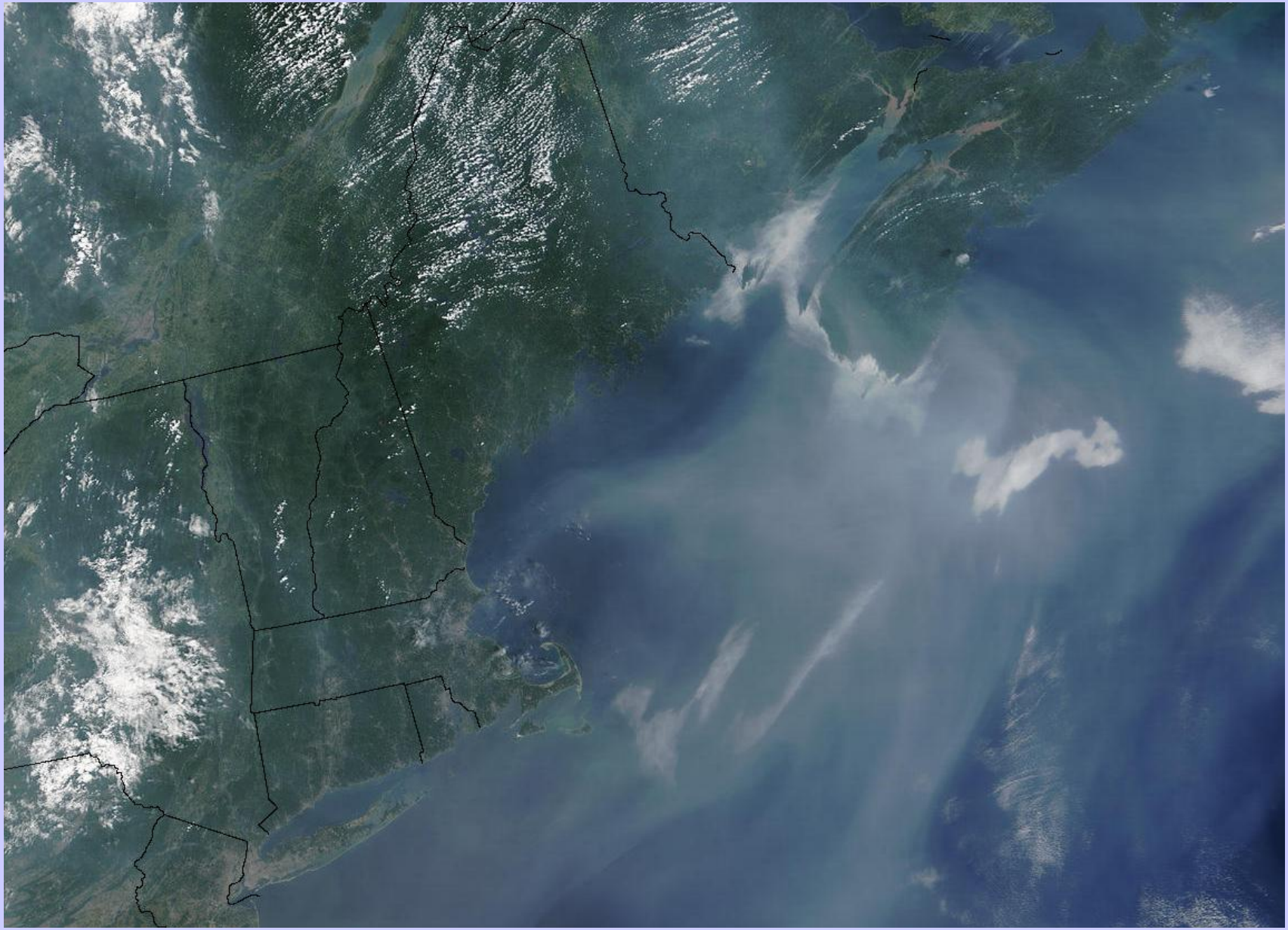

True color composite

AOT (0.55 um)

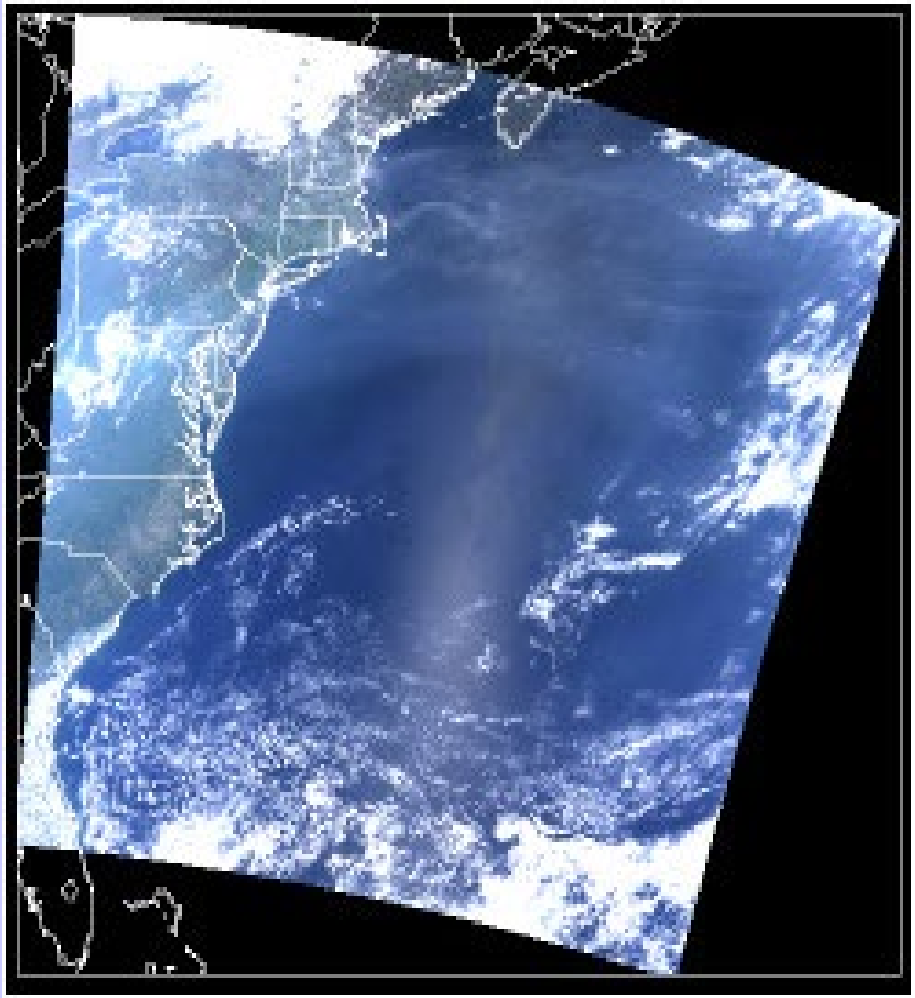

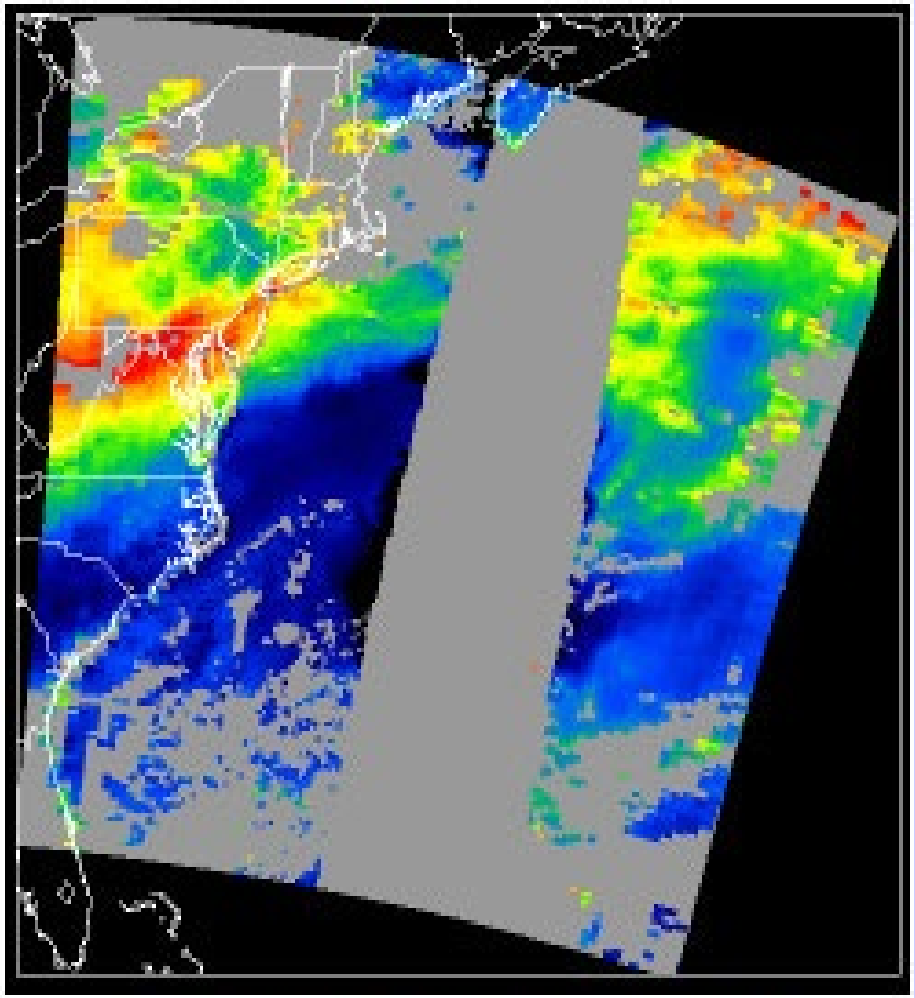

Ohio Valley pollution heading over N. Atlantic

τ_a (0.56 µm)

Effect of aerosol on climate:

Cooling past climates, possibly warming future climates

Effect of aerosol on hydrologic cycle:

Less evaporation from cooler land and ocean, more stable atmosphere, less clouds and precipitation.

Effect of aerosol on health:

May be more important then ozone in causing cancer and heart problems.

Effect on agriculture, vegetation:

Shift of precipitation away from polluted land, less sunlight to vegetation

Does Population cause Pollution ?

POLDER aerosol index Feb. 1997 & population density

(Kaufman, Tanré & Boucher, Nature 2002)

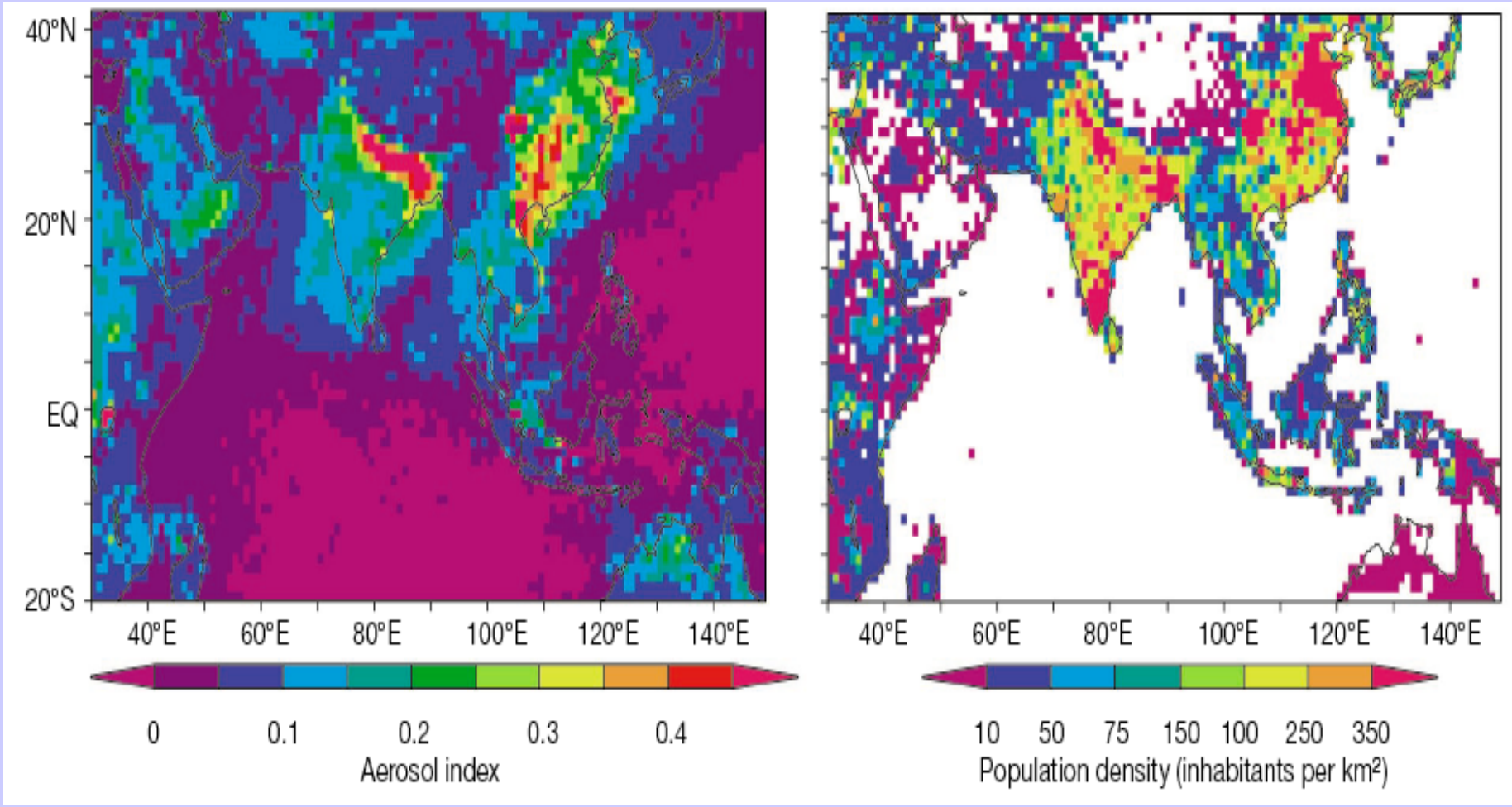

Aerosol Optical Thickness
(Coarse Particle Mode)

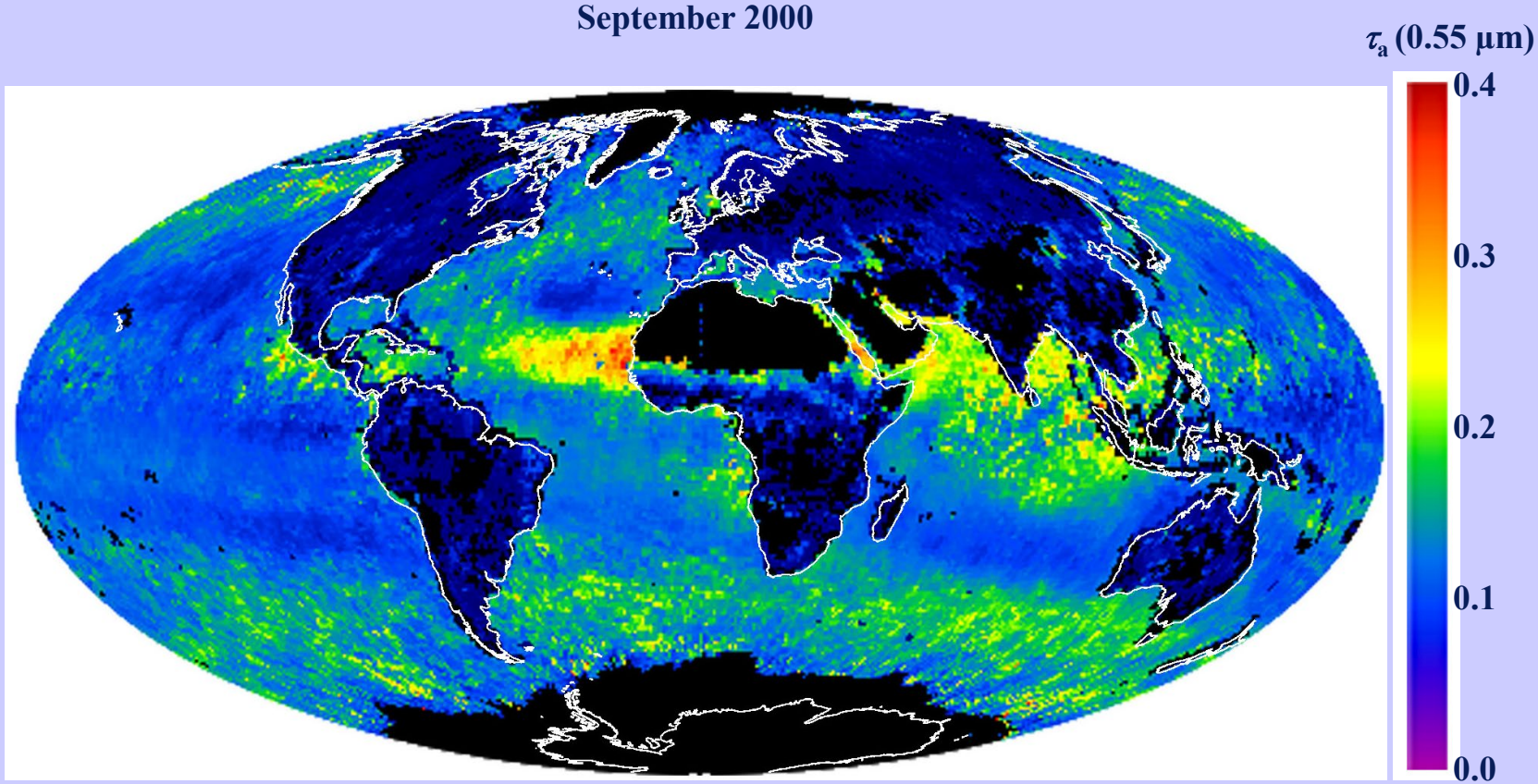

bands for aerosol retrieval over ocean (550, 660, 865, 1230, 1640, 2130 nm)

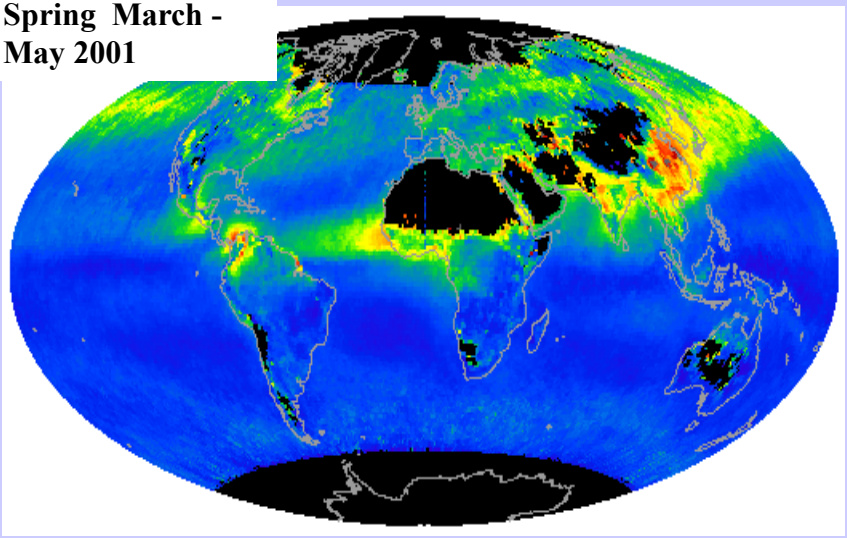

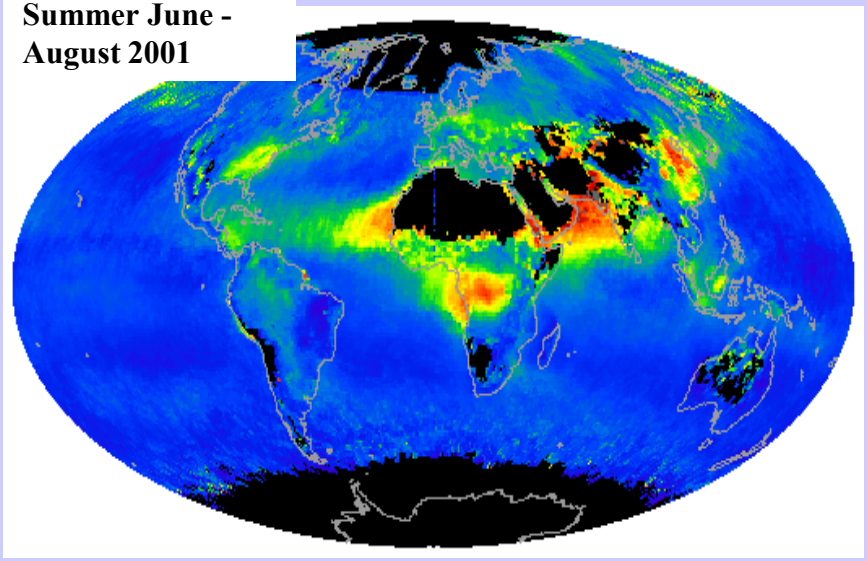

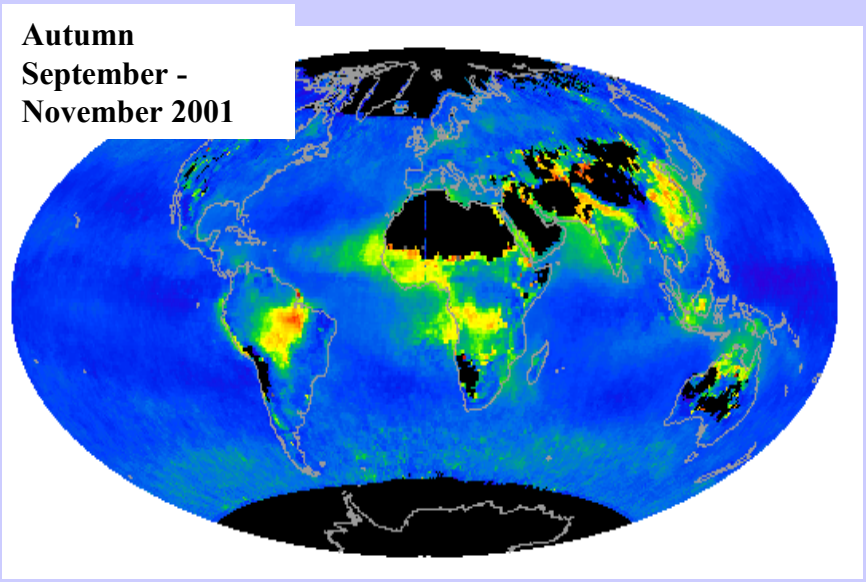

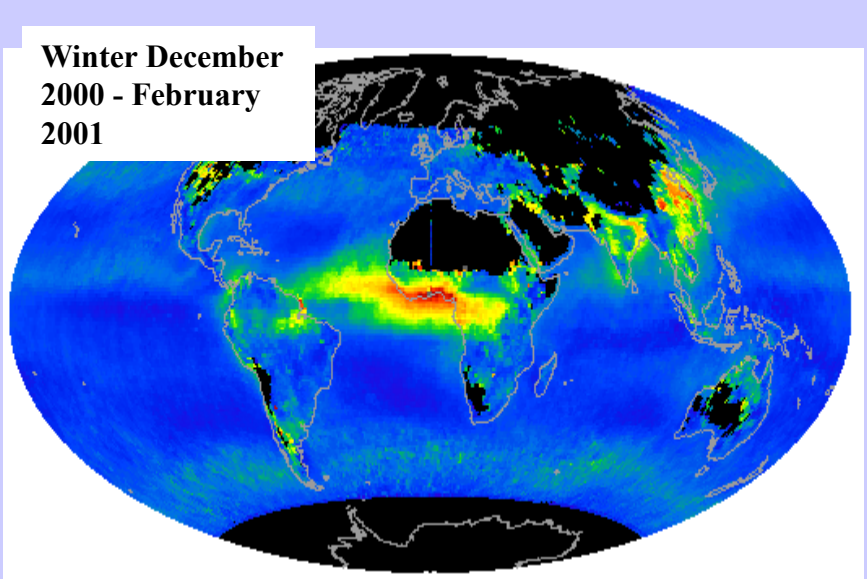

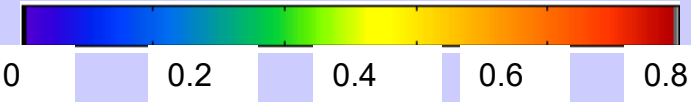

Average optical thickness

Global aerosol AOT trends

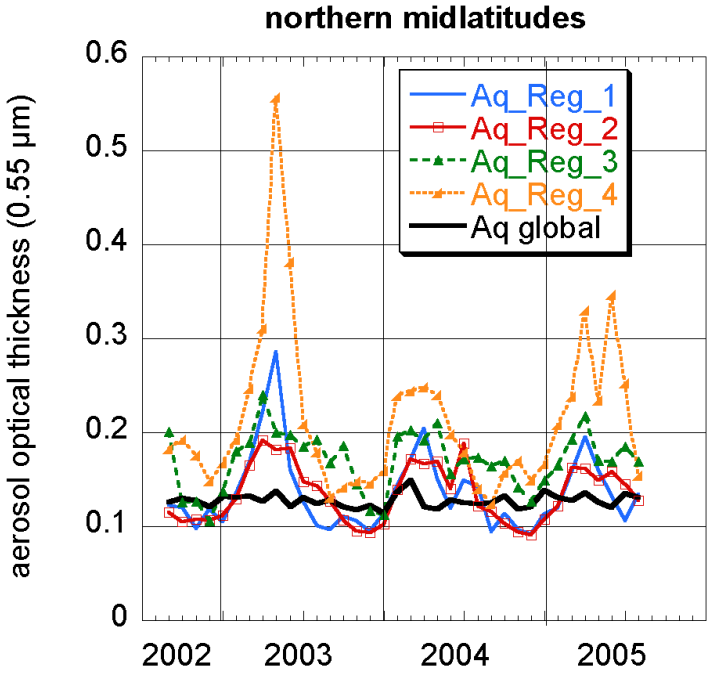

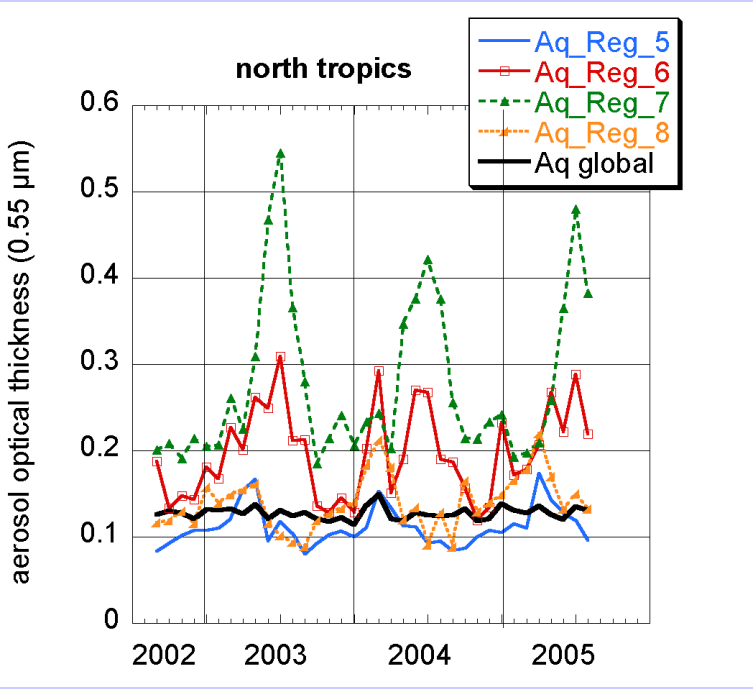

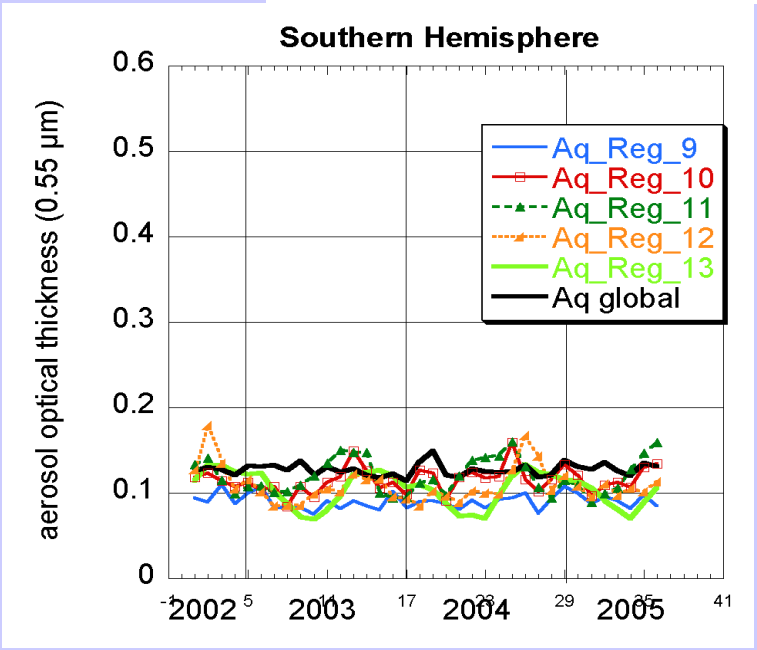

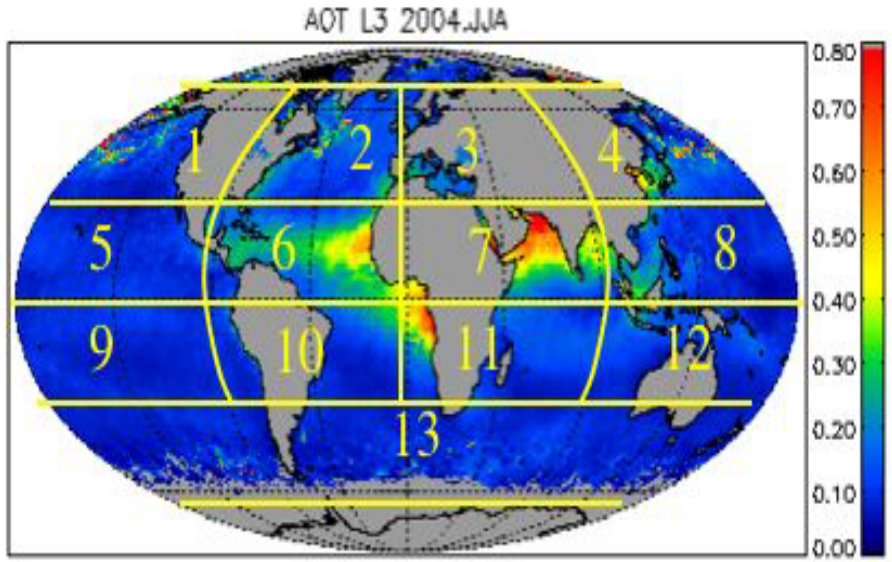

Aerosol optical thickness (0.55 μm)

Aerosol effects on cloud cover over the Atlantic Ocean - several aerosol types interact with clouds

June-Aug 2002

Pollution zone

Dust zone

Smoke zone

Marine aerosol

aerosol forcing increased cloud cover 5% (~ 6 W/m2) and height 40 hPa (~ 400 m) in June-Aug 02 over Atlantic Ocean

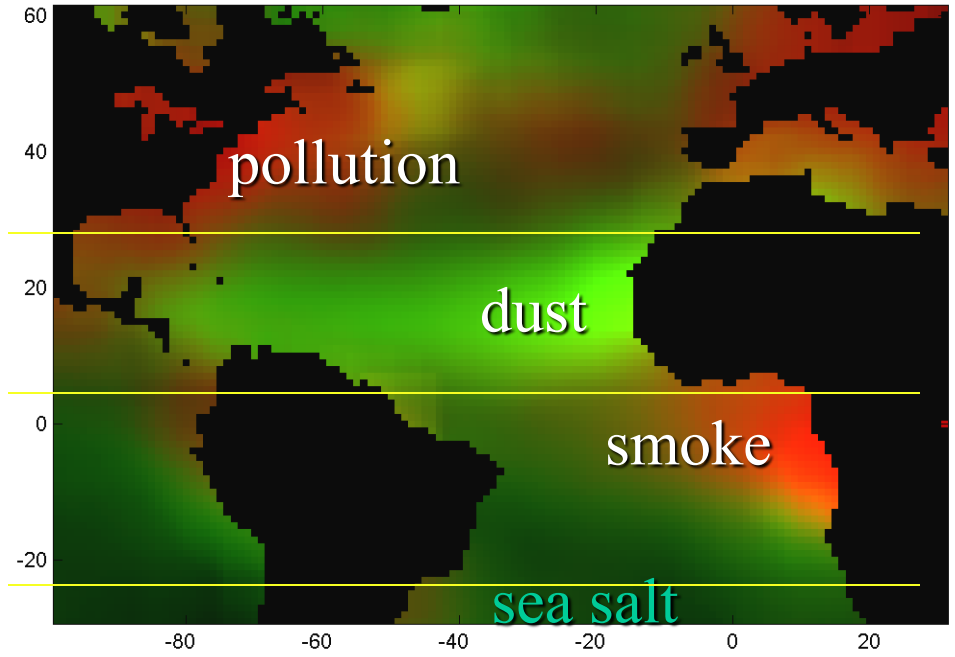

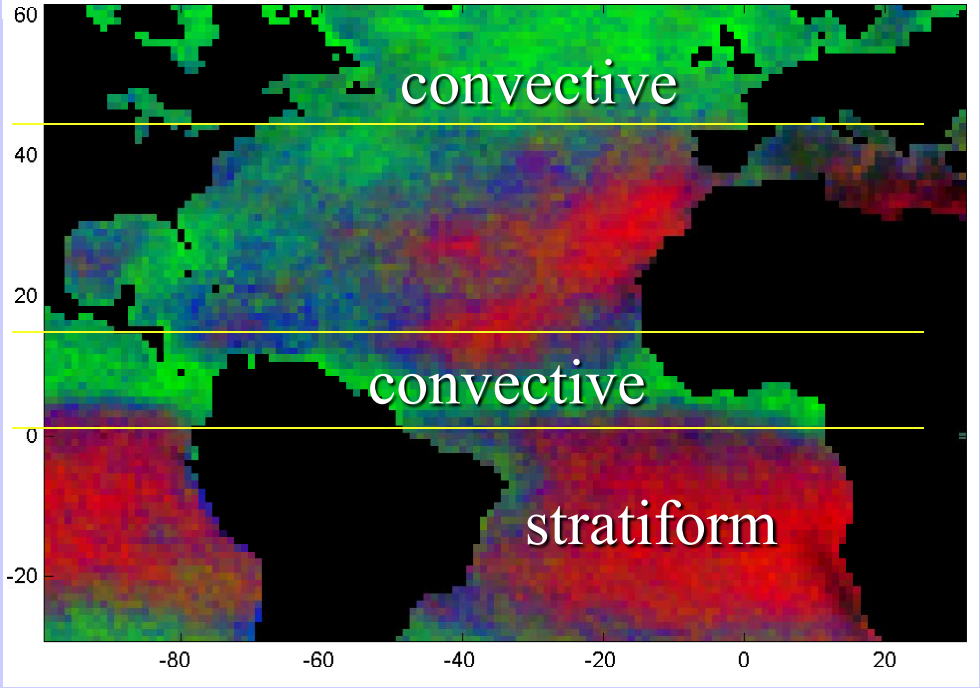

Dust

Stratus and trade cumulus Clouds

Smoke

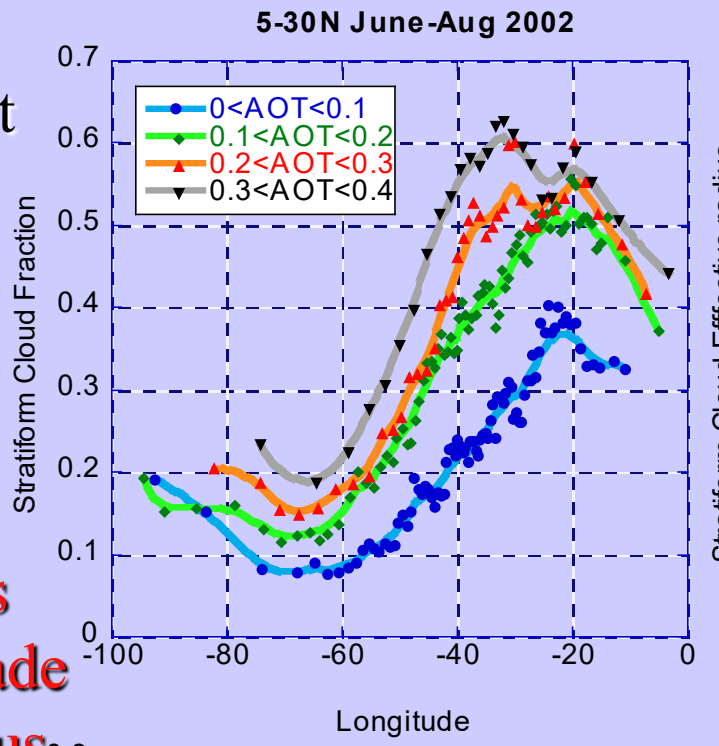

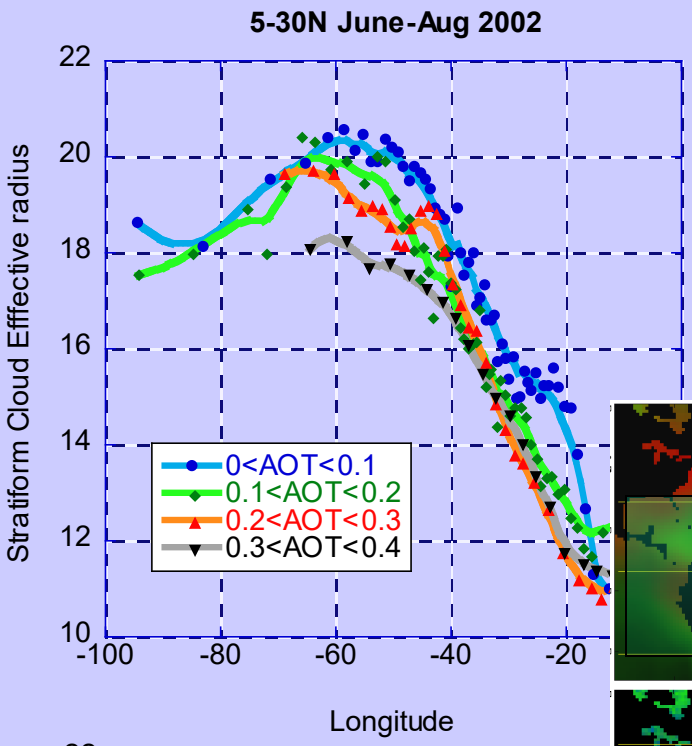

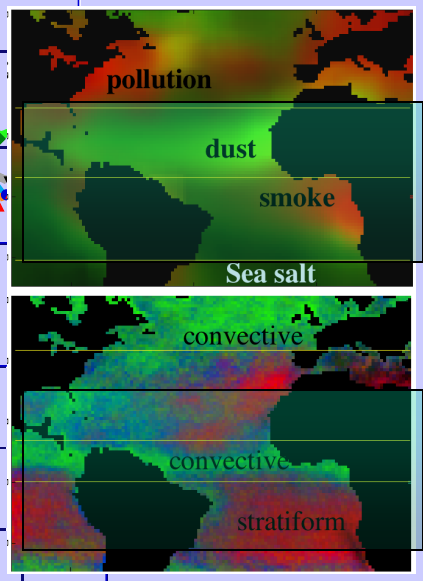

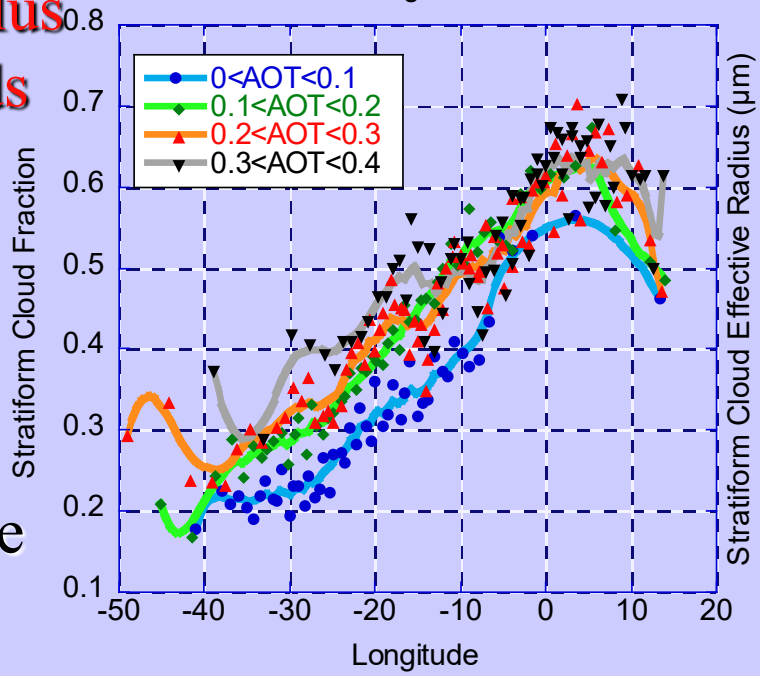

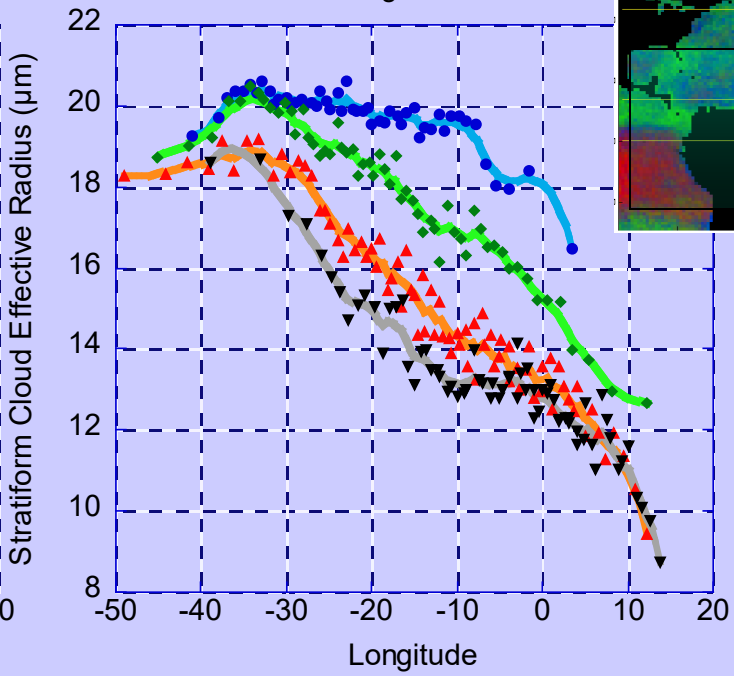

clean

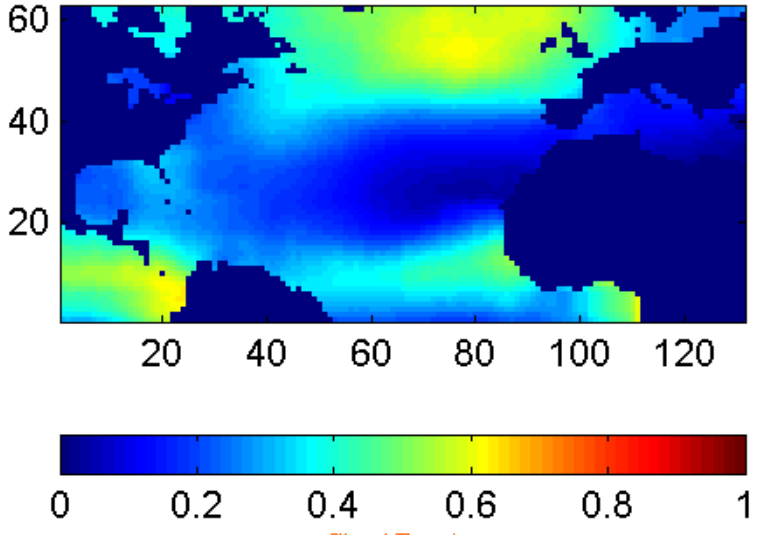

Cloud fraction

hazy

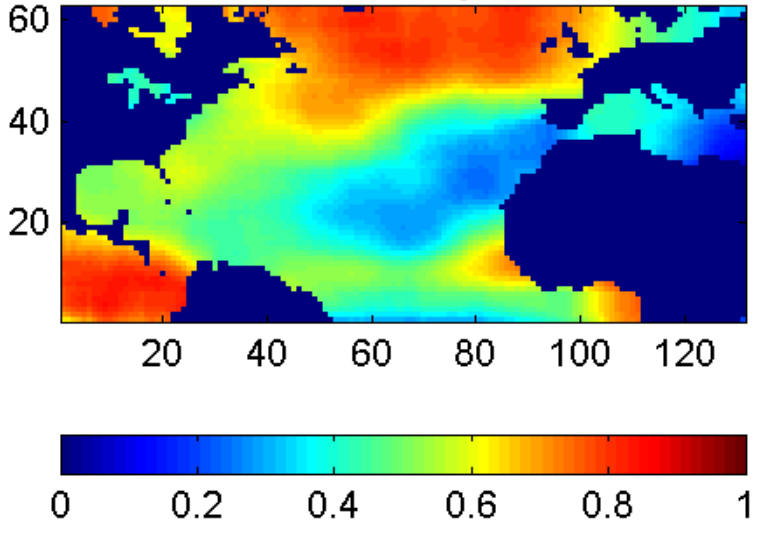

Cloud fraction

clean

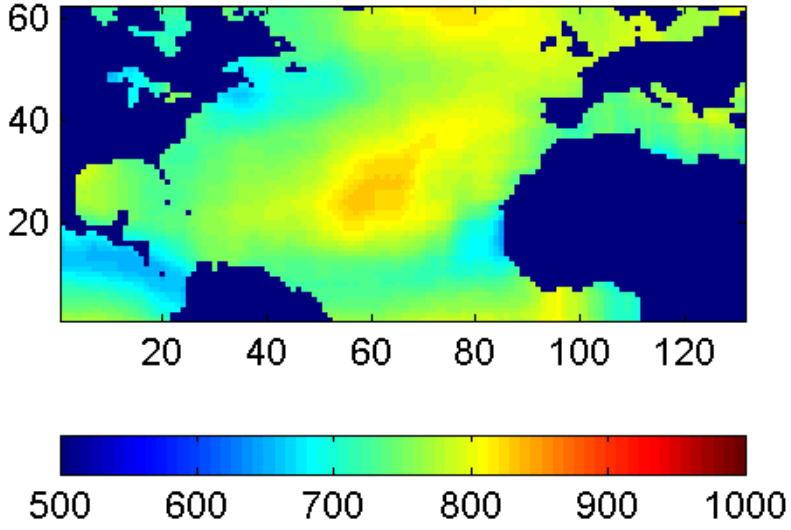

Cloud top pressure

hazy

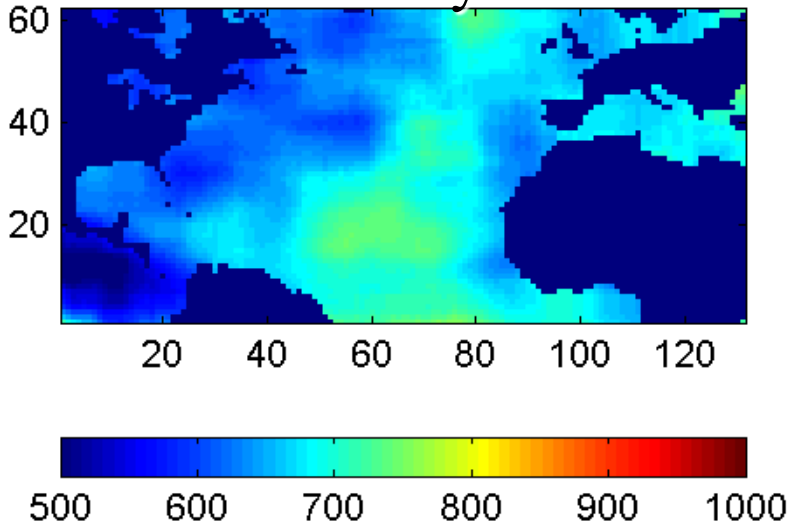

Cloud top pressure

Active Fire Detection

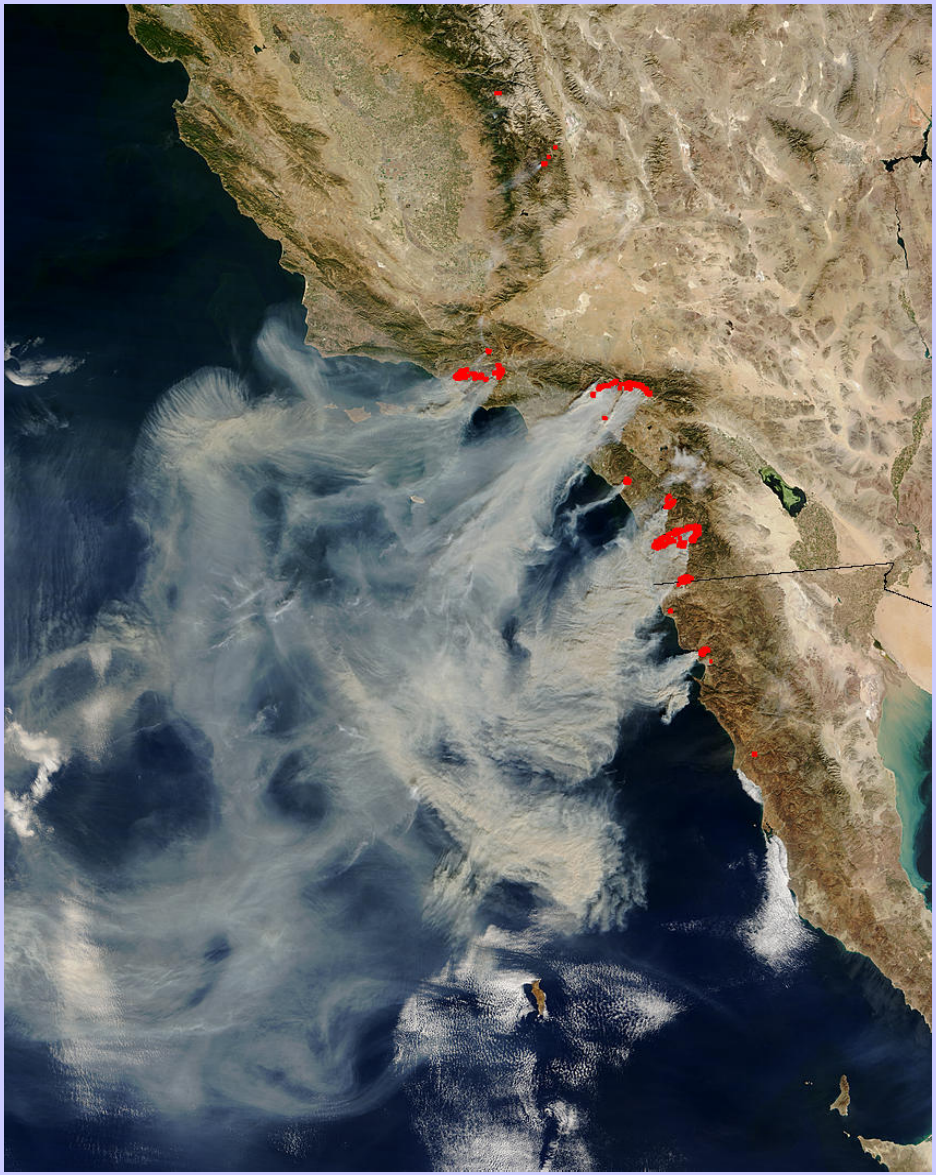

California – 10/26/03

- Same code as the "offical" MOD14 thermal anomalies product
- Contextual algorithm (Giglio et al., 2003)
- The algorithm considers the spectral signature (in middle and thermal infrared) of each pixel and compares it to the non-burning surrounding pixels
- The natural variability of the surrounding background is taken into account
- Fewer false detections than traditional threshold-based algorithms
- Sensitive enough to detect small fires
- Current version: v4.3.2 (March 2003)

Biscuit and Tiller Fires in California and Oregon (08/14/02)

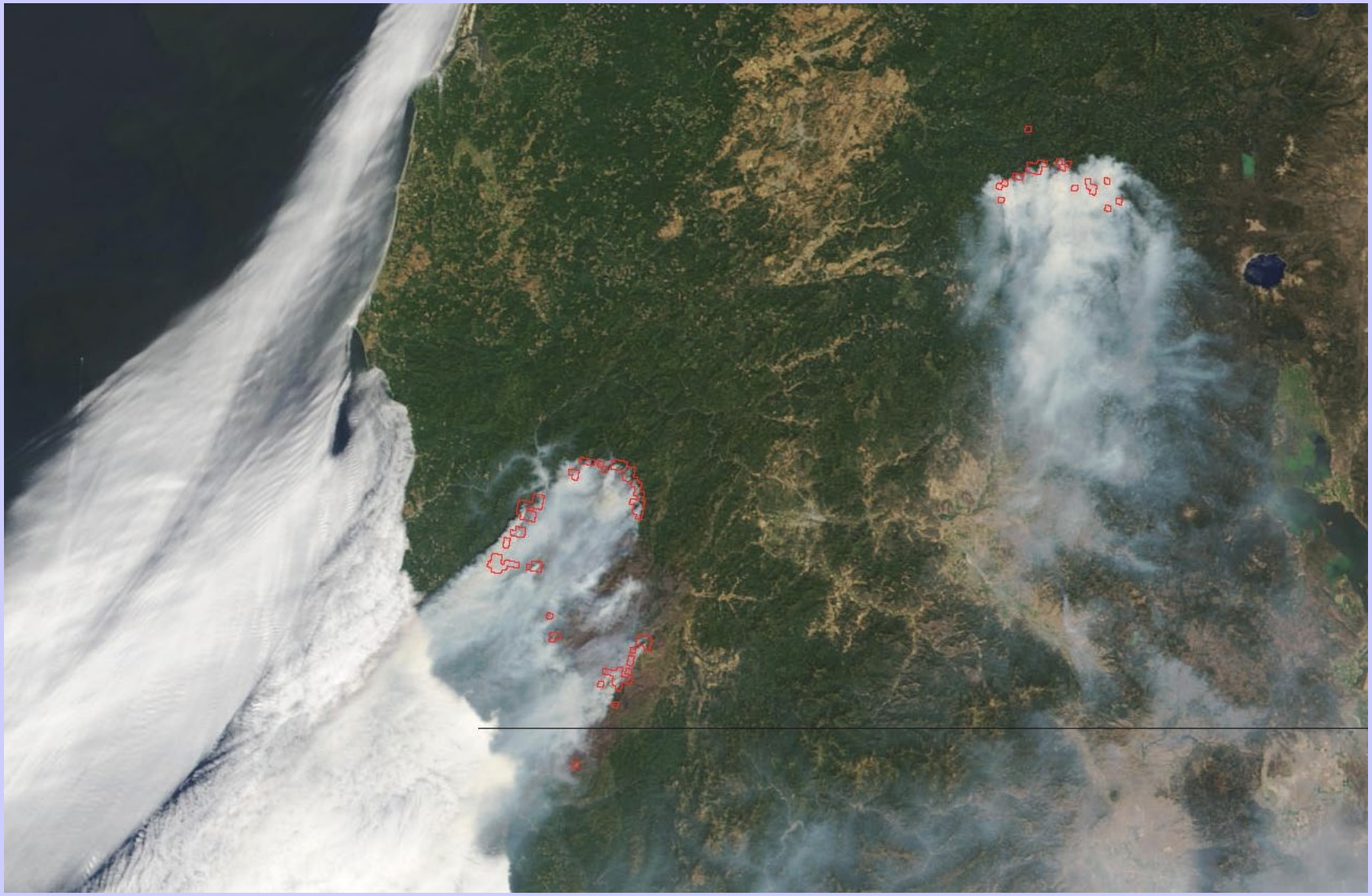

Fire Monitoring: http://rapidfire.sci.gsfc.nasa.gov/realtime

Cooperative Development of Advanced Products

Mapping Burn Severity With MODIS

The Devil Fire Susanville, California May 2001

These MODIS images were obtained shortly after containment of the 4,200 acre Devil Fire on June 3, 2001.

Two models were run on the subset area using Erdas Imagine:

- NDVI (Normalized Difference Vegetation Index)
- NDBR (Normalized Difference Burn Ratio), developed by the USGS.

Unsupervised classifications were then performed on these 2 images as well as on the false color NIR image.

Ground truthing would be required to determine the accuracy of each technique as well as the burned severity of the perimeter area.

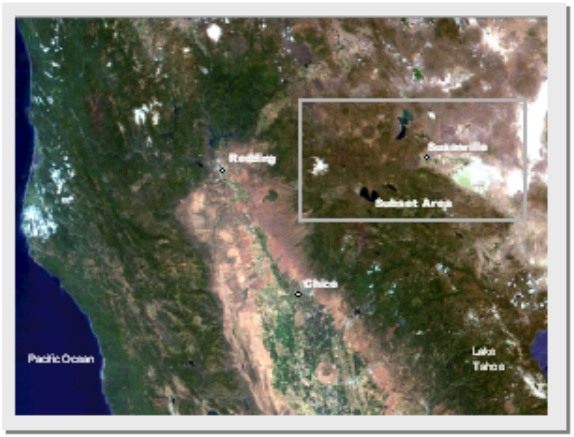

True Color MODIS Image of Northern California June 3, 2001

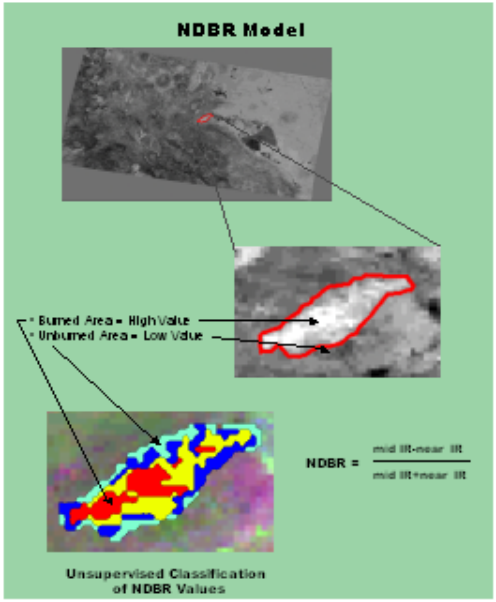

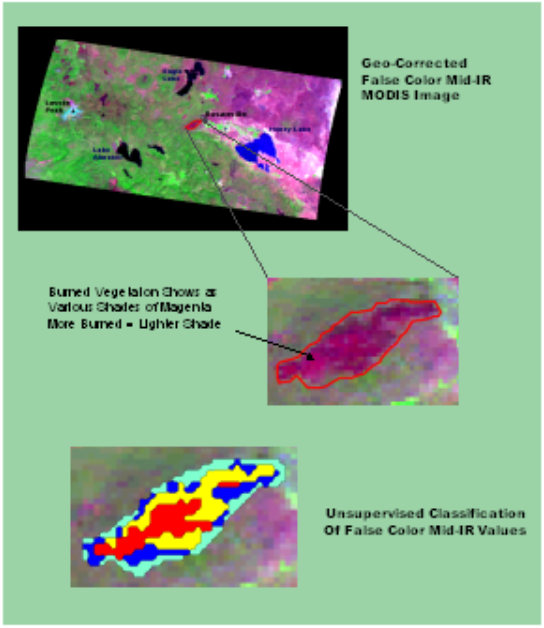

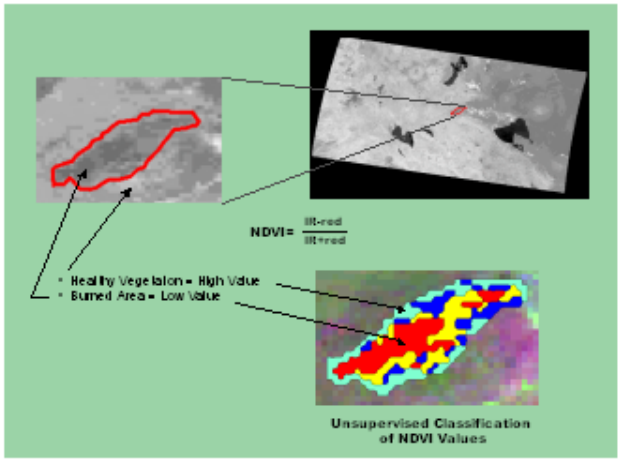

The fire extent and temperature within a field of view can be determined by considering the upwelling thermal radiance values obtained by both channels (Matson and Dozier, 1981; Dozier, 1981). For a given channel, λ, the radiative transfer equation indicates

$$R_\lambda(T) = \varepsilon_\lambda B_\lambda(Ts)\, \tau_\lambda(s) + \int_0^1 B_\lambda(T)\, d\tau_\lambda$$

When the GOES radiometer senses radiance from a pixel containing a target of blackbody temperature T_t occupying a portion p (between zero and one) of the pixel and a background of blackbody temperature T_b occupying the remainder of the pixel (1-p), the following equations represent the radiance sensed by the instrument at 4 and 11 micron.

$$R_4(T_4) = p\, R_4(T_t) + \varepsilon_4\, (1-p)\, R_4\, (T_b) + (1-\varepsilon_4)\, \tau_4(s)\, R_4(solar)$$

$$R_{11}(T_{11}) = p\, R_{11}(T_t) + \varepsilon_{11}\, (1-p)\, R_{11}(T_b)$$

The observed short wave window radiance also contains contributions due to solar reflection that must be distinguished from the ground emitted radiances; solar reflection is estimated from differences in background temperatures in the 4 and 11 micron channels. Once T_b is estimated from nearby pixels, these two nonlinear equations can be solved for T_t and p. In this study, the solution to the set of equations is found by applying a globally convergent bisection technique followed by Newton's method.

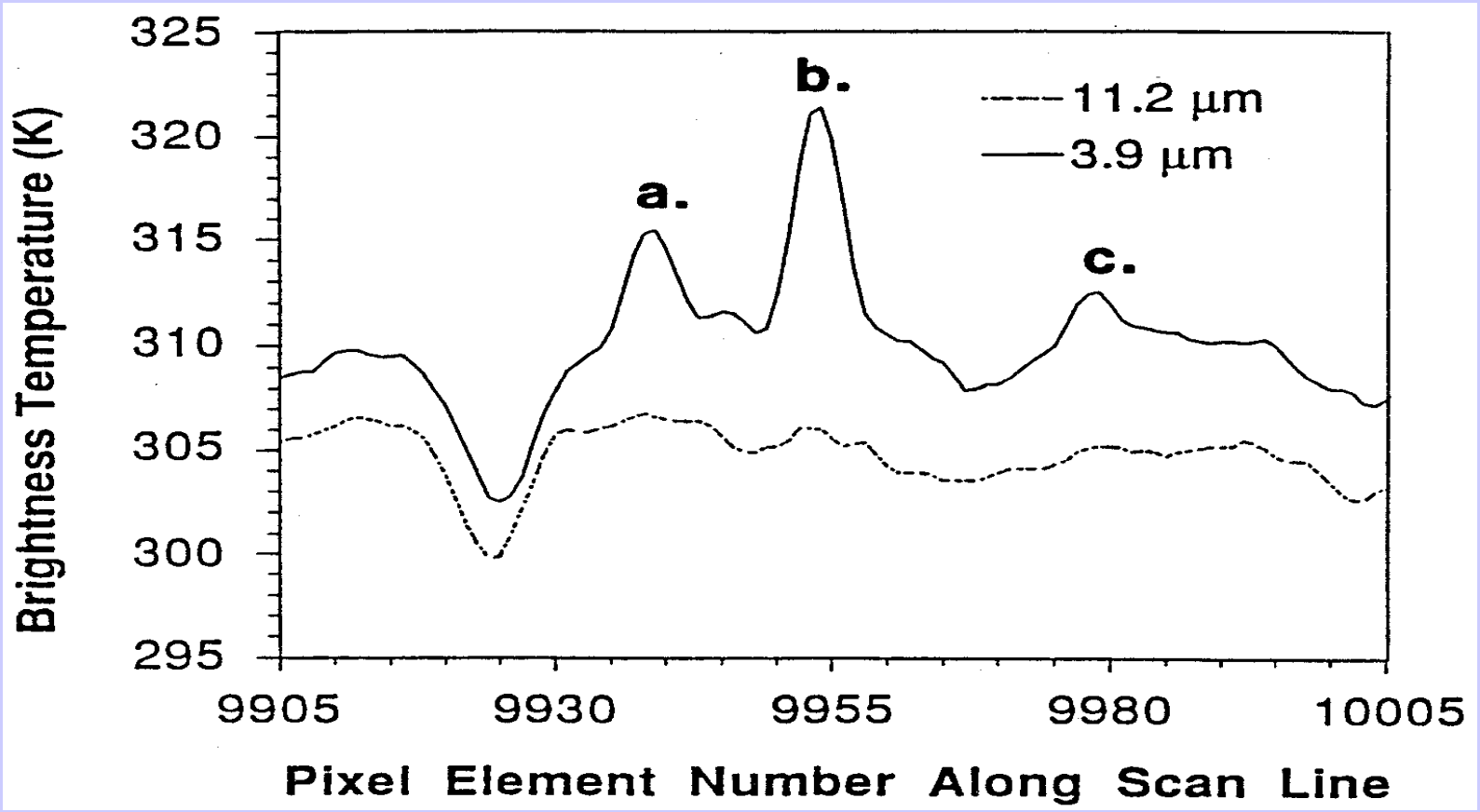

3.9 and 11.2 microns plotted for one scan line over grassland burning in South America; fires are likely at a, b, and c.

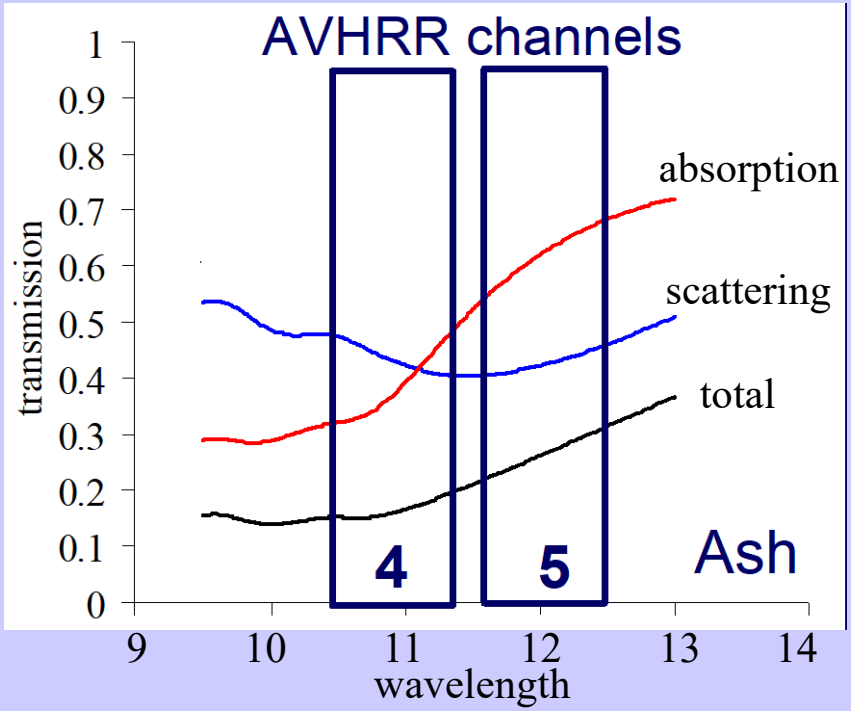

Investigating with Multi-spectral Combinations

Given the spectral response of a surface or atmospheric feature

Select a part of the spectrum where the reflectance or absorption changes with wavelength

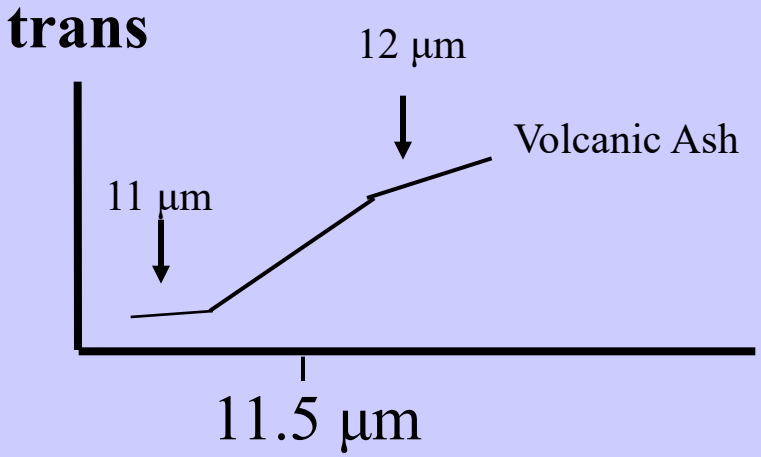

e.g. transmission through ash

If 11 μm sees the same or higher BT than 12 μm the atmosphere viewed does not contain volcanic ash; if 12 μm sees considerably higher BT than 11 μm then the atmosphere probably contains volcanic ash

Ash Plume Detection

Mt. Cleveland Eruption 19 Feb 2001

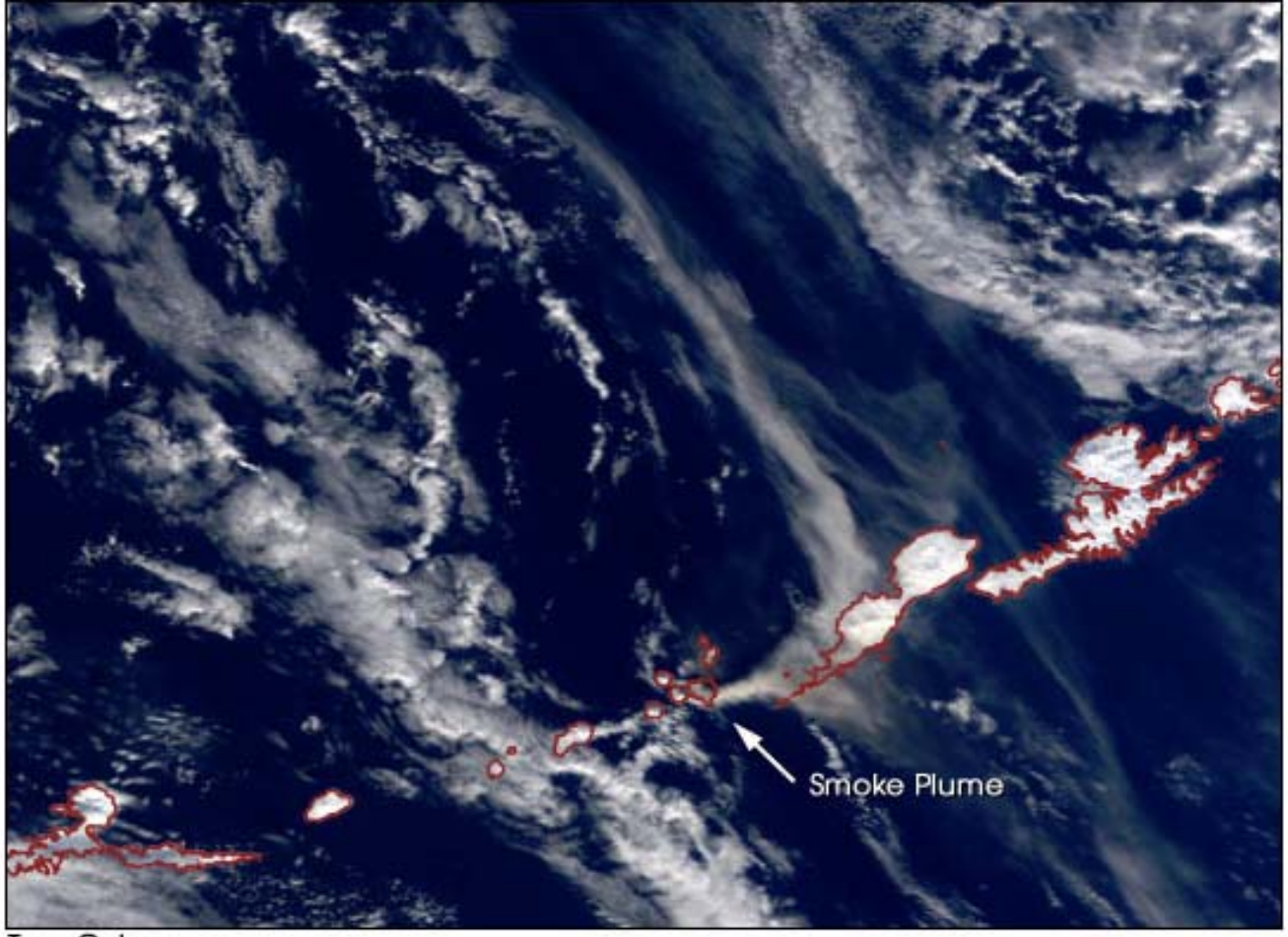

True Color

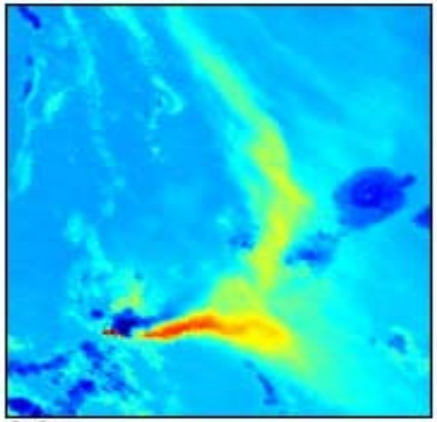

3.9μm

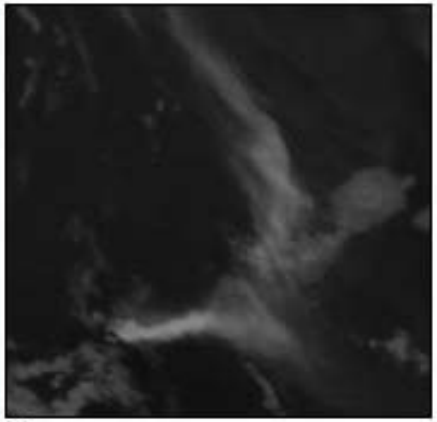

11μm

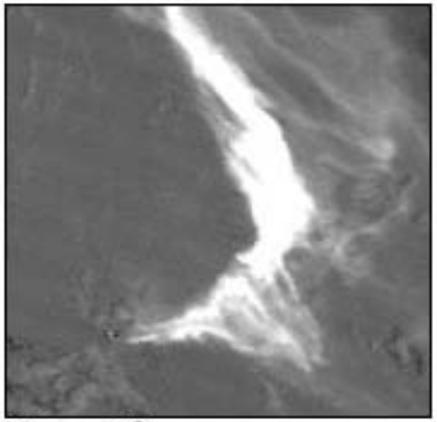

11μm - 12μm

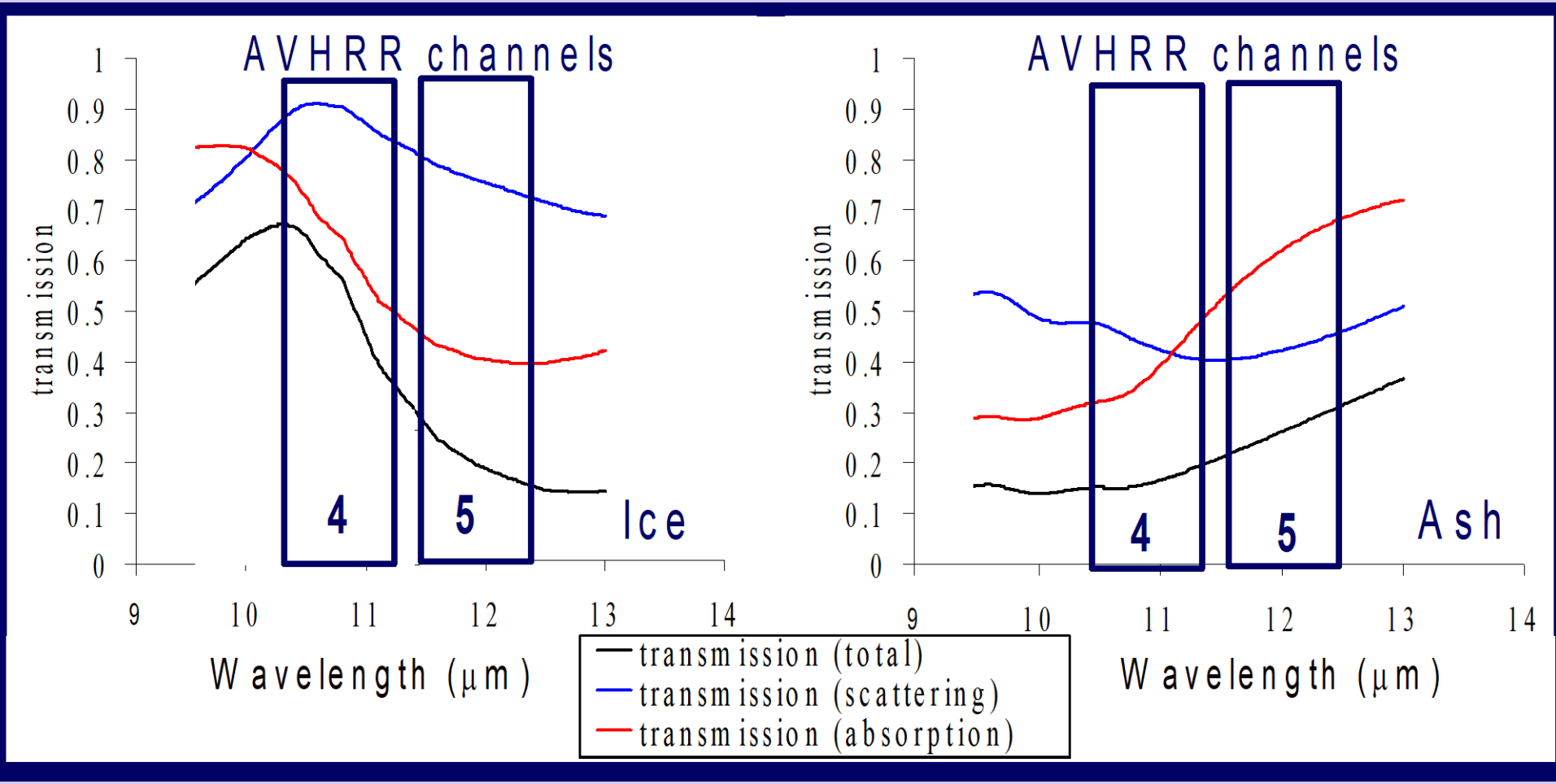

BT11-BT12 > 0 for ice
BT11-BT12 < 0 for volcanic ash

Frank Honey 1980s

MODIS detects ship tracks

Ship Tracks occur in marine stratocumulus regions of the globe

- California, Azores, Namibia, and Peru

Conditions for formation

- High humidity
- Small air-sea temperature difference
- Low wind speed
- Boundary layer between 300 and 750 m deep

Enhanced reflectance of clouds at 3.7 μm

- Larger number of small droplets arising from particulate emission from ships

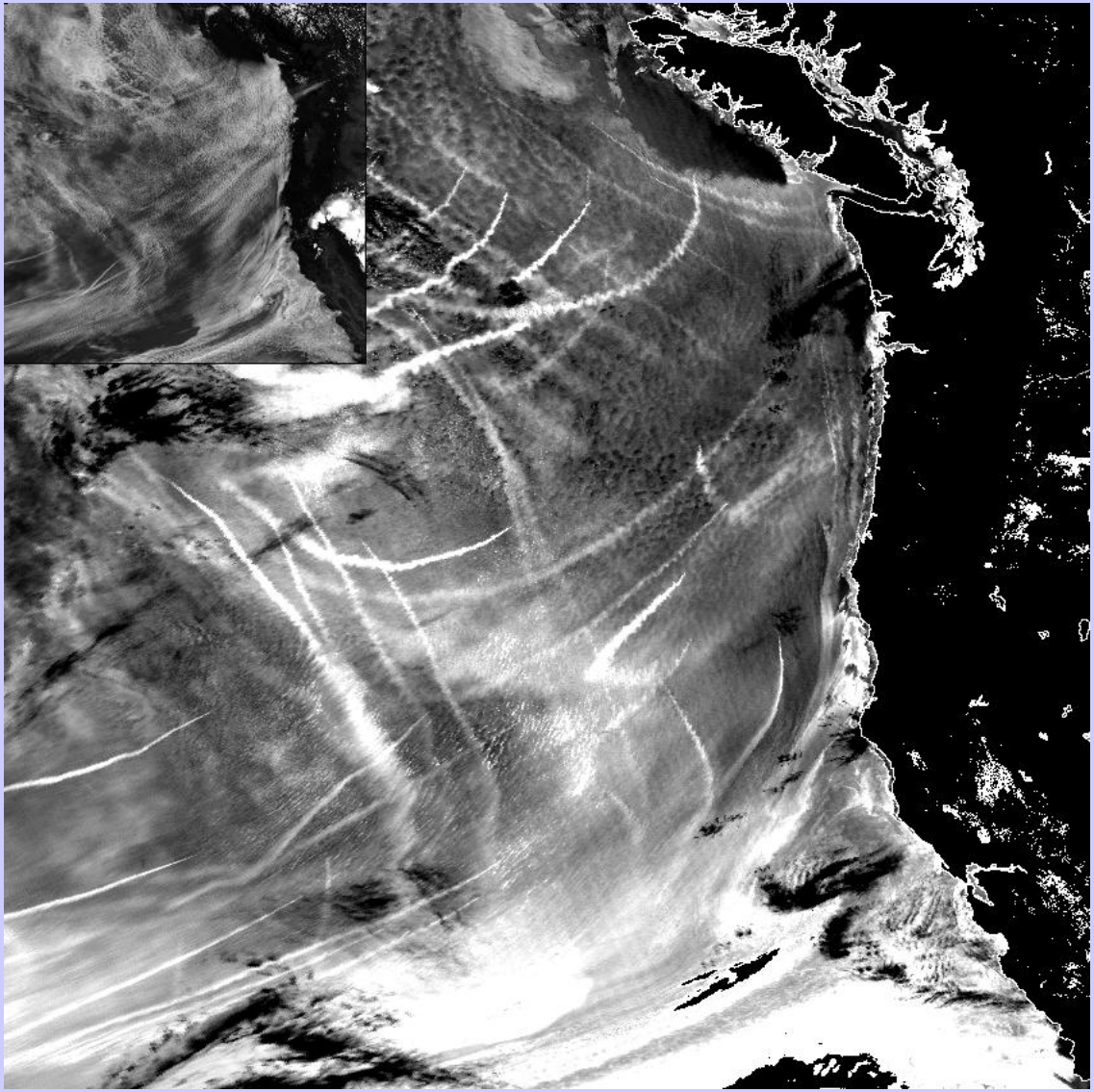

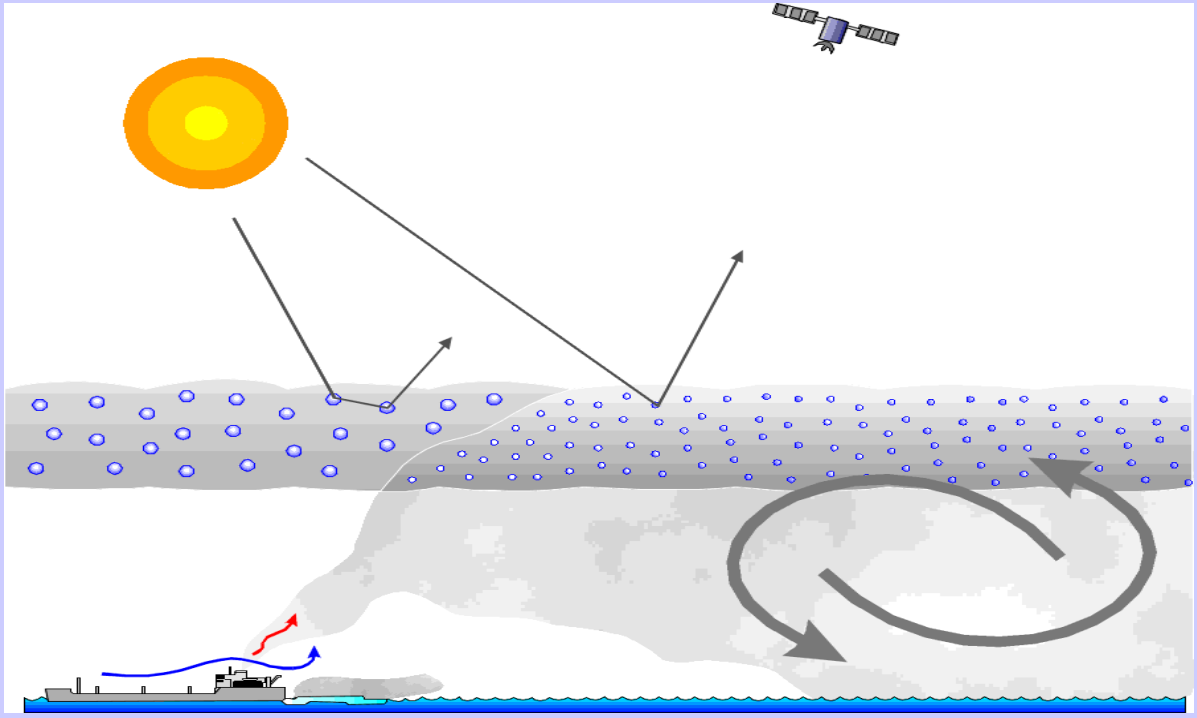

* Particles emitted by ships increase concentration of cloud condensation nuclei (CCN) in the air
* Increased CCN increase concentration of cloud droplets and reduce average size of the droplets
* Increased concentration and smaller particles reduce production of drizzle (100 μm radius) droplets in clouds
* Liquid water content increases because loss of drizzle particles is suppressed
* Clouds are *optically thicker* and brighter along ship track

Ship tracks off France (01/27/03)

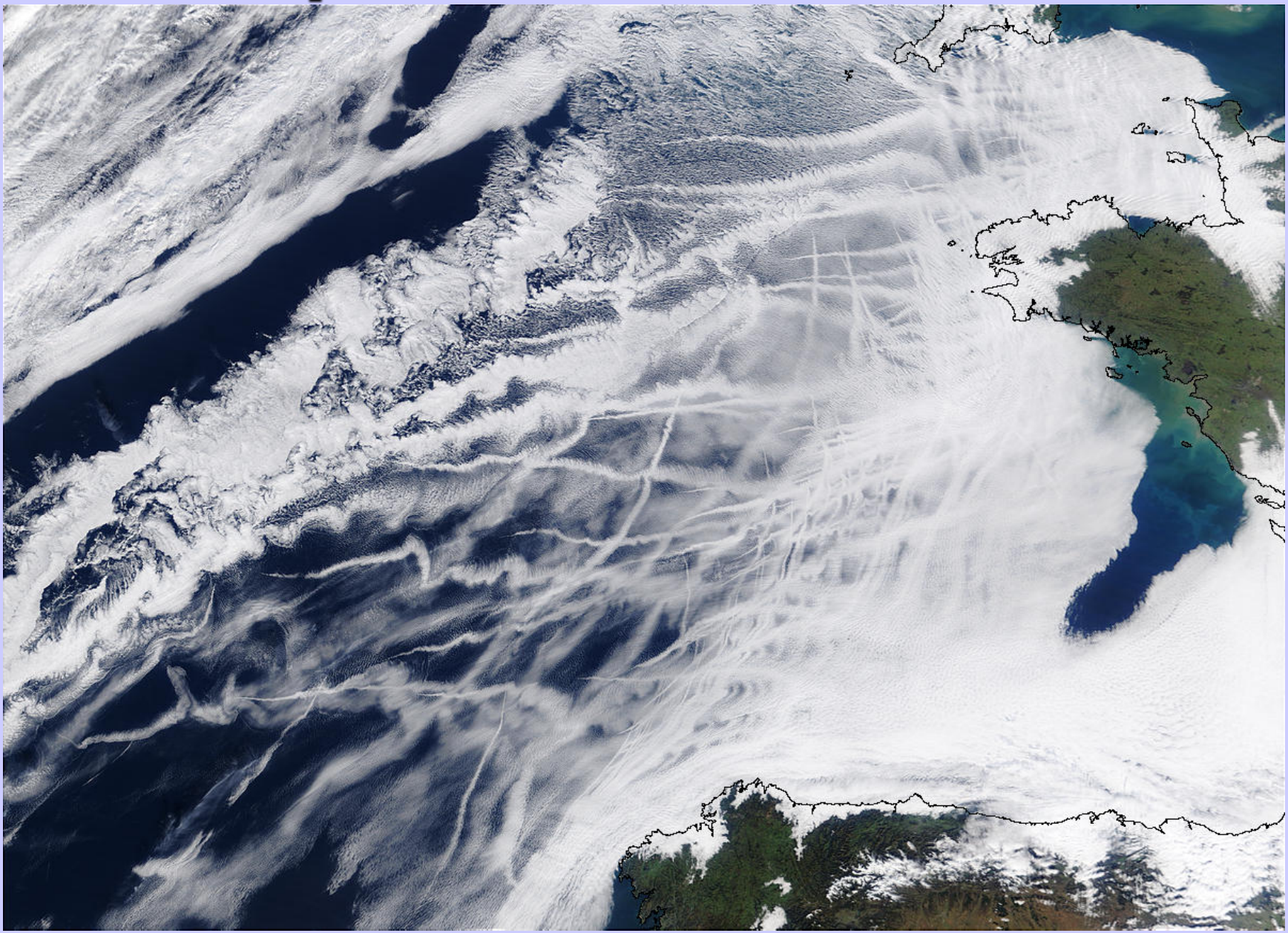

Application Opportunities with Multispectral Remote Sensing Data

Satellite Remote Sensing
Energy Balance
VIS, IR, and MW Radiative Transfer
EOS Terra & Aqua MODIS
Multispectral Applications
(Ocean Color, Snow/Ice, Vegetation, Aerosols, Fires, Volcanic Ash, Clouds, Moisture)
Detecting Climate Trends

Relevant Material in Applications of Meteorological Satellites

ATMOSPHERE-SOLAR RADIATION

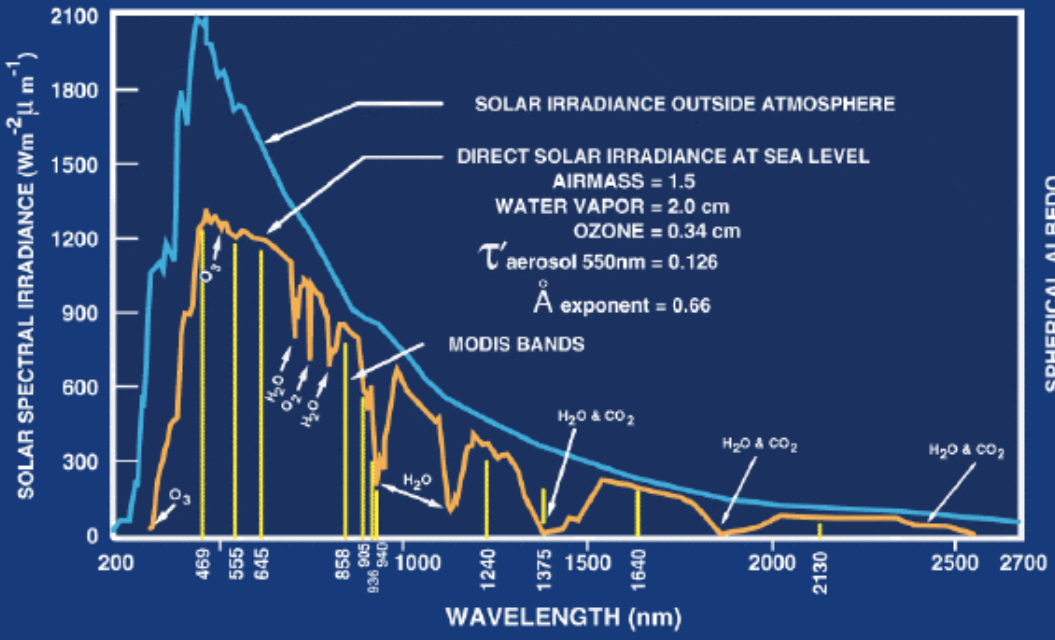

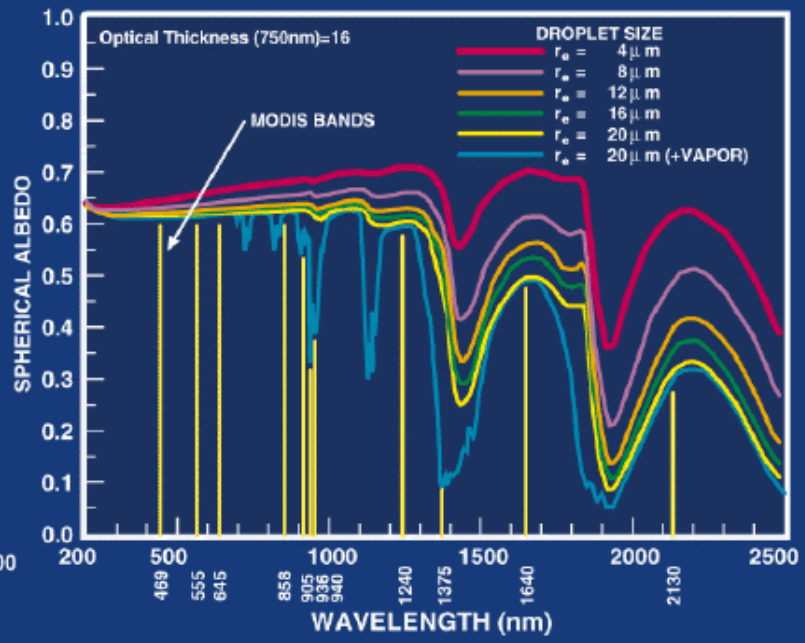

ATMOSPHERE - CLEAR SKY
THERMAL EMISSION

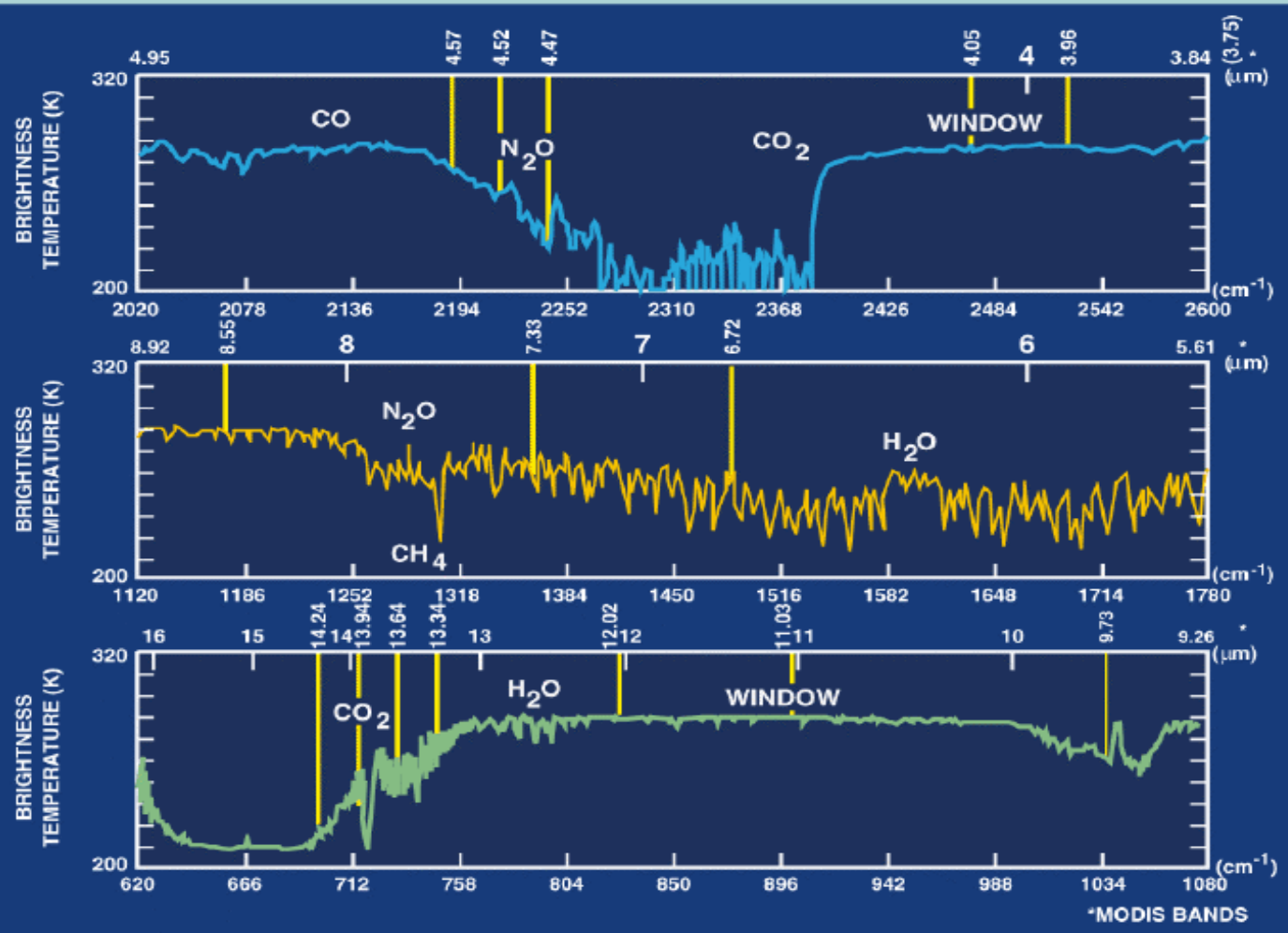

002 11/92

ATMOSPHERE - THERMAL RADIATION

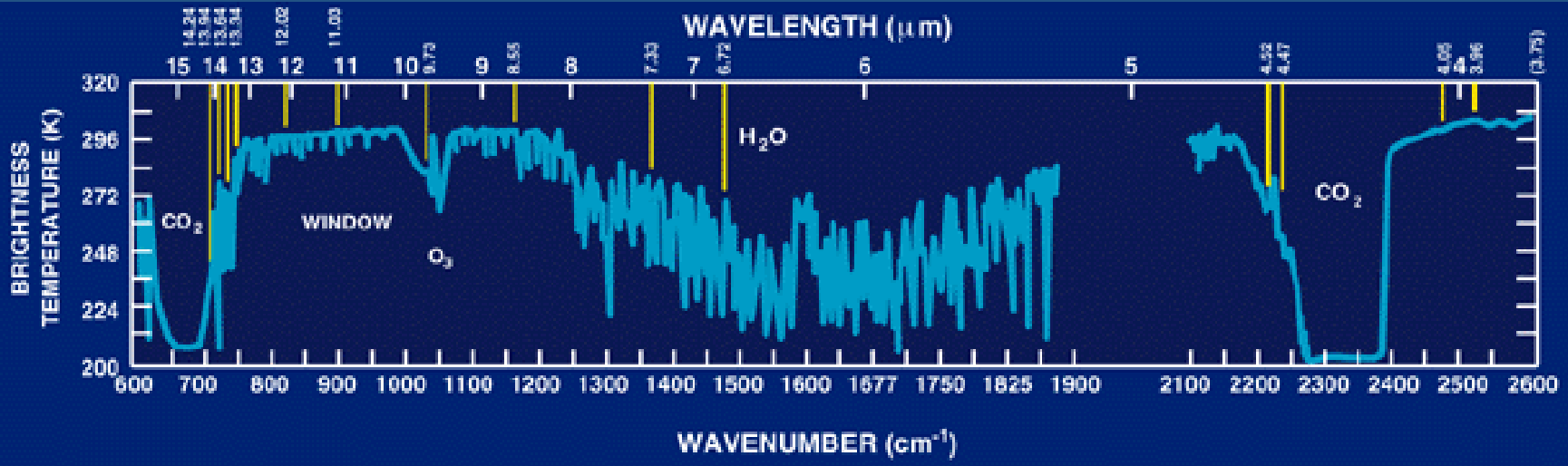

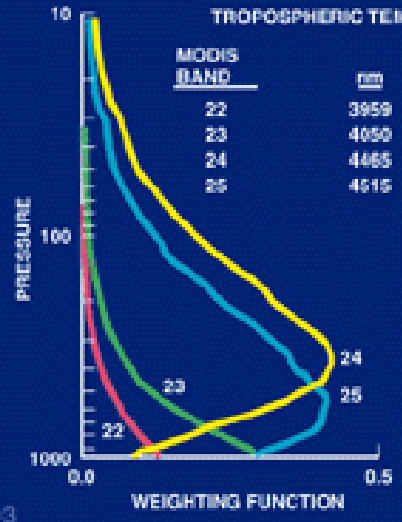

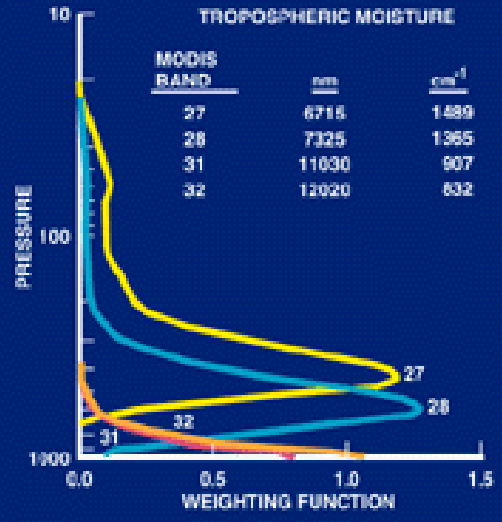

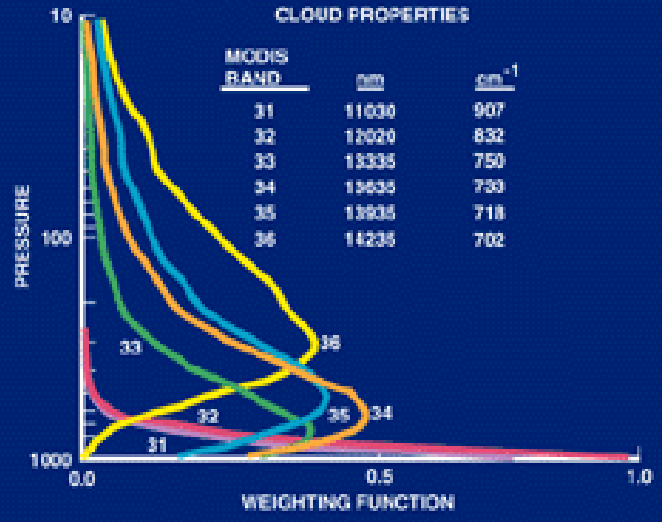

E351.002 5/93

Optical properties of cloud particles: imaginary part of refraction index

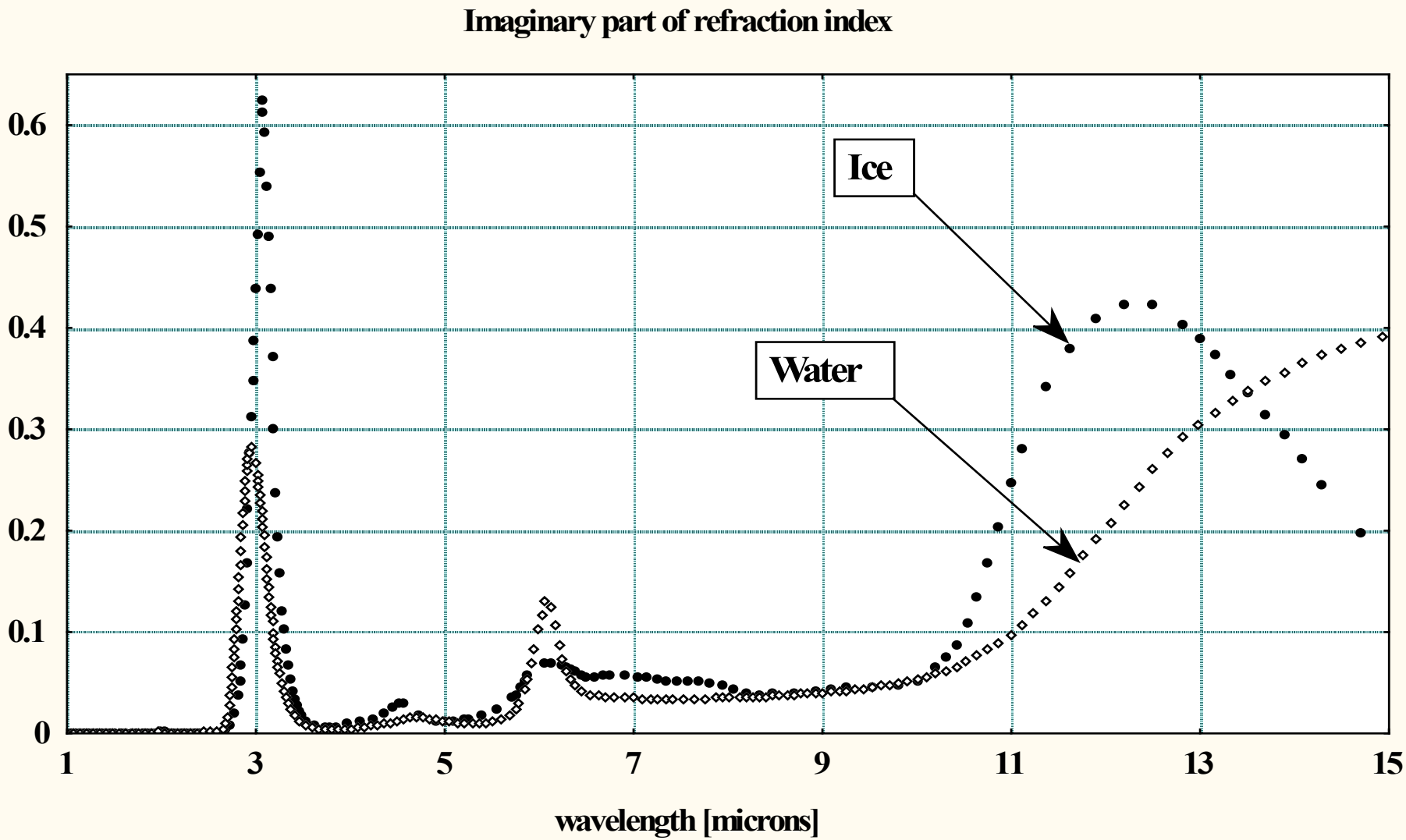

BT[8.6] – BT[11] will be positive for ice clouds

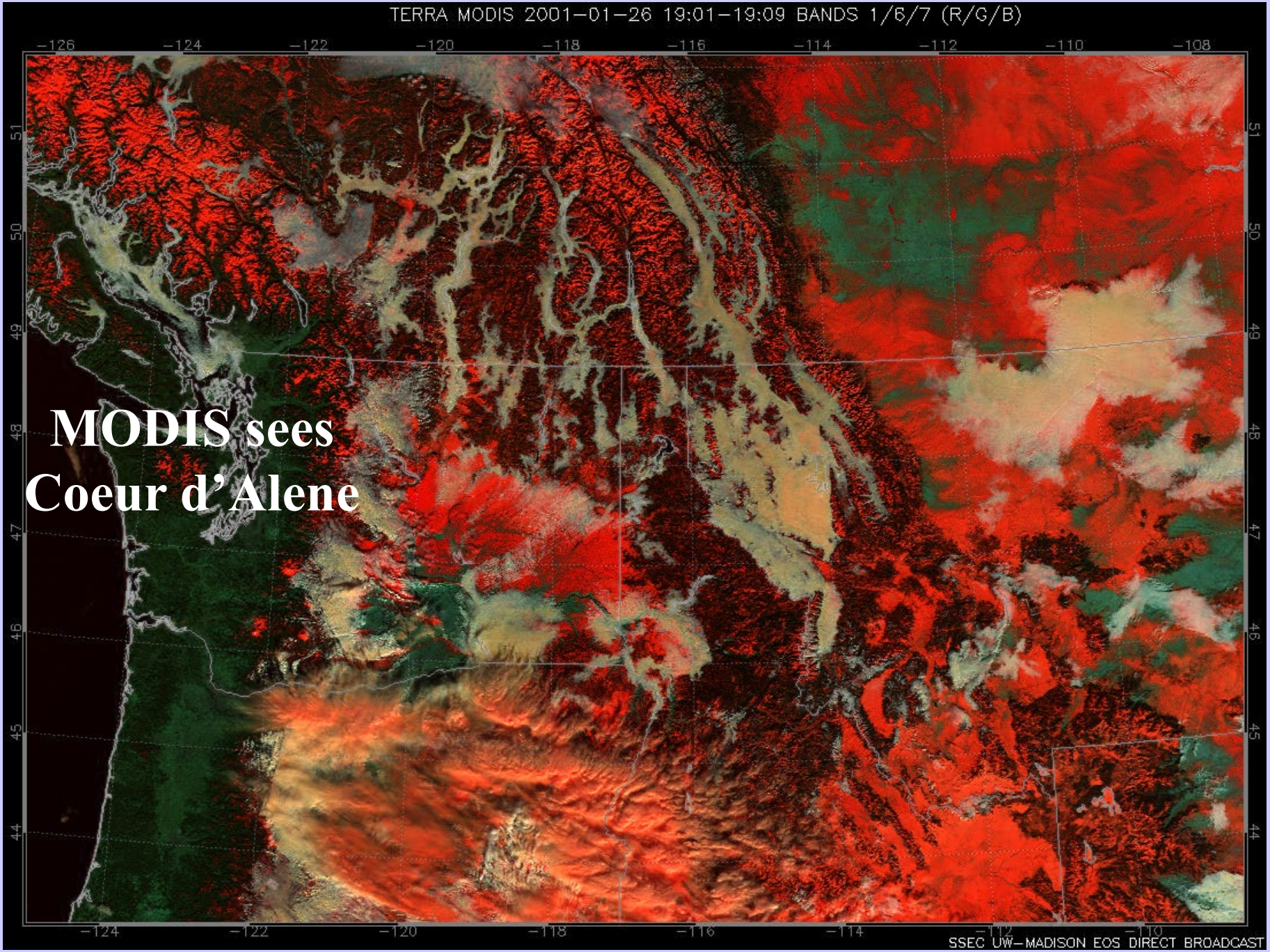
TERRA MODIS 2001-01-26 19:01-19:09 BANDS 1/6/7 (R/G/B)
-126
-124
-122
-120
-118
-116
-114
-112
-110
-108
51
50
49
48
47
46
45
44
MODIS sees
Coeur d'Alene
SSEC UW-MADISON EOS DIRECT BROADCAST

MODIS identifies cloud classes

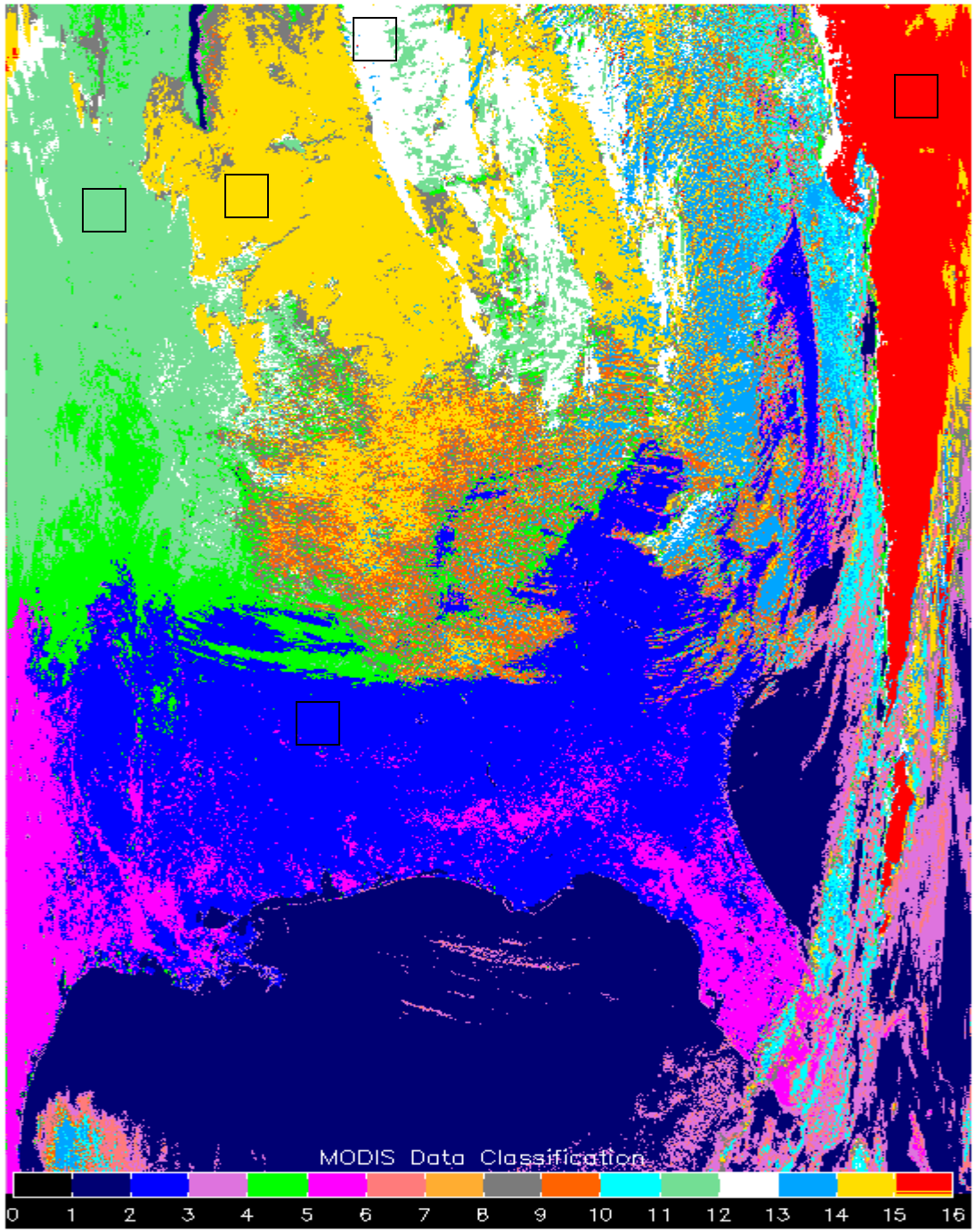

Hi cld

Mid cld

Lo cld

Snow

clr

Clouds separate into classes when multispectral radiance information is viewed

vis

LSD 1.6 um

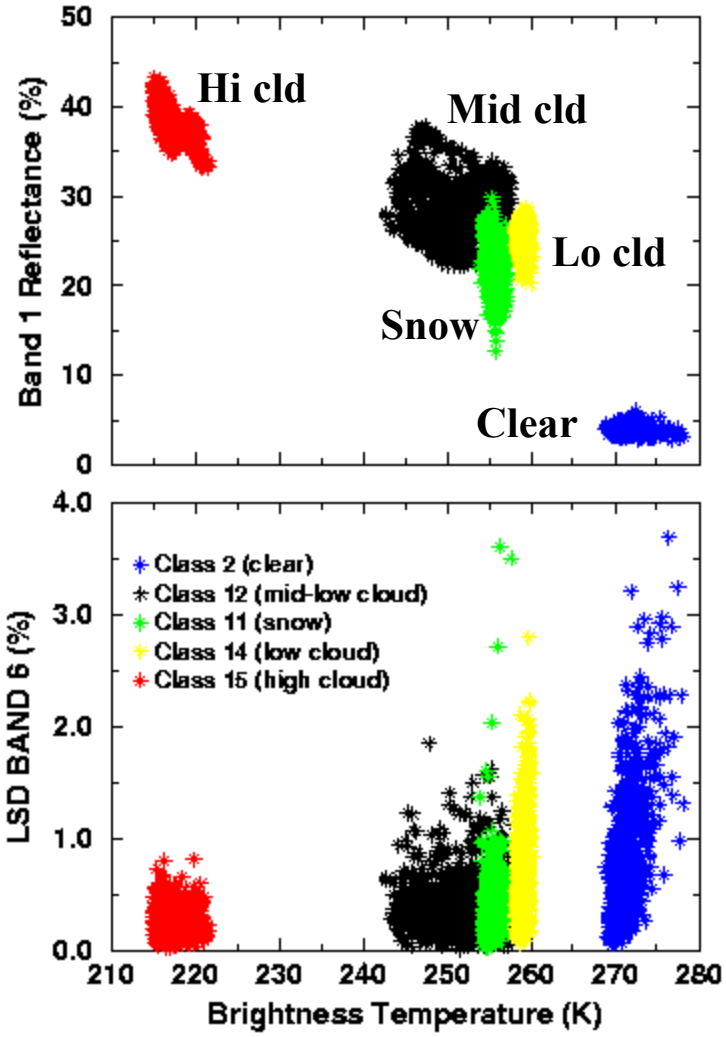

11 um

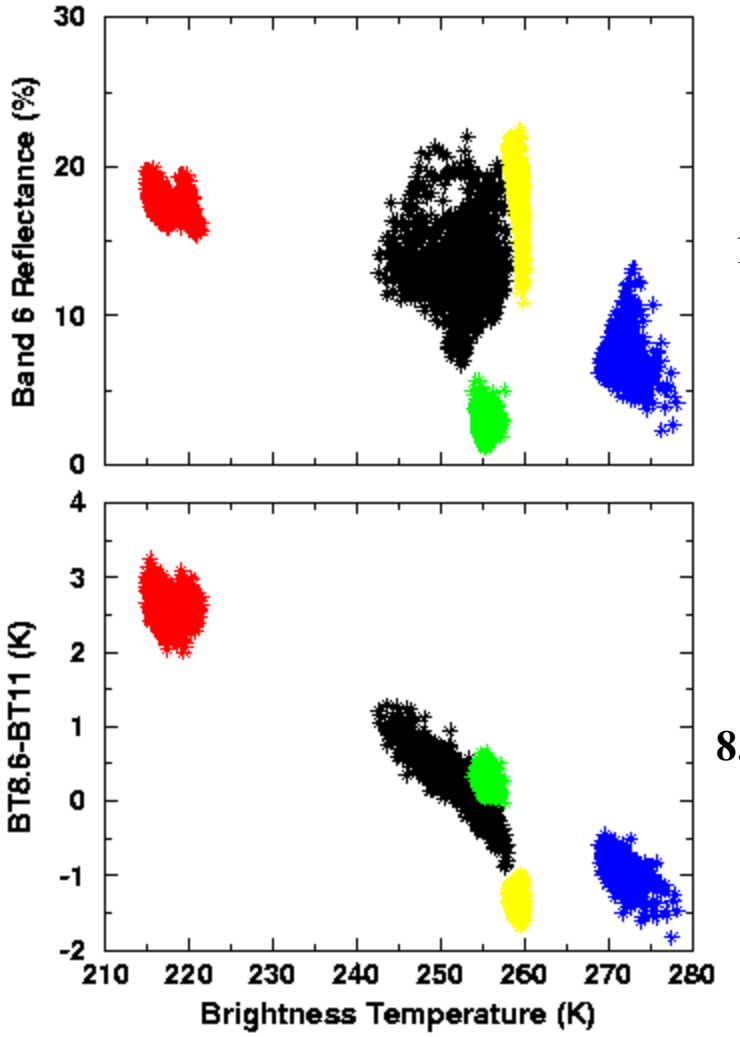

1.6 um

8.6-11 um

11 um

Cloud Properties

True Color Image
Cloud Mask
Land Classification
Cloud Opt Thickness
Cloud Eff Radius
Cloud Top Temp
Bispectral Phase

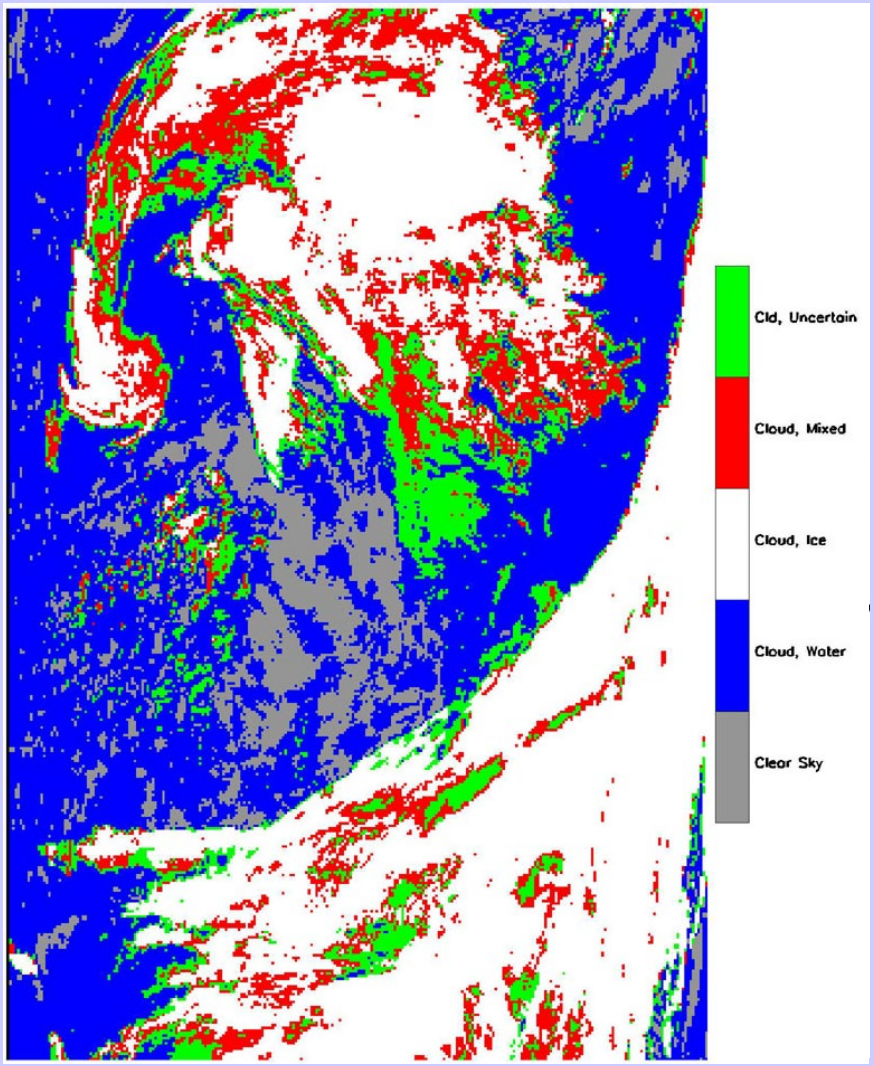

October 1, 2001

Cloud optical, microphysical properties

retrieval space example

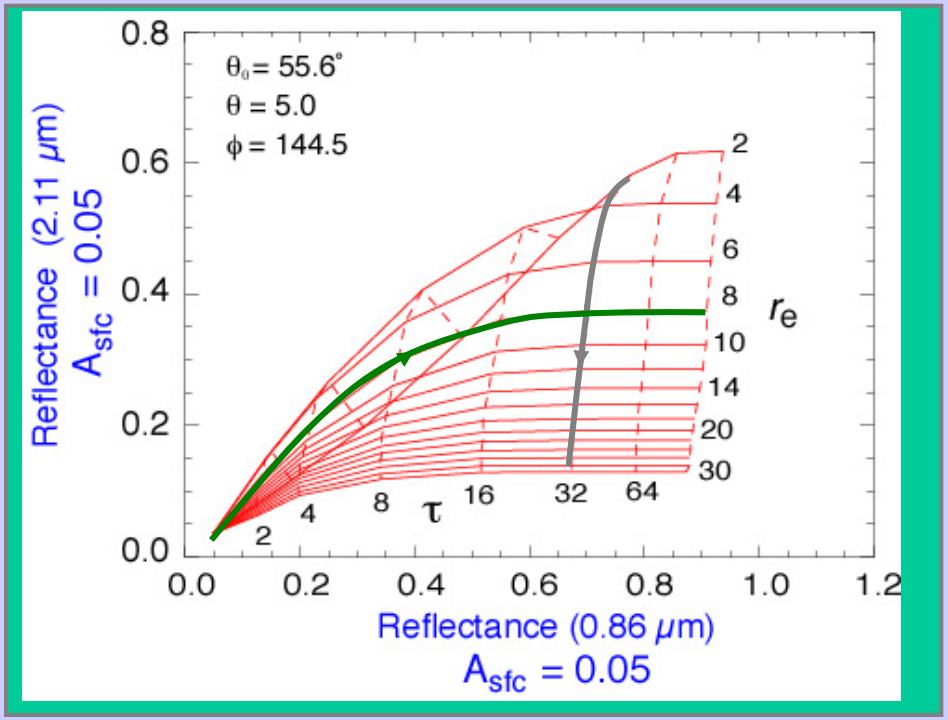

2.1 μm absorption increases with particle size, little effect at 0.86 μm

2.1 μm reflectance reaches limiting values with optical thickness

Liquid water cloud
ocean surface

Radiance from a partly cloudy FOV

Cloud Parameter Determinations from Satellite Measured Radiances
for a given field of view (FOV) partly clear and partly cloudy

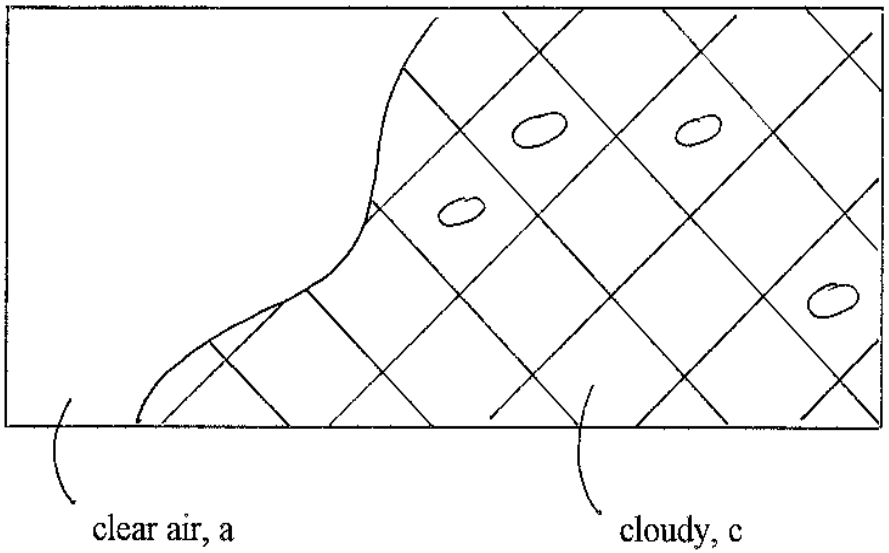

$$R = [1 - N] R_a + N R_c$$

but if b indicates opaque "black" cloud

$$R_c = [1 - \varepsilon] R_a + \varepsilon R_b(p_c)$$

so together

$$R = [1 - N\varepsilon] R_a + N\varepsilon R_b(p_c)$$

Two unknowns, ε and Pc, require two measurements

RTE in Cloudy Conditions

$$I_\lambda = \eta I^{cd}_\lambda + (1 - \eta) I^{clr}_\lambda \quad \text{where cd = cloud, clr = clear, } \eta \text{ = cloud fraction}$$

$$I^{clr}_\lambda = B_\lambda(T_s)\, \tau_\lambda(p_s) + \int_{p_s}^{o} B_\lambda(T(p))\, d\tau_\lambda \, .$$

$$I^{cd}_\lambda = (1-\varepsilon_\lambda)\, B_\lambda(T_s)\, \tau_\lambda(p_s) + (1-\varepsilon_\lambda) \int_{p_s}^{p_c} B_\lambda(T(p))\, d\tau_\lambda$$

$$+ \varepsilon_\lambda\, B_\lambda(T(p_c))\, \tau_\lambda(p_c) + \int_{p_c}^{o} B_\lambda(T(p))\, d\tau_\lambda$$

ε_λ is emittance of cloud. First two terms are from below cloud, third term is cloud contribution, and fourth term is from above cloud. After rearranging

$$I_\lambda - I_\lambda^{clr} = \eta\varepsilon_\lambda \int_{p_s}^{p_c} \tau(p)\, \frac{dB_\lambda}{dp}\, dp \, .$$

CO2 channels see to different levels in the atmosphere

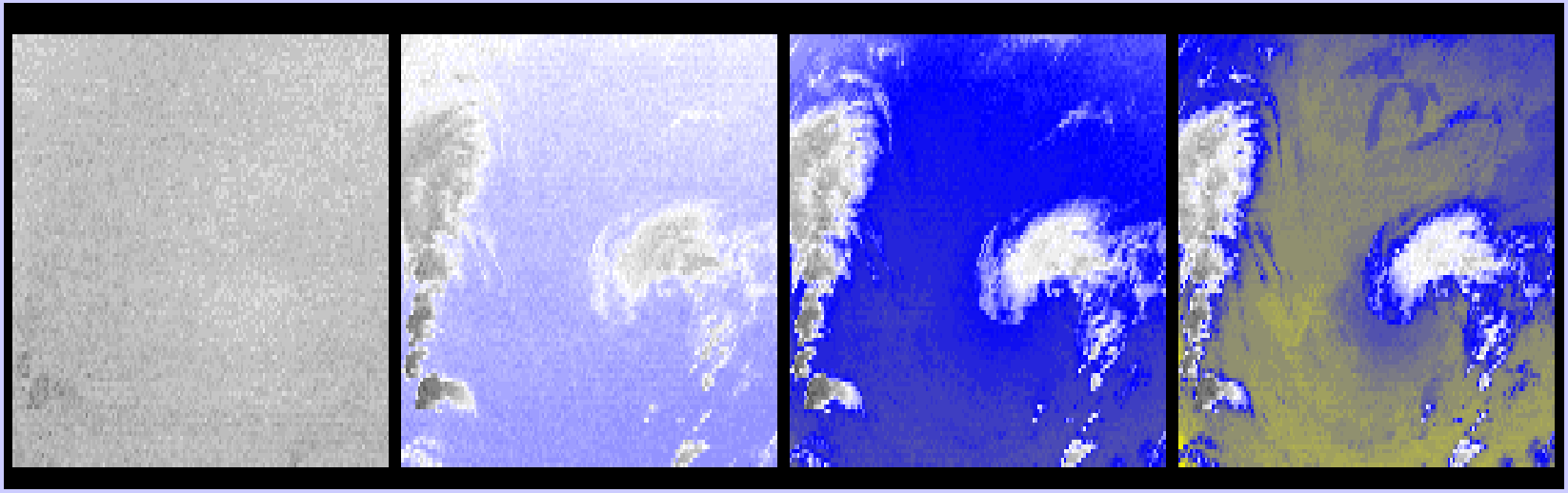

14.2 um 13.9 um 13.6 um 13.3 um

Cloud Properties from CO2 Slicing

RTE for cloudy conditions indicates dependence of cloud forcing (observed minus clear sky radiance) on cloud amount ($\eta\varepsilon_\lambda$) and cloud top pressure (p_c)

$$(I_\lambda - I_\lambda^{clr}) = \eta\varepsilon_\lambda \int_{p_s}^{p_c} \tau_\lambda \, dB_\lambda \, .$$

Higher colder cloud or greater cloud amount produces greater cloud forcing; dense low cloud can be confused for high thin cloud. Two unknowns require two equations.

p_c can be inferred from radiance measurements in two spectral bands where cloud emissivity is the same. $\eta\varepsilon_\lambda$ is derived from the infrared window, once p_c is known.

Different ratios reveal cloud properties at different levels

hi - 14.2/13.9
mid - 13.9/13.6
low - 13.6/13.3

Meas **Calc**

$$\frac{(I_{\lambda 1}-I_{\lambda 1}^{clr})}{(I_{\lambda 2}-I_{\lambda 2}^{clr})} = \frac{\eta\varepsilon_{\lambda 1}\int_{p_s}^{p_c}\tau_{\lambda 1}\,dB_{\lambda 1}}{\eta\varepsilon_{\lambda 2}\int_{p_s}^{p_c}\tau_{\lambda 2}\,dB_{\lambda 2}}$$

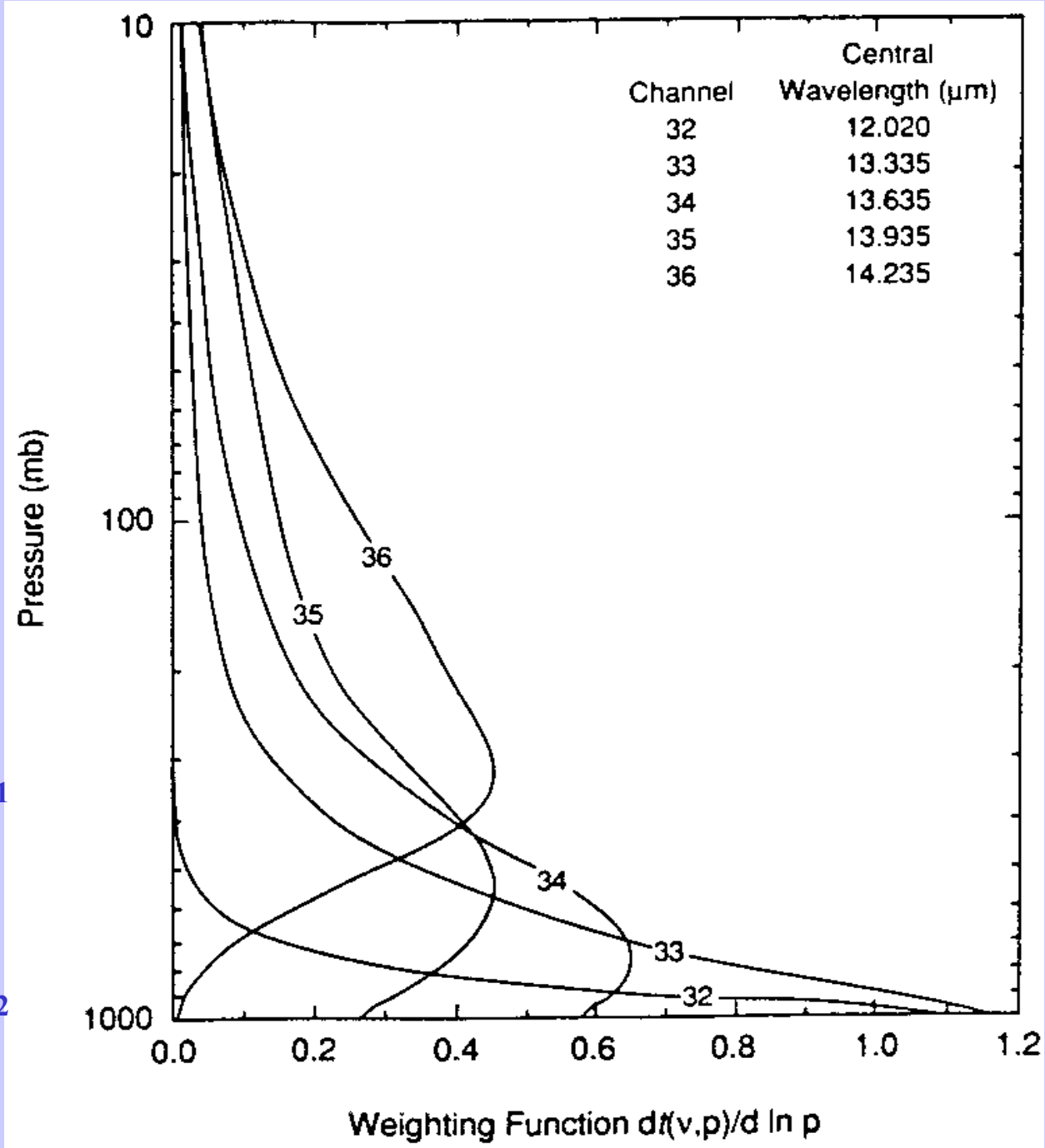

BTs in and out of clouds for MODIS CO_2 bands

demonstrate weighting functions and cloud top algorithm

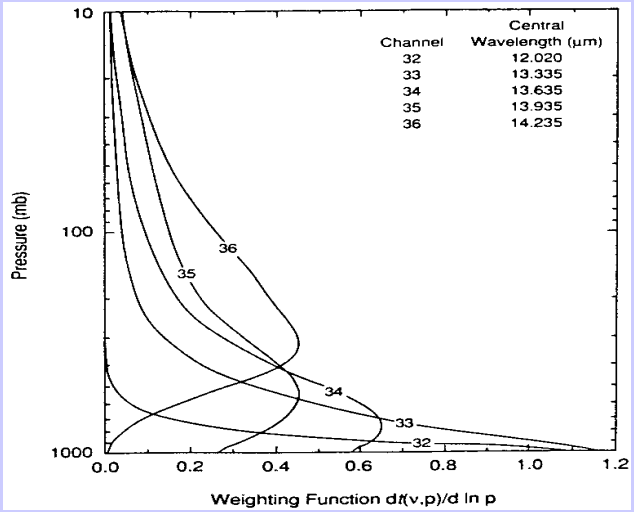

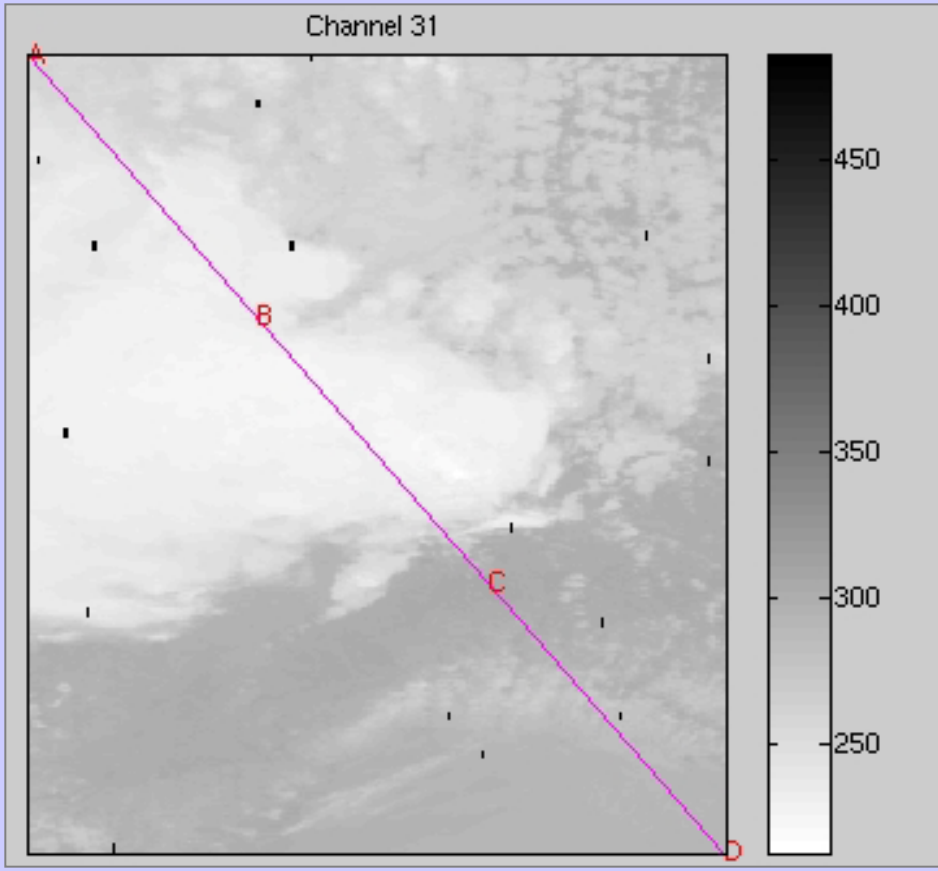

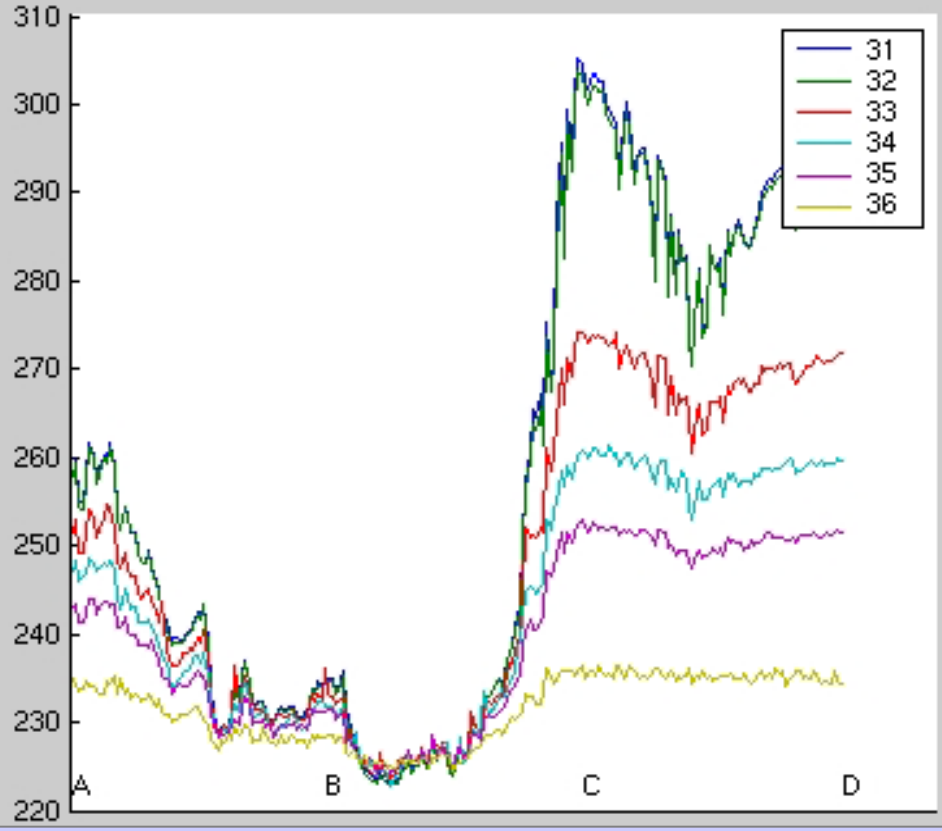

AQUA/MODIS BAND1 2300UTC 8/24/02

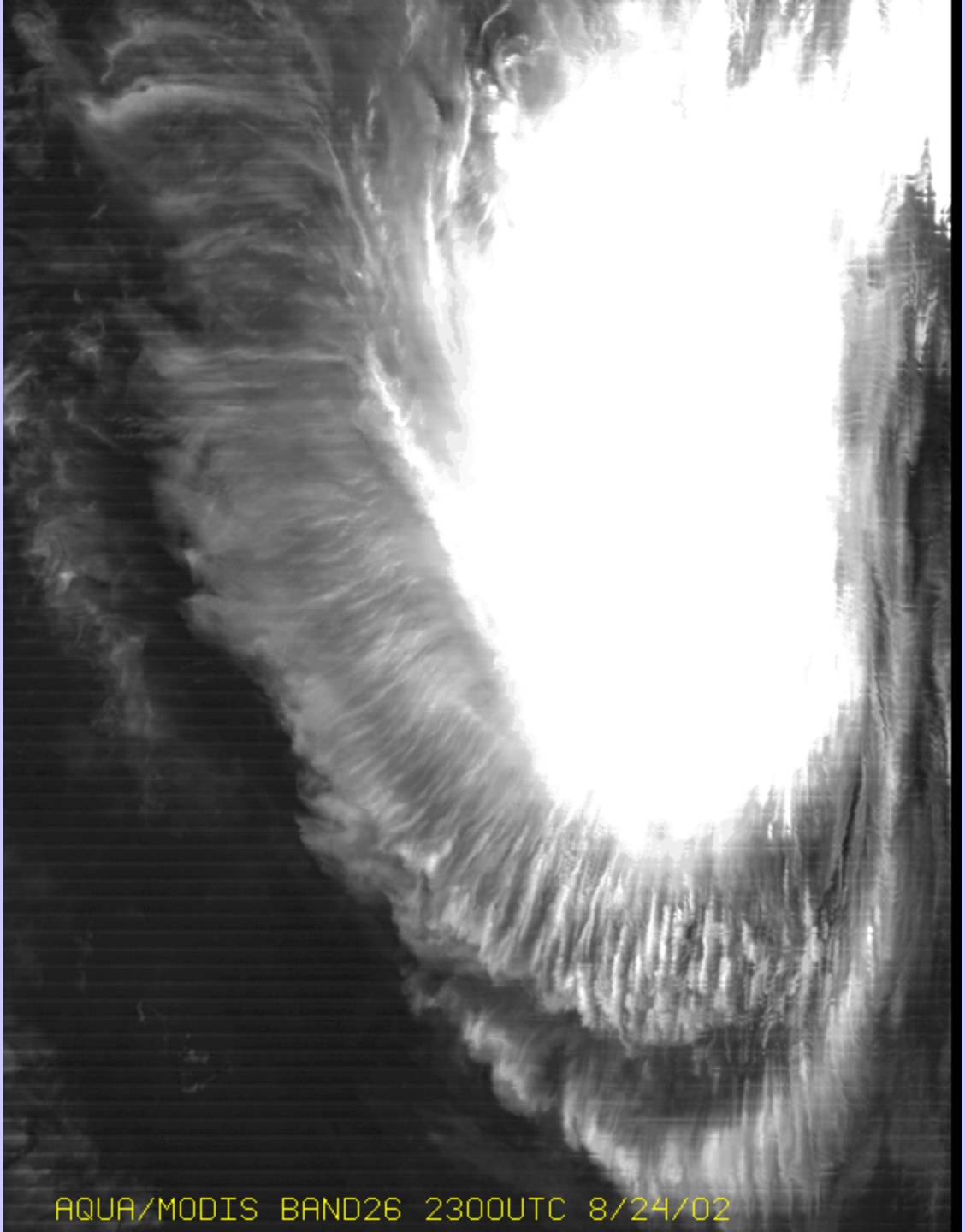
AQUA/MODIS BAND26 2300UTC 8/24/02

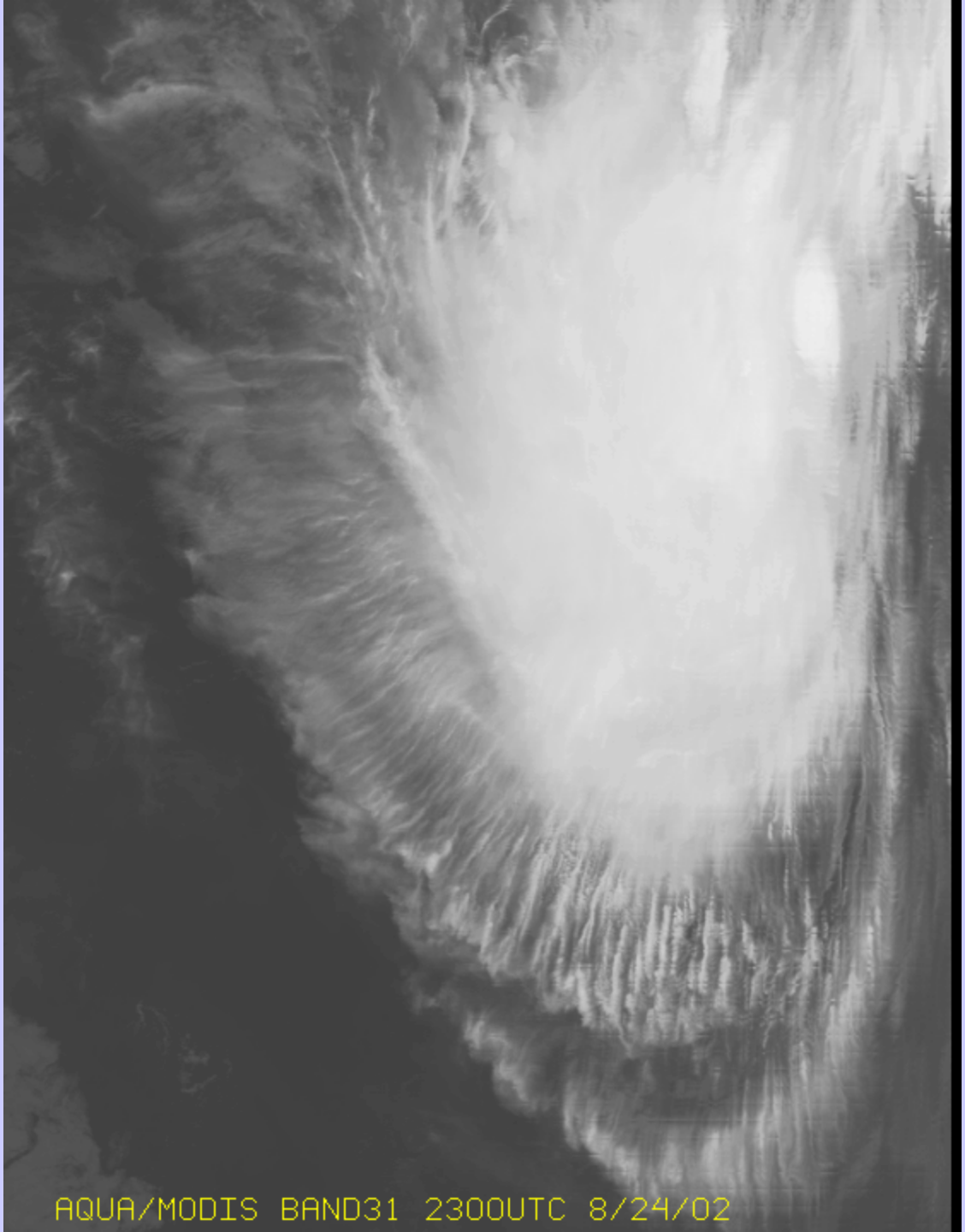
AQUA/MODIS BAND31 2300UTC 8/24/02

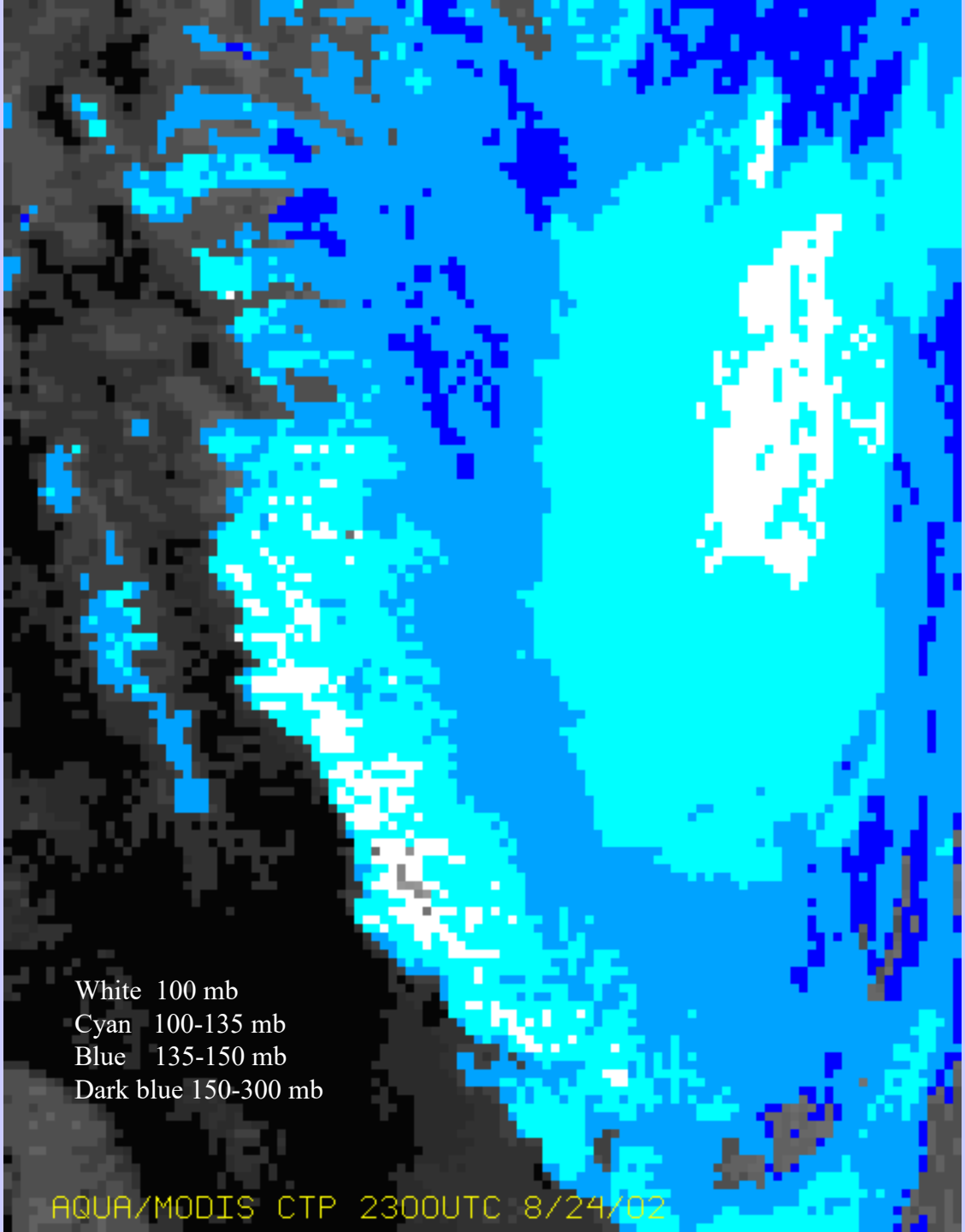
White 100 mb
Cyan 100-135 mb
Blue 135-150 mb
Dark blue 150-300 mb
AQUA/MODIS CTP 2300UTC 8/24/02

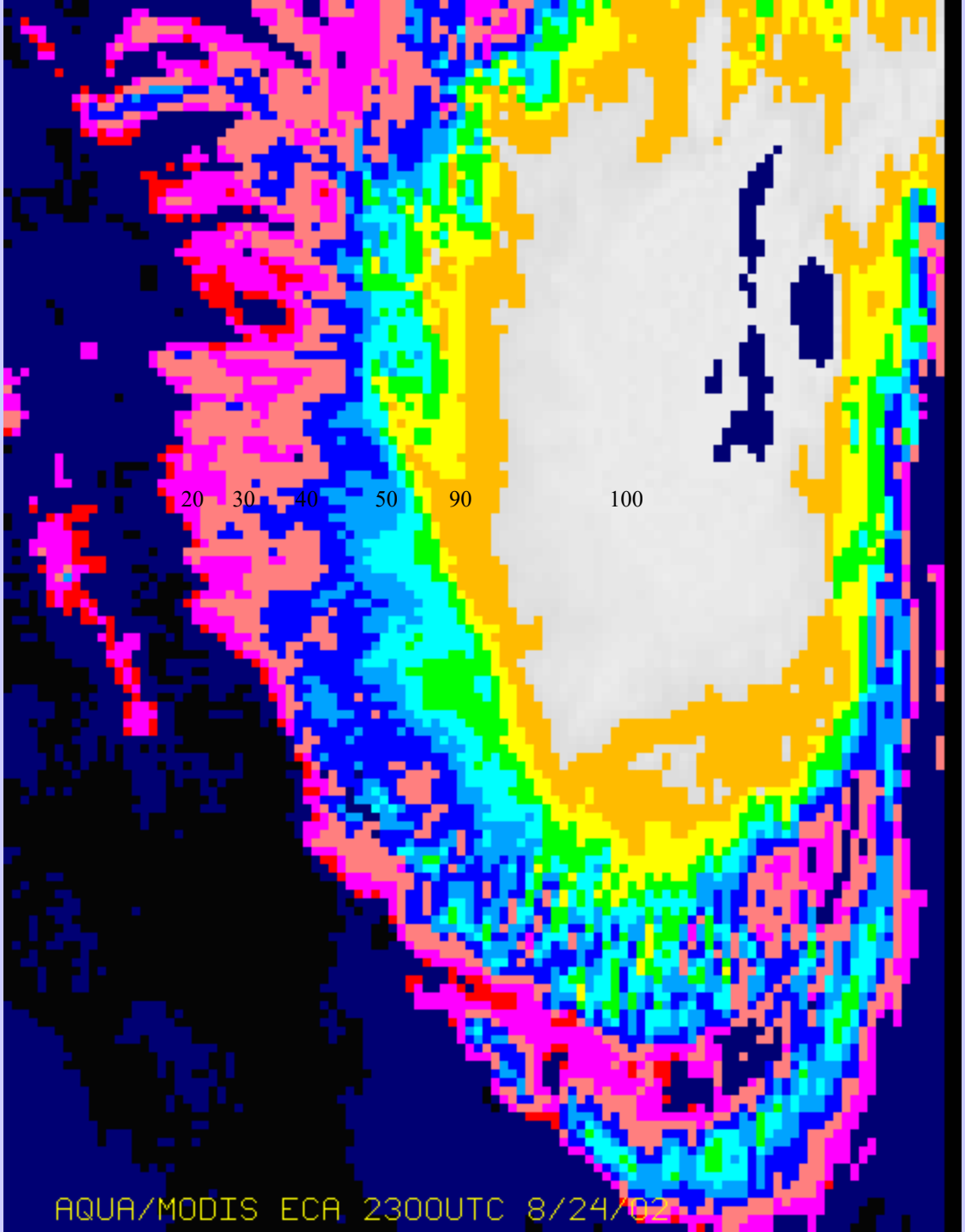
L
20
30
40
50
90
100
AQUA/MODIS ECA 2300UTC 8/24/02

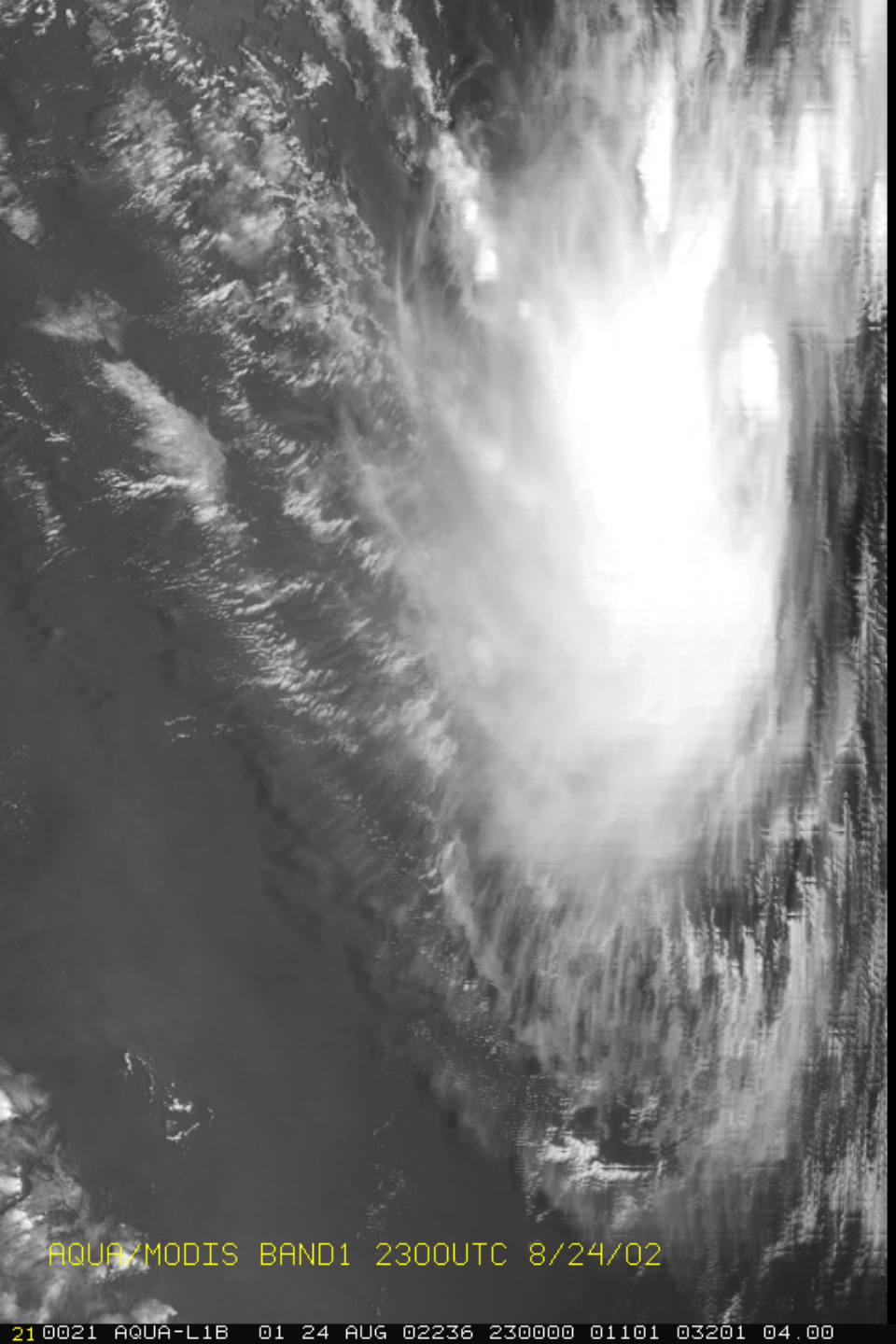

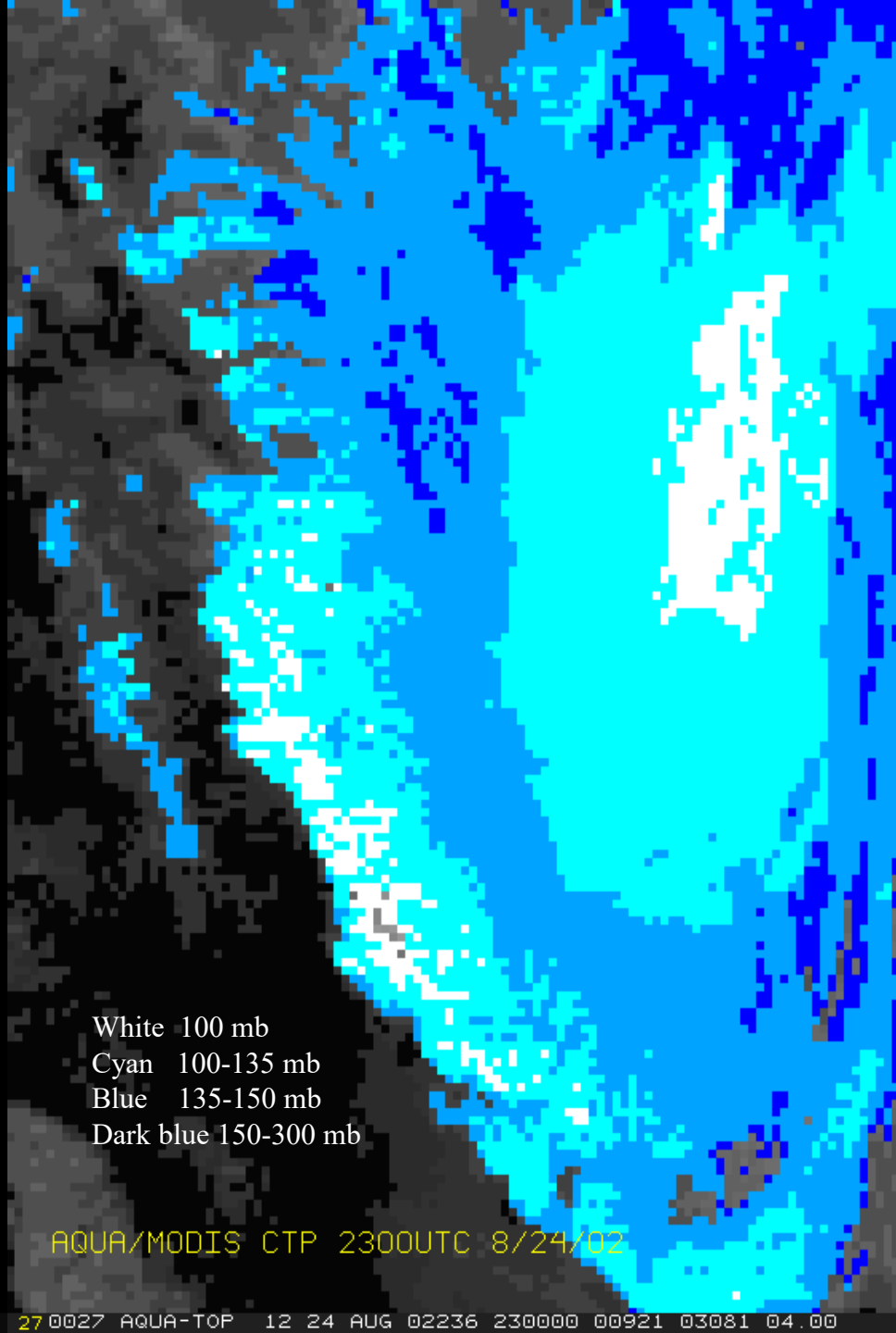

21 0021 AQUA-L1B 01 24 AUG 02236 230000 01101 03201 04.00

27 0027 AQUA-TOP 12 24 AUG 02236 230000 00921 03081 04.00

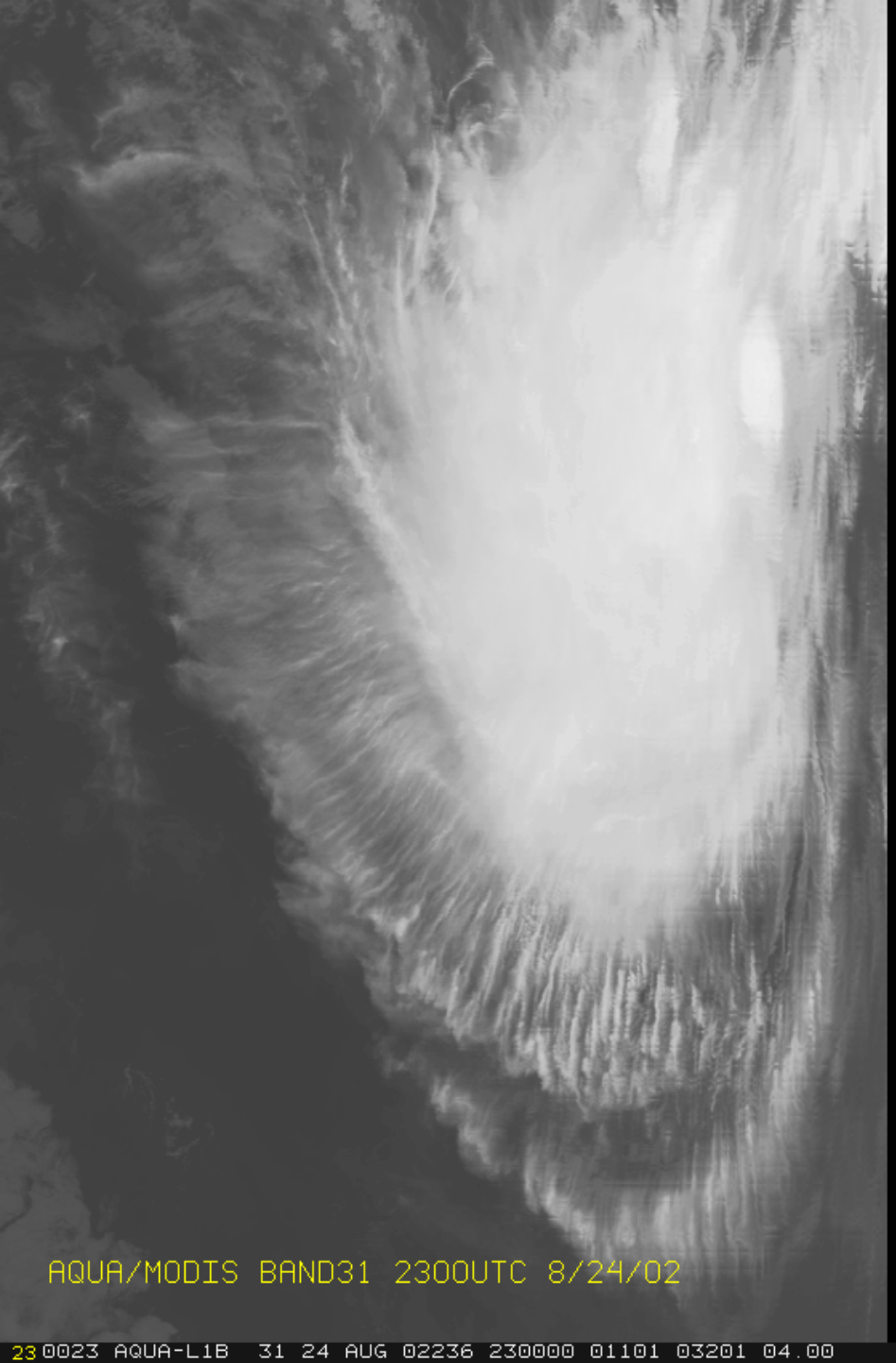

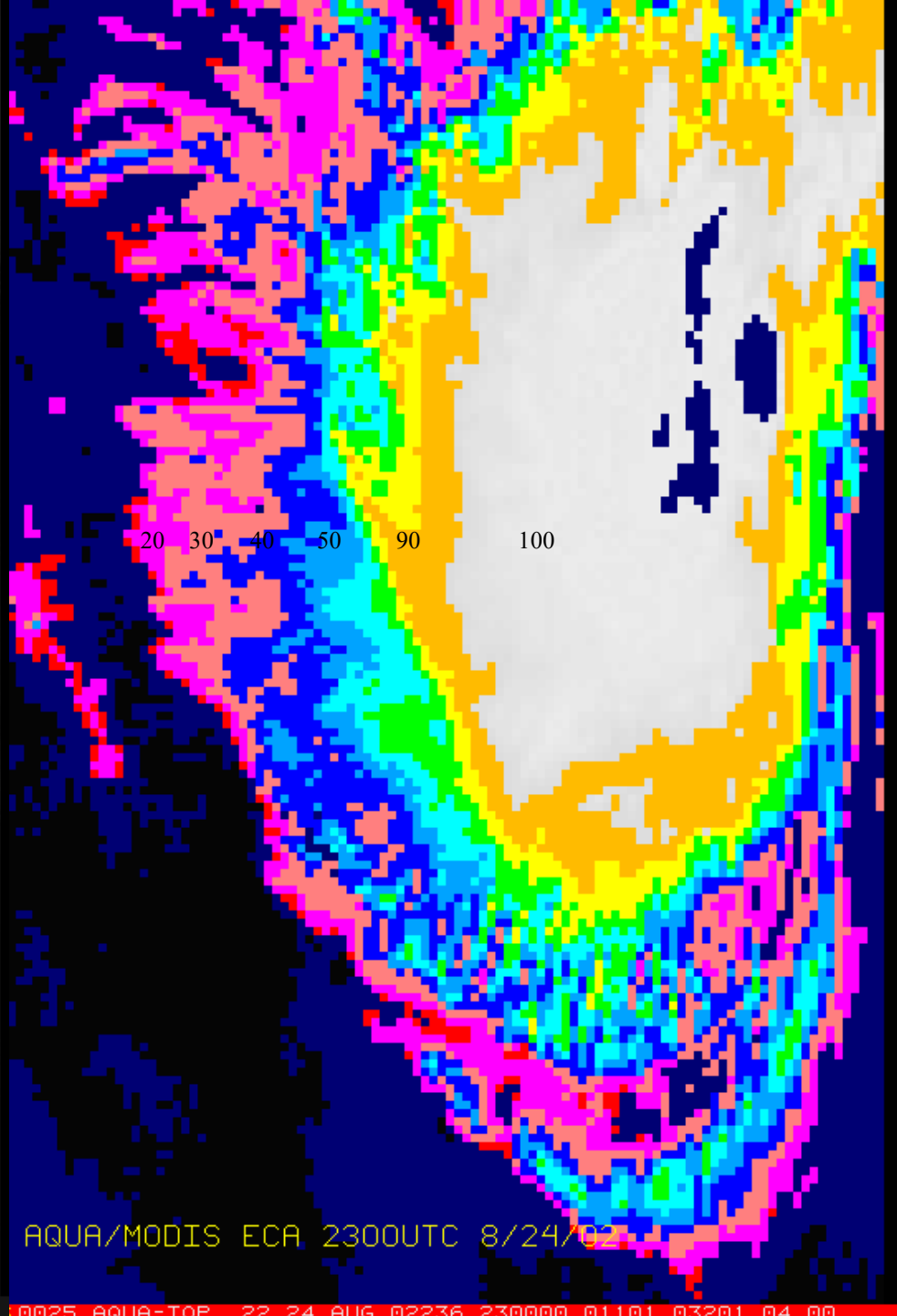

23 0023 AQUA-L1B 31 24 AUG 02236 230000 01101 03201 04.00
0025 AQUA-TOP 22 24 AUG 02236 230000 01101 03201 04.00

January 2001: MODIS High Clouds (0–400 mb)

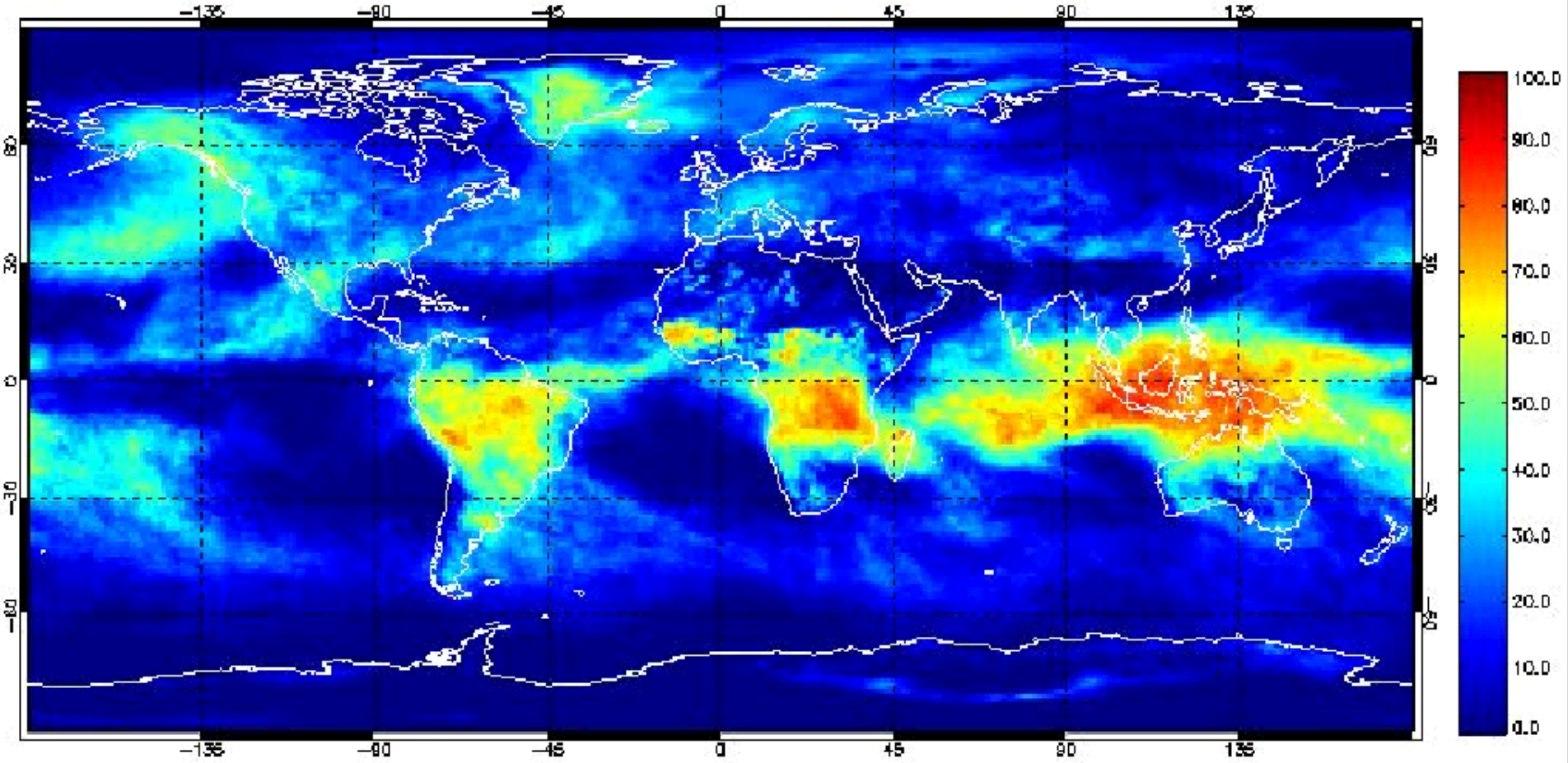

Simulations of Ice and Water Phase Clouds
8.5 - 11 μm BT Differences

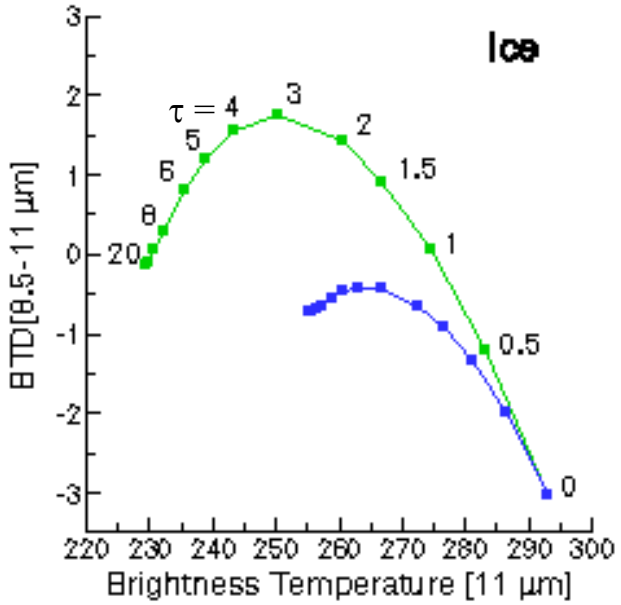

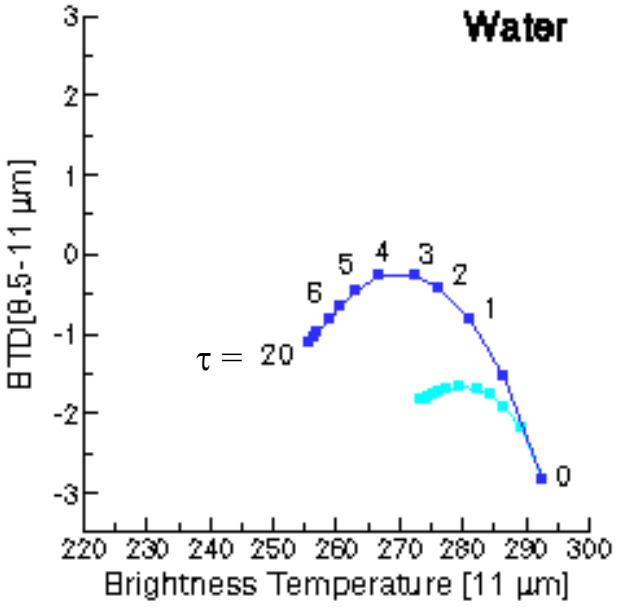

High Ice clouds

- BTD[8.5-11] > 0 over a large range of optical thicknesses τ
- T_{cld} = 228 K

Midlevel clouds

- BTD[8.5-11] values are similar (*i.e.*, negative) for both water and ice clouds
- T_{cld} = 253 K

Low-level, warm clouds

- BTD[8.5-11] values always negative
- T_{cld} = 273 K

Ice: Cirrus model derived from FIRE-I in-situ data (Nasiri et al, 2002)
Water: r_e=10 μm
Angles: θ_o = 45°, θ = 20°, and ϕ = 40°
Profile: midlatitude summer

MODIS Direct Broadcast

May 14, 2003 at 1458 UTC (Terra)
1-km resolution

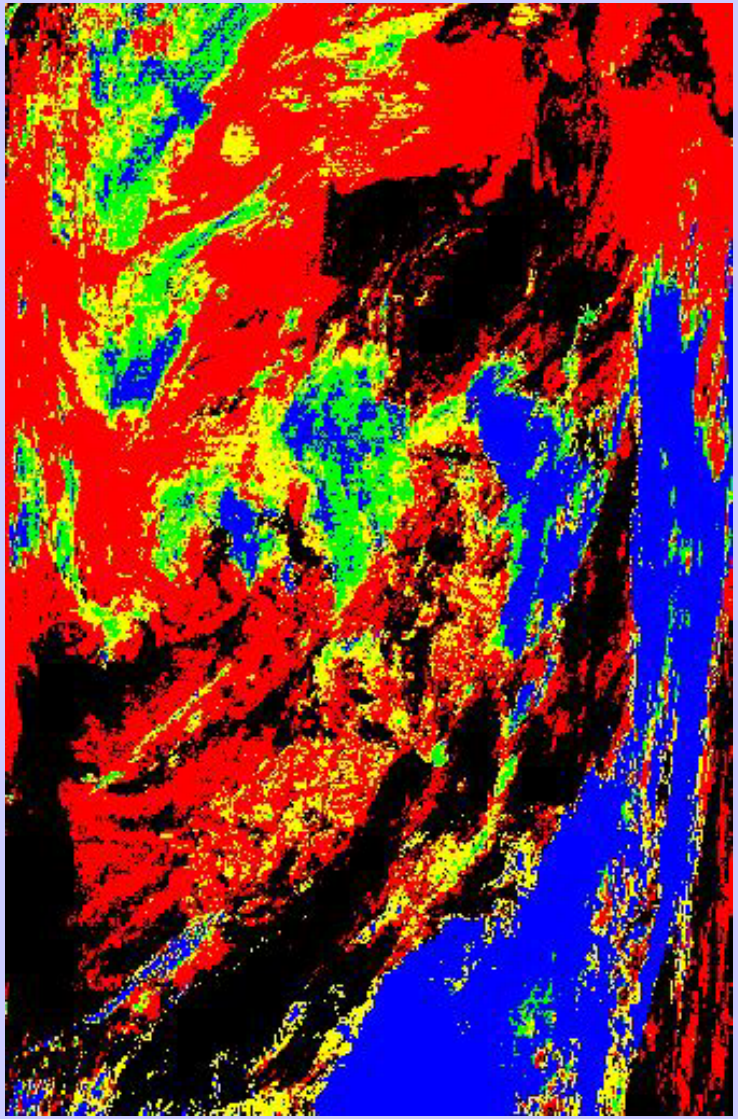

MODIS Frequency of Co-occurrence Water Phase with 253 K < T_{cld} < 268 K 05 Nov. 2000 - Daytime Only

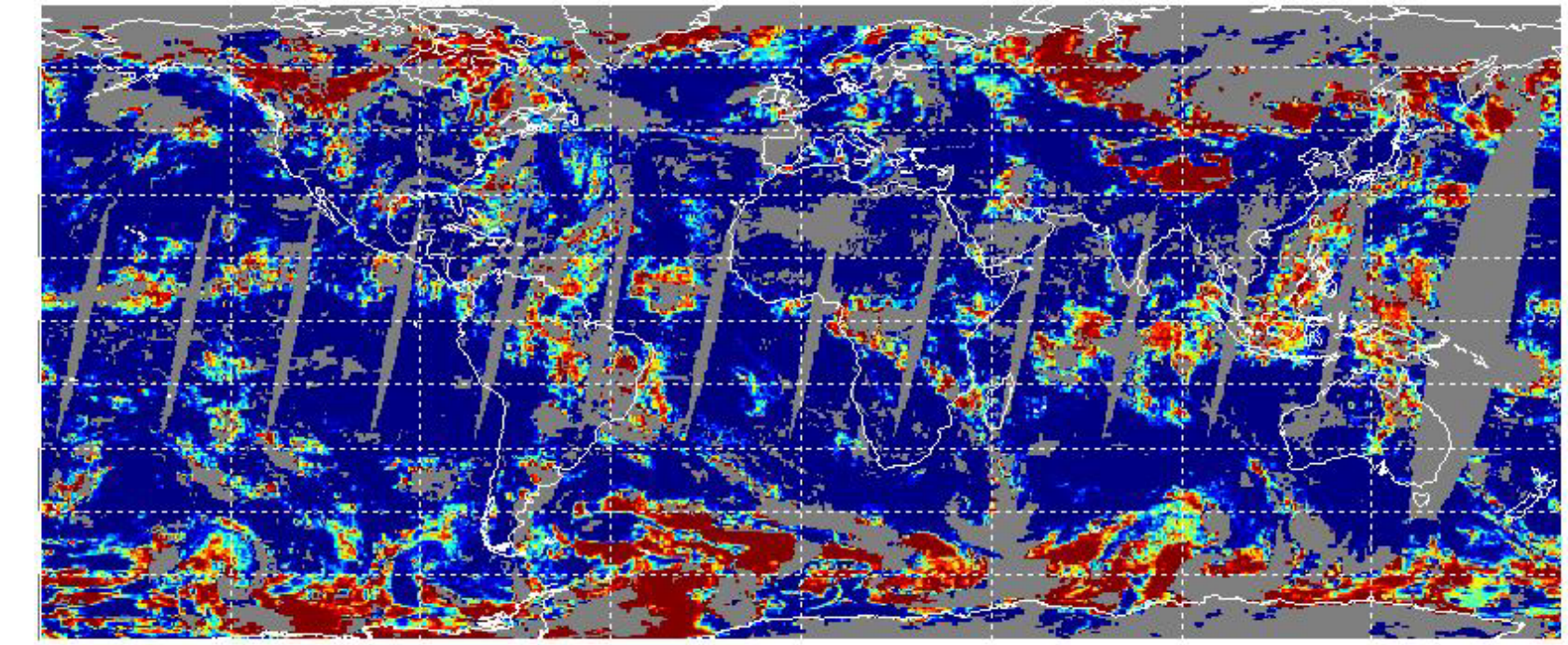

frequency of occurrence in percent (%)

MODIS Frequency of Co-occurrence
Water Phase with 253 K < T_{cld} < 268 K
05 Nov. 2000 - Nighttime Only

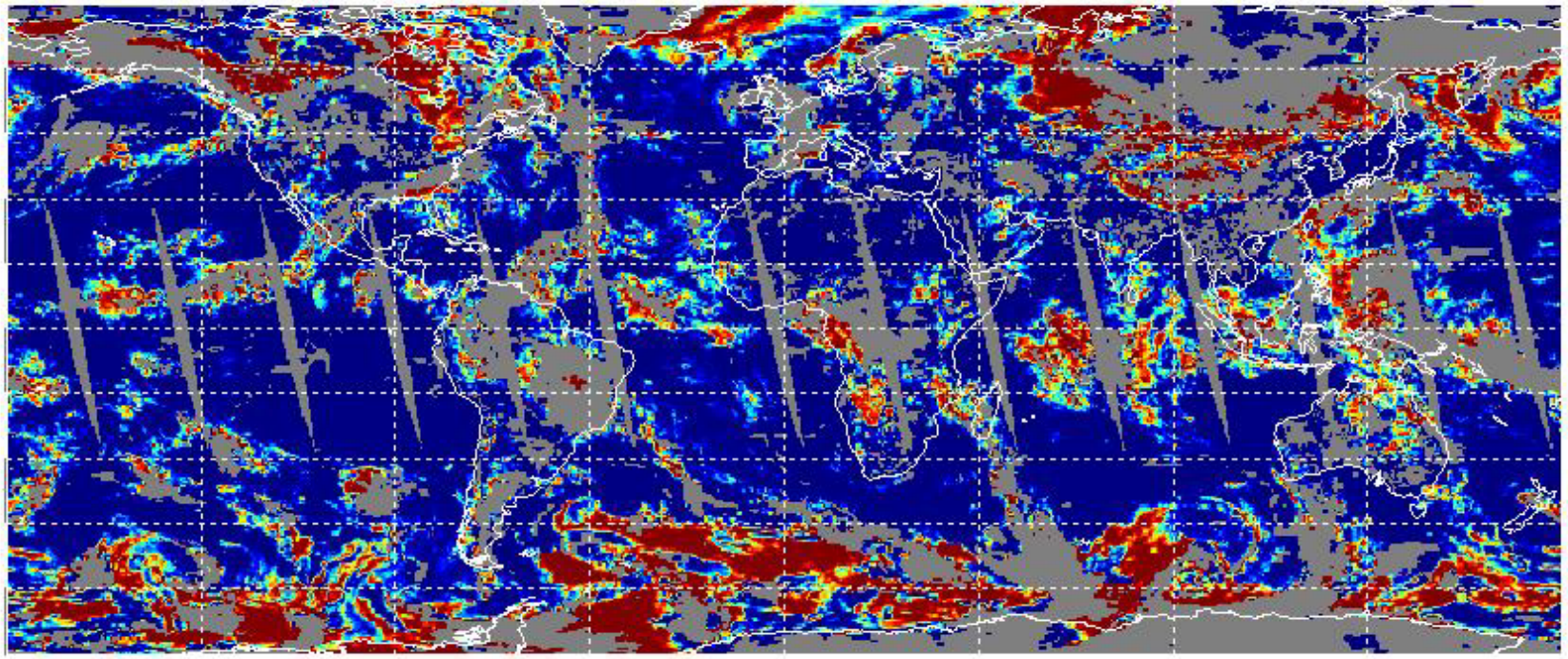

frequency of occurrence in percent (%)

CIRRUS FORMATION BY CONTRAILS OVER CENTRAL U.S. IN GOES-8 IR IMAGERY October 26, 1996

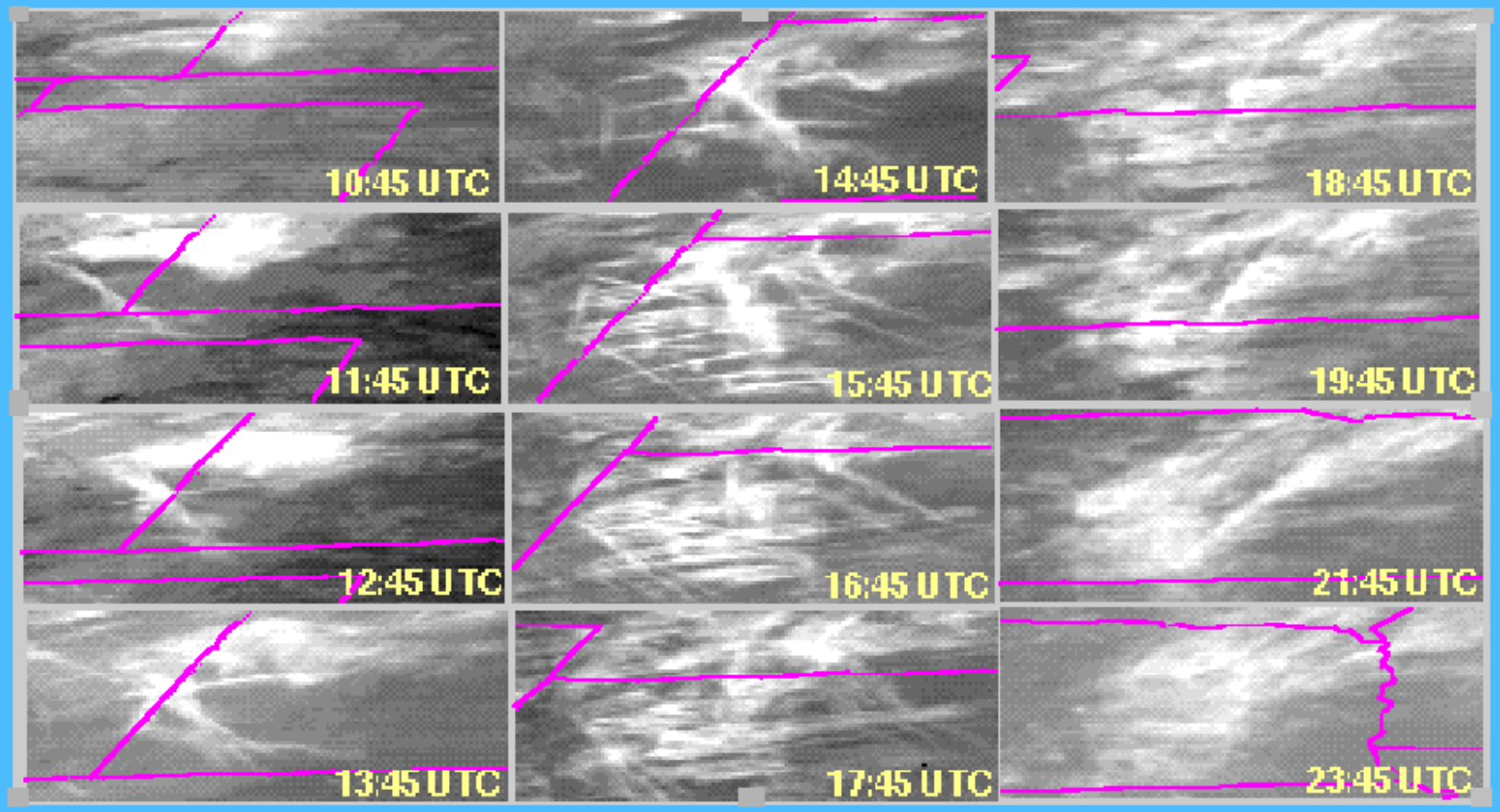

Minnis et al., *Science*, 1999

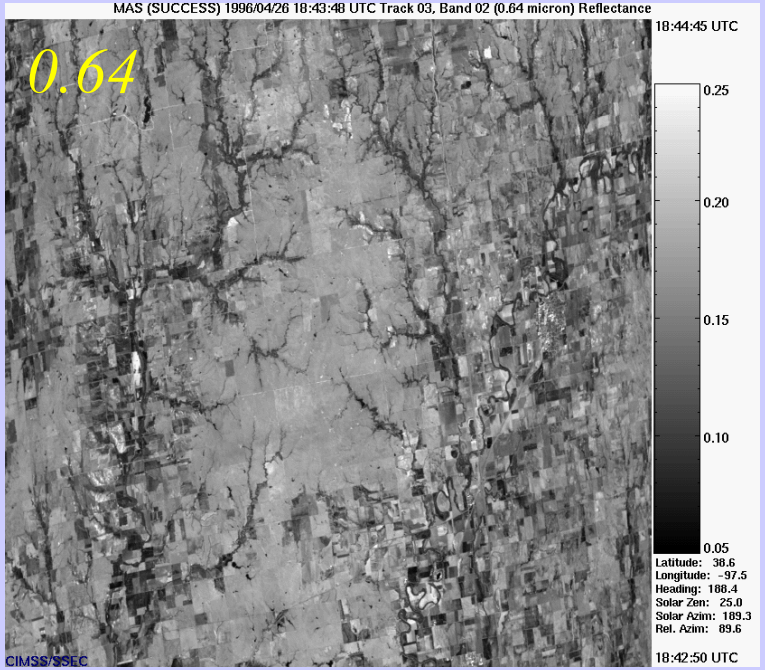
MAS (SUCCESS) 1996/04/26 18:43:48 UTC Track 03, Band 02 (0.64 micron) Reflectance
0.64
18:44:45 UTC
0.25
0.20
0.15
0.10
0.05
Latitude: 38.6
Longitude: -97.5
Heading: 188.4
Solar Zen: 25.0
Solar Azim: 189.3
Rel. Azim: 89.6
18:42:50 UTC
CIMSS/SSEC

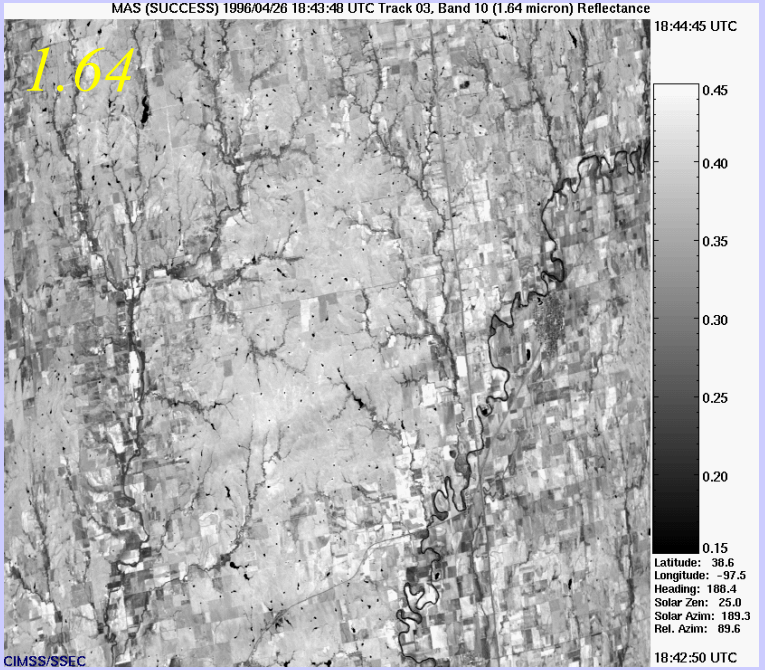
MAS (SUCCESS) 1996/04/26 18:43:48 UTC Track 03, Band 10 (1.64 micron) Reflectance
1.64
18:44:45 UTC
0.45
0.40
0.35
0.30
0.25
0.20
0.15
Latitude: 38.6
Longitude: -97.5
Heading: 188.4
Solar Zen: 25.0
Solar Azim: 189.3
Rel. Azim: 89.6
18:42:50 UTC
CIMSS/SSEC

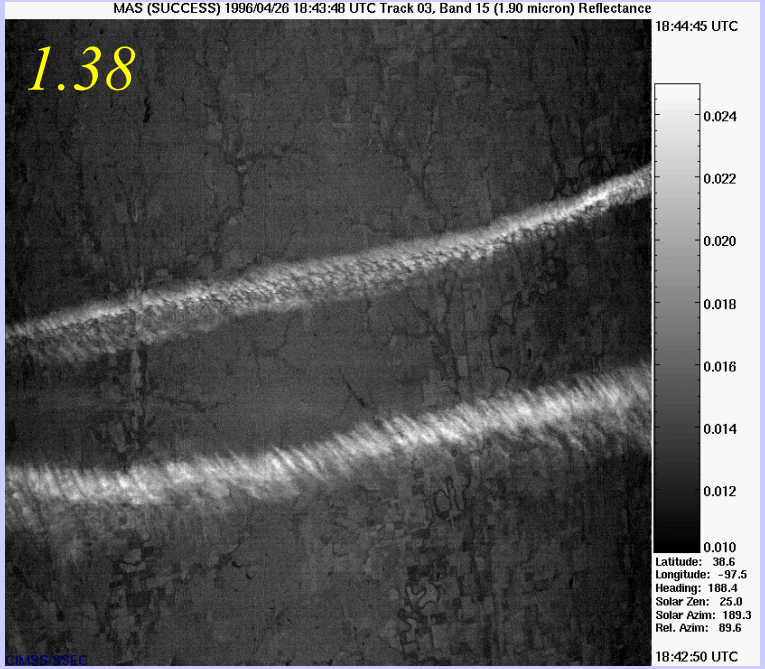
MAS (SUCCESS) 1996/04/26 18:43:48 UTC Track 03, Band 15 (1.90 micron) Reflectance
1.38
18:44:45 UTC
0.024
0.022
0.020
0.018
0.016
0.014
0.012
0.010
Latitude: 38.6
Longitude: -97.5
Heading: 188.4
Solar Zen: 25.0
Solar Azim: 189.3
Rel. Azim: 89.6
18:42:50 UTC
CIMSS/SSEC

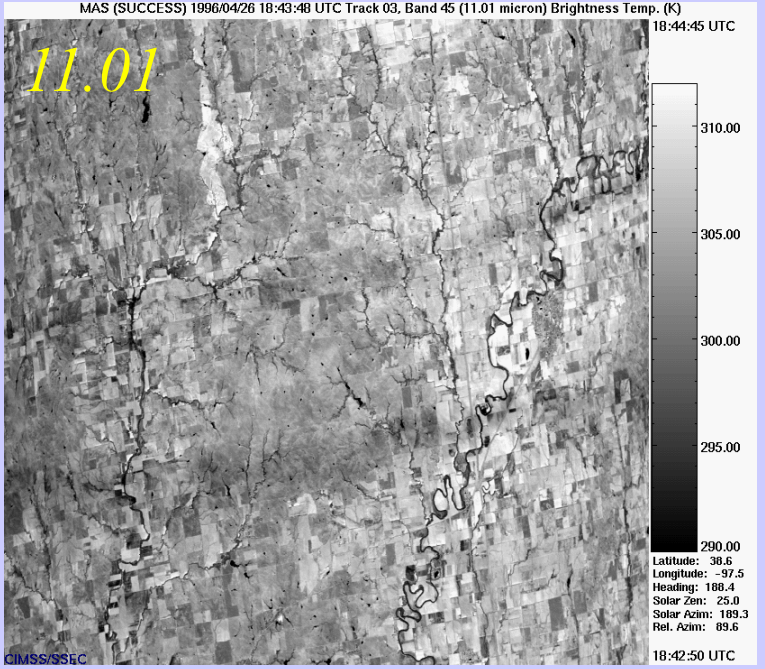
MAS (SUCCESS) 1996/04/26 18:43:48 UTC Track 03, Band 45 (11.01 micron) Brightness Temp. (K)
11.01
18:44:45 UTC
310.00
305.00
300.00
295.00
290.00
Latitude: 38.6
Longitude: -97.5
Heading: 188.4
Solar Zen: 25.0
Solar Azim: 189.3
Rel. Azim: 89.6
18:42:50 UTC
CIMSS/SSEC

Is cirrus related to air traffic?

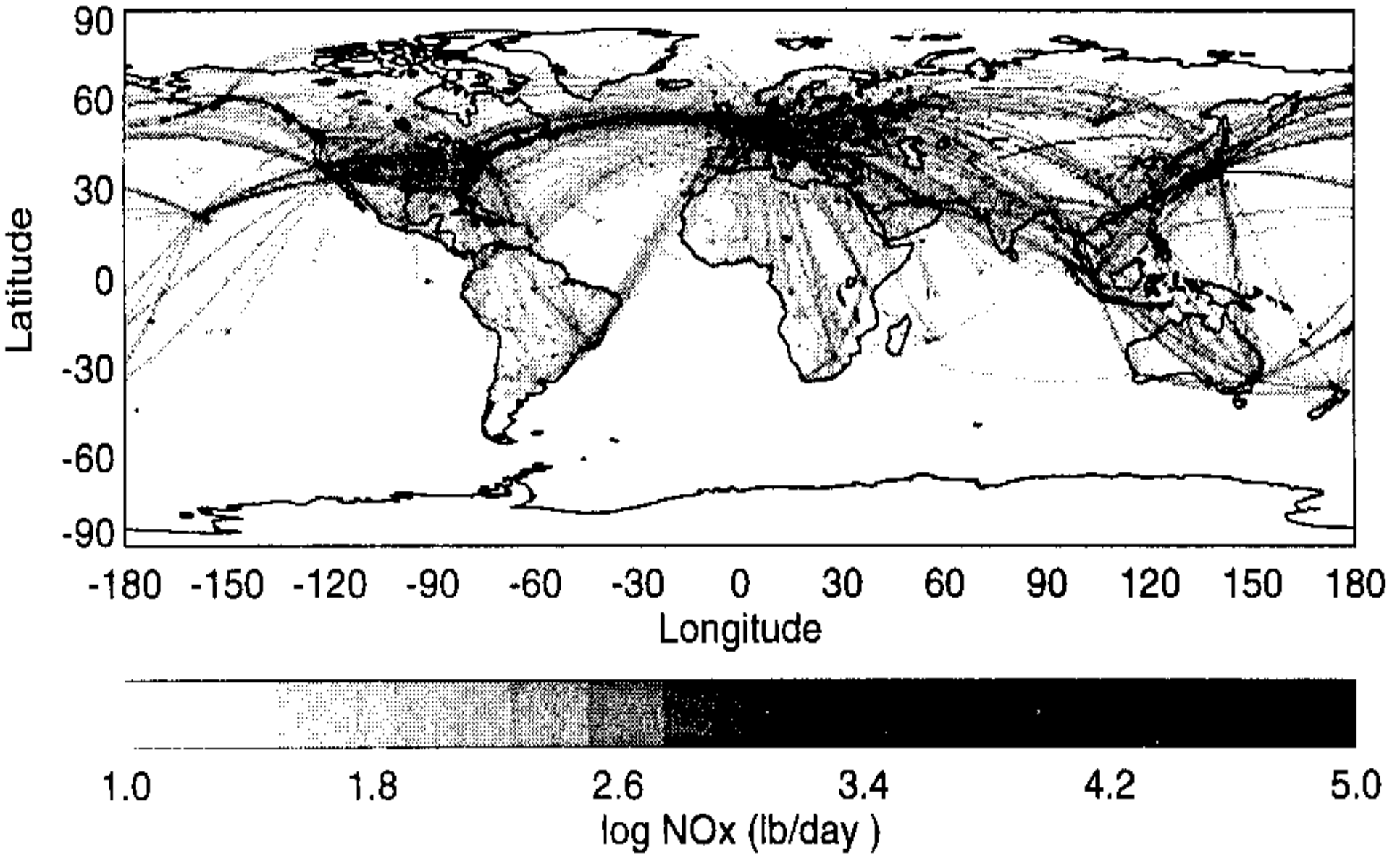

Cloud Clearing

For a single layer of clouds, radiances in one spectral band vary linearly with those of another as cloud amount varies from one field of view (fov) to another

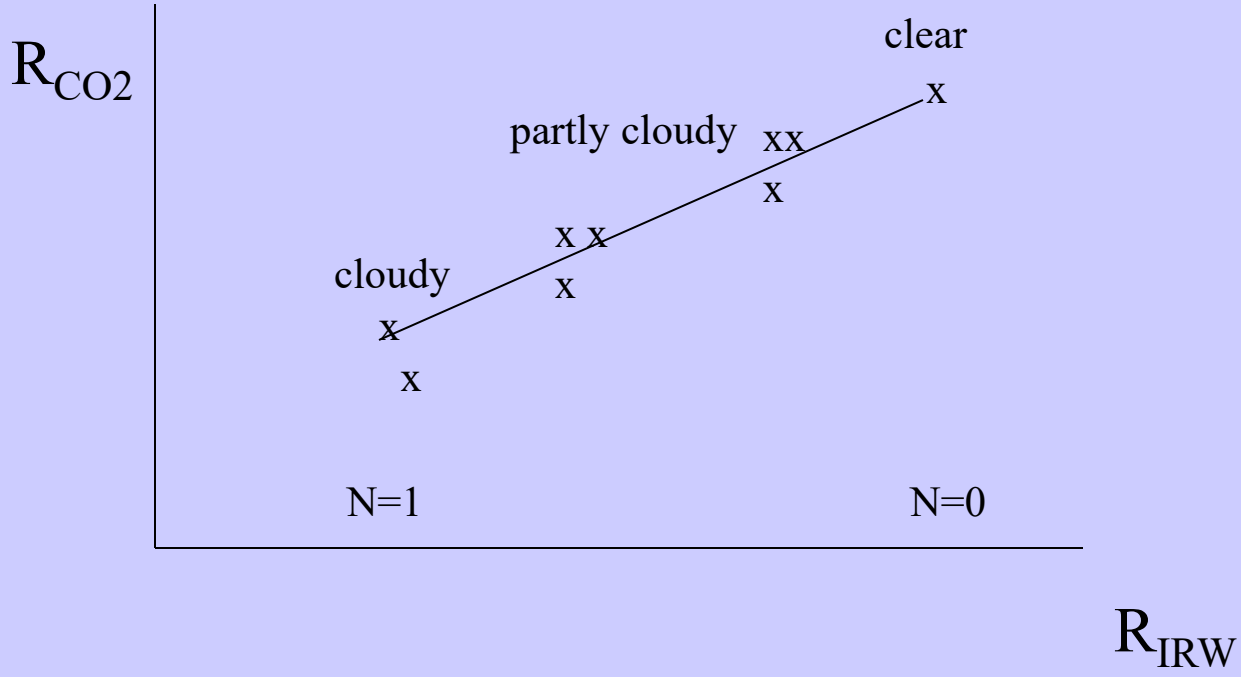

Clear radiances can be inferred by extrapolating to cloud free conditions.

Paired field of view proceeds as follows. For a given wavelength λ, radiances from two spatially independent, but geographically close, fields of view are written

$$I_{\lambda,1} = \eta_1 I_{\lambda,1}^{cd} + (1 - \eta_1) I_{\lambda,1}^{c} \quad ,$$

$$I_{\lambda,2} = \eta_2 I_{\lambda,2}^{cd} + (1 - \eta_2) I_{\lambda,2}^{c} \quad ,$$

If clouds are at uniform altitude, and clear air radiance is in each FOV

$$I_\lambda^{cd} = I_{\lambda,1}^{cd} = I_{\lambda,2}^{cd}$$

$$I_\lambda^{c} = I_{\lambda,1}^{c} = I_{\lambda,2}^{c}$$

$$\frac{\eta_1 \ (I_\lambda^{cd} - I_\lambda^{c})}{\eta_2 \ (I_\lambda^{cd} - I_\lambda^{c})} = \frac{\eta_1}{\eta_2} = \eta^* = \frac{I_{\lambda,1} - I_\lambda^{c}}{I_{\lambda,2} - I_\lambda^{c}} \ ,$$

where η^* is the ratio of the cloud amounts for the two geographically independent fields of view of the sounding radiometer. Therefore, the clear air radiance from an area possessing broken clouds at a uniform altitude is given by

$$I_\lambda^{c} = [\, I_{\lambda,1} - \eta^* I_{\lambda,2}] \,/[1 - \eta^*]$$

where η^* still needs to be determined. Given an independent measurement of surface temperature, T_s, and measurements $I_{w,1}$ and $I_{w,2}$ in a spectral window channel, then η^* can be determined by

$$\eta^* = [I_{w,1} - B_w(T_s)] \,/\, [I_{w,2} - B_w(T_s)]$$

and I_λ^c for different spectral channels can be solved.

First Order Estimation of TPW

Moisture attenuation in atmospheric windows varies linearly with optical depth.

$$\tau_\lambda = e^{-k_\lambda u} = 1 - k_\lambda u$$

For same atmosphere, deviation of brightness temperature from surface temperature is a linear function of absorbing power. Thus moisture corrected SST can inferred by using split window measurements and extrapolating to zero k_λ

$$T_s = T_{bw1} + [\, k_{w1} / (k_{w2} - k_{w1}) \,] \, [T_{bw1} - T_{bw2}] \; .$$

Moisture content of atmosphere inferred from slope of linear relation.

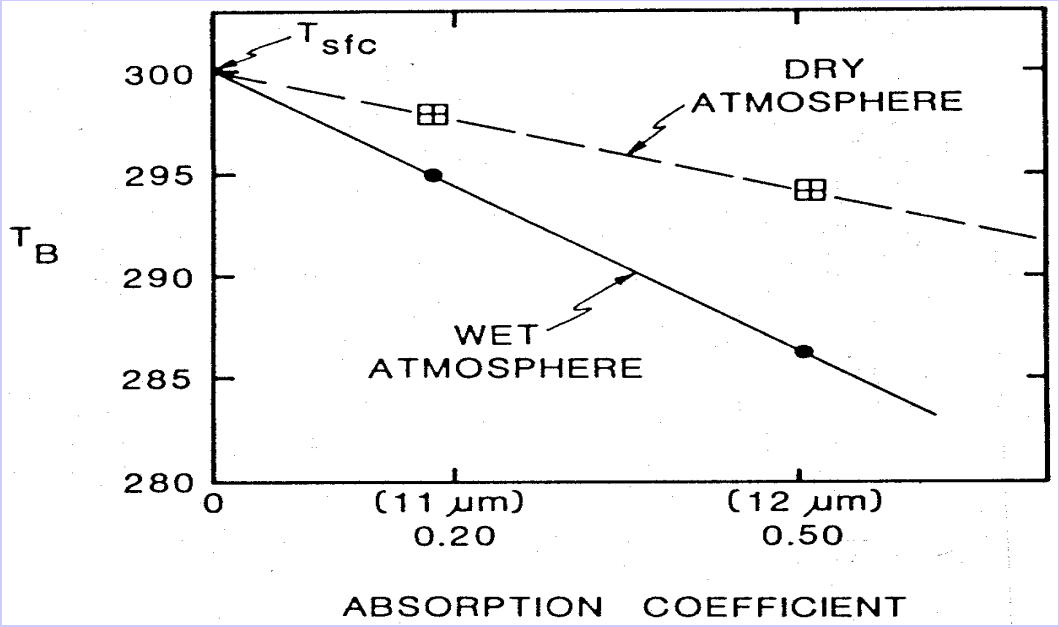

Water vapour evaluated in multiple infrared window channels where absorption is weak, so that

$$\tau_w = \exp[-k_w u] \sim 1 - k_w u \text{ where w denotes window channel}$$

and

$$d\tau_w = -k_w du$$

What little absorption exists is due to water vapour, therefore, u is a measure of precipitable water vapour. RTE in window region

$$I_w = B_{sw}(1-k_w u_s) + k_w \int_o^{u_s} B_w du$$

u_s represents total atmospheric column absorption path length due to water vapour, and s denotes surface. Defining an atmospheric mean Planck radiance, then

$$I_w = B_{sw}(1-k_w u_s) + k_w u_s \bar{B}_w \text{ with } \bar{B}_w = \int_o^{u_s} B_w du \Big/ \int_o^{u_s} du$$

Since B_{sw} is close to both I_w and B_w, first order Taylor expansion about the surface temperature T_s allows us to linearize the RTE with respect to temperature, so

$T_{bw} = T_s(1-k_w u_s) + k_w u_s \bar{T}_w$, where T_w is mean atmospheric temperature corresponding to B_w.

For two window channels (11 and 12um) the following ratio can be determined.

$$\frac{T_s - T_{bw1}}{T_s - T_{bw2}} = \frac{k_{w1} u_s (T_s - \bar{T}_{w1})}{k_{w1} u_s (T_s - \bar{T}_{w2})} = \frac{k_{w1}}{k_{w2}}$$

where the mean atmospheric temperature measured in the one window region is assumed to be comparable to that measured in the other, $T_{w1} \sim T_{w2}$,

Thus it follows that

$$T_s = T_{bw1} + \frac{k_{w1}}{k_{w2} - k_{w1}} [T_{bw1} - T_{bw2}]$$

and

$$u_s = \frac{T_{bw} - T_s}{k_w (\bar{T}_w - T_s)} .$$

Obviously, the accuracy of the determination of the total water vapour concentration depends upon the contrast between the surface temperature, T_s, and

the effective temperature of the atmosphere $\bar{T}_w$

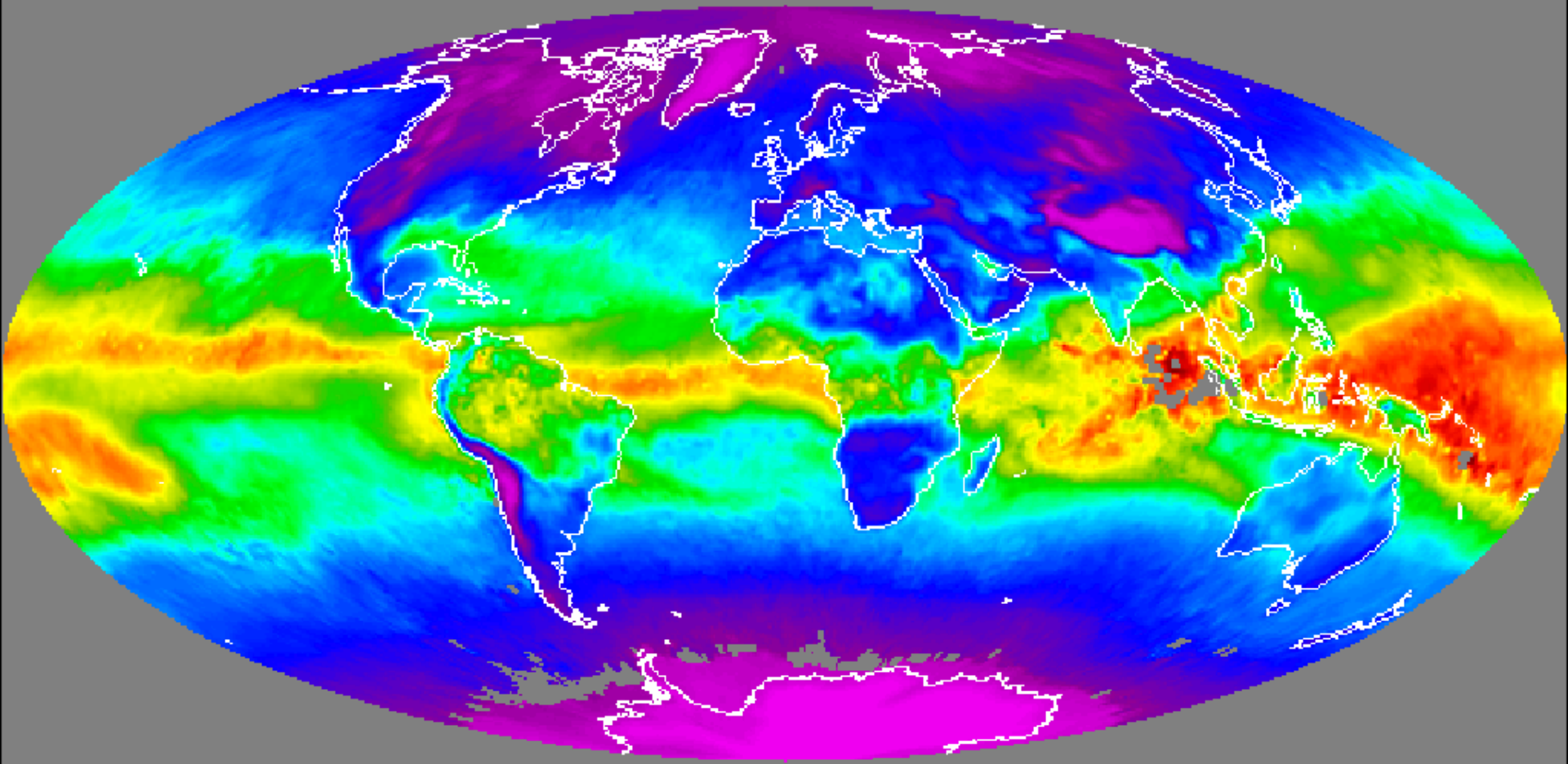

Global TPW from Seemann

T(p)

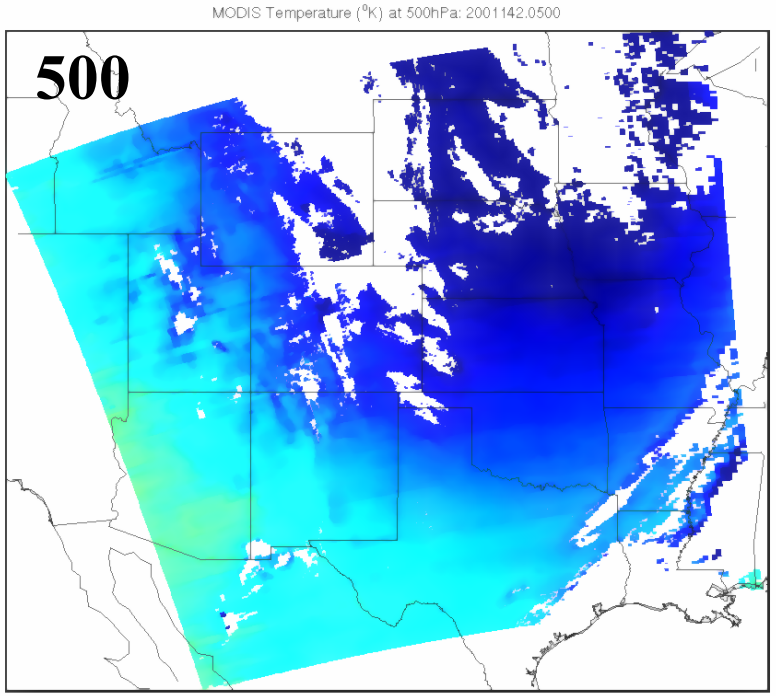
MODIS Temperature (°K) at 500hPa: 2001142.0500
500

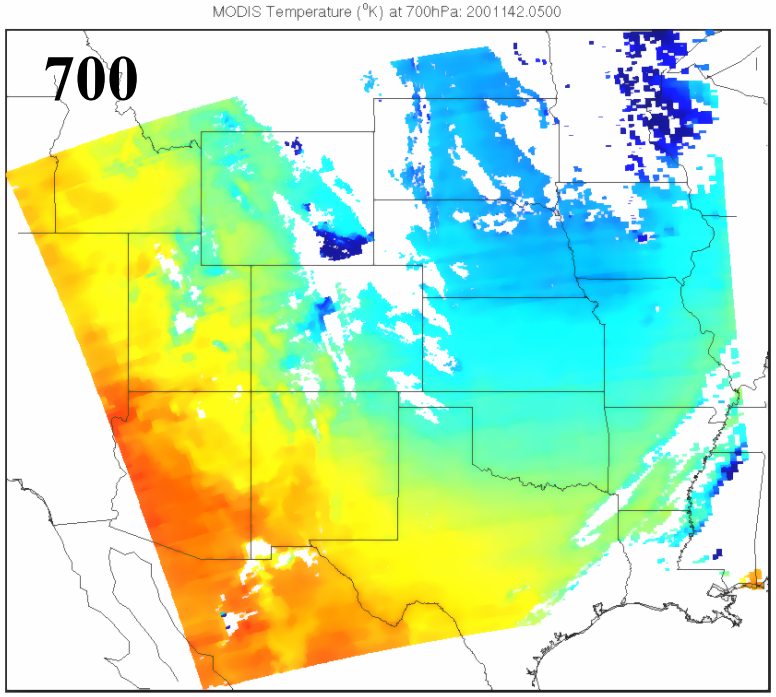
MODIS Temperature (°K) at 700hPa: 2001142.0500
700

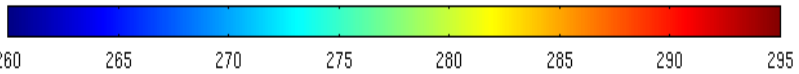
260
265
270
275
280
285
290
295

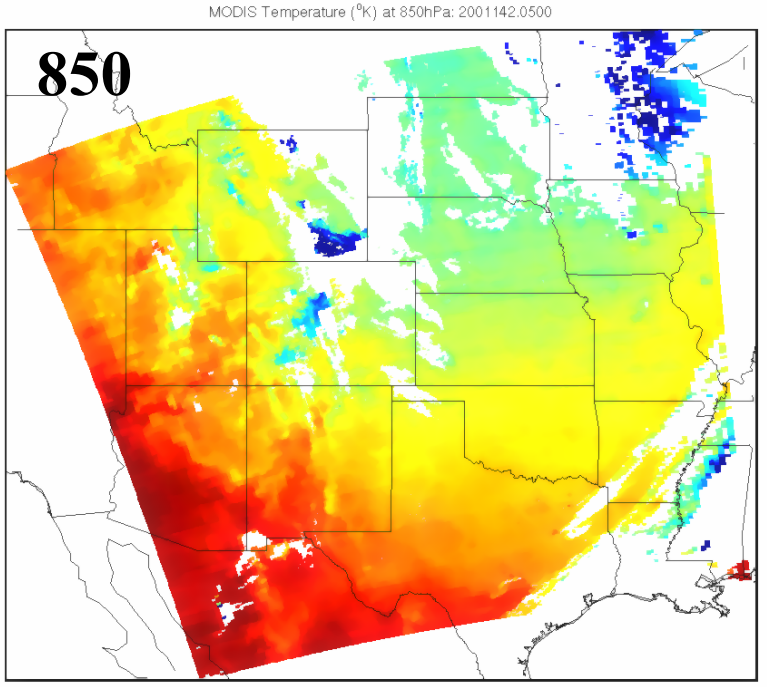
MODIS Temperature (°K) at 850hPa: 2001142.0500
850

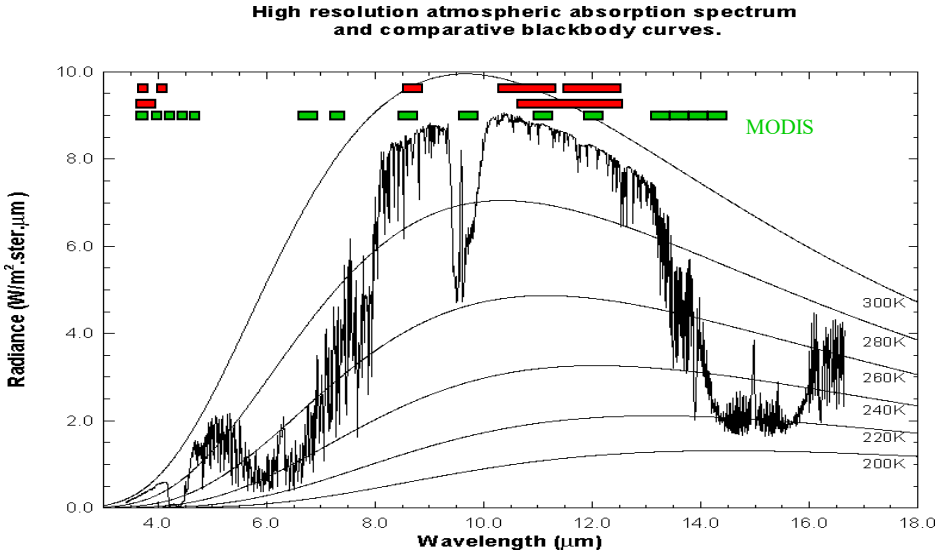
High resolution atmospheric absorption spectrum
and comparative blackbody curves.
MODIS
300K
280K
260K
240K
220K
200K
Radiance (W/m².ster.μm)
Wavelength (μm)
0.0
2.0
4.0
6.0
8.0
10.0
4.0
6.0
8.0
10.0
12.0
14.0
16.0
18.0

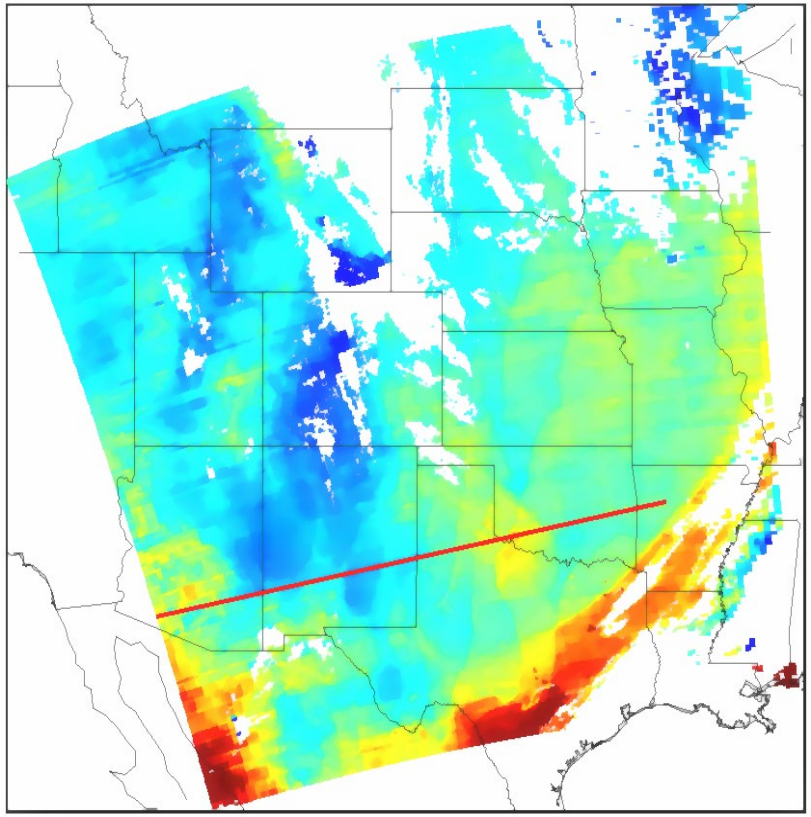

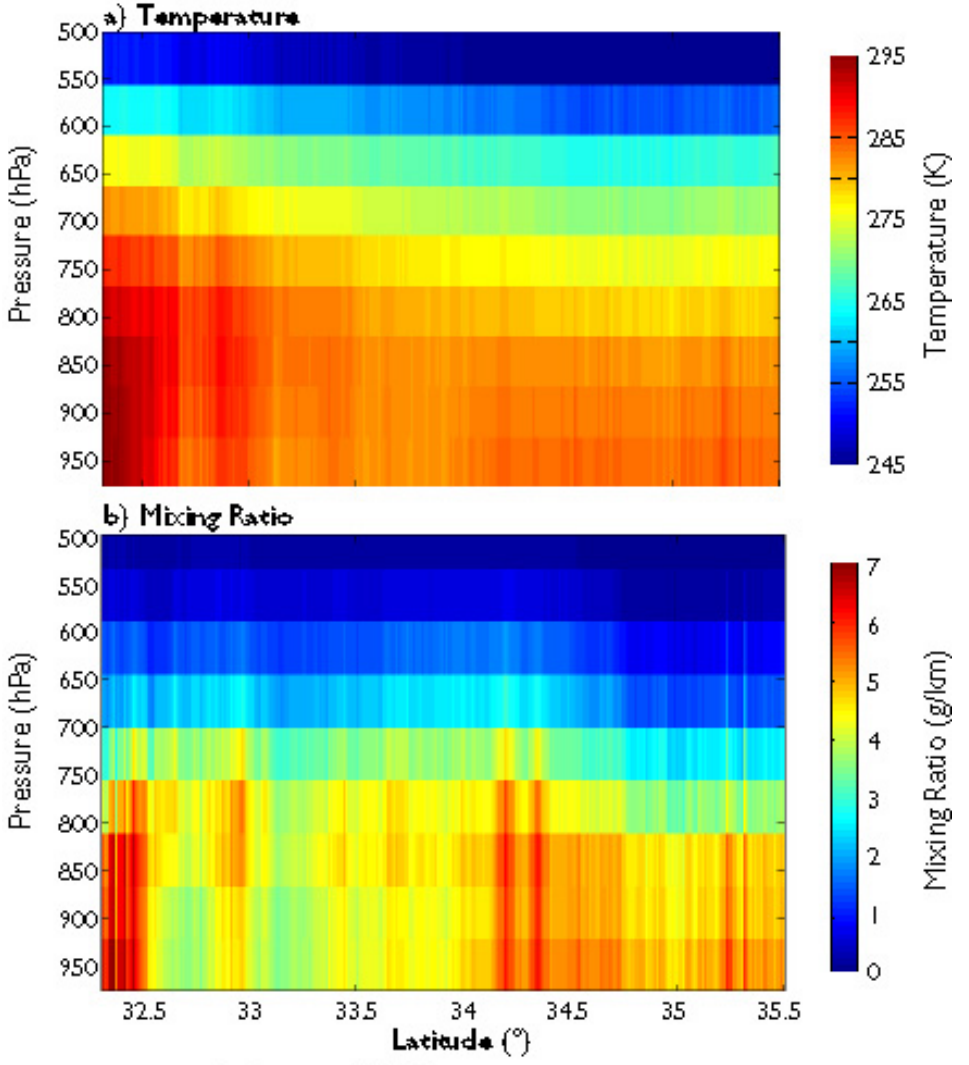

Clear sky layers of temperature and moisture

Application Opportunities with Multispectral Remote Sensing Data

Satellite Remote Sensing
Energy Balance
VIS, IR, and MW Radiative Transfer
EOS Terra & Aqua MODIS
Multispectral Applications
(Ocean Color, Snow/Ice, Vegetation, Aerosols, Fires, Volcanic Ash, Clouds, Moisture)
Detecting Climate Trends

Climate System Energy Balance

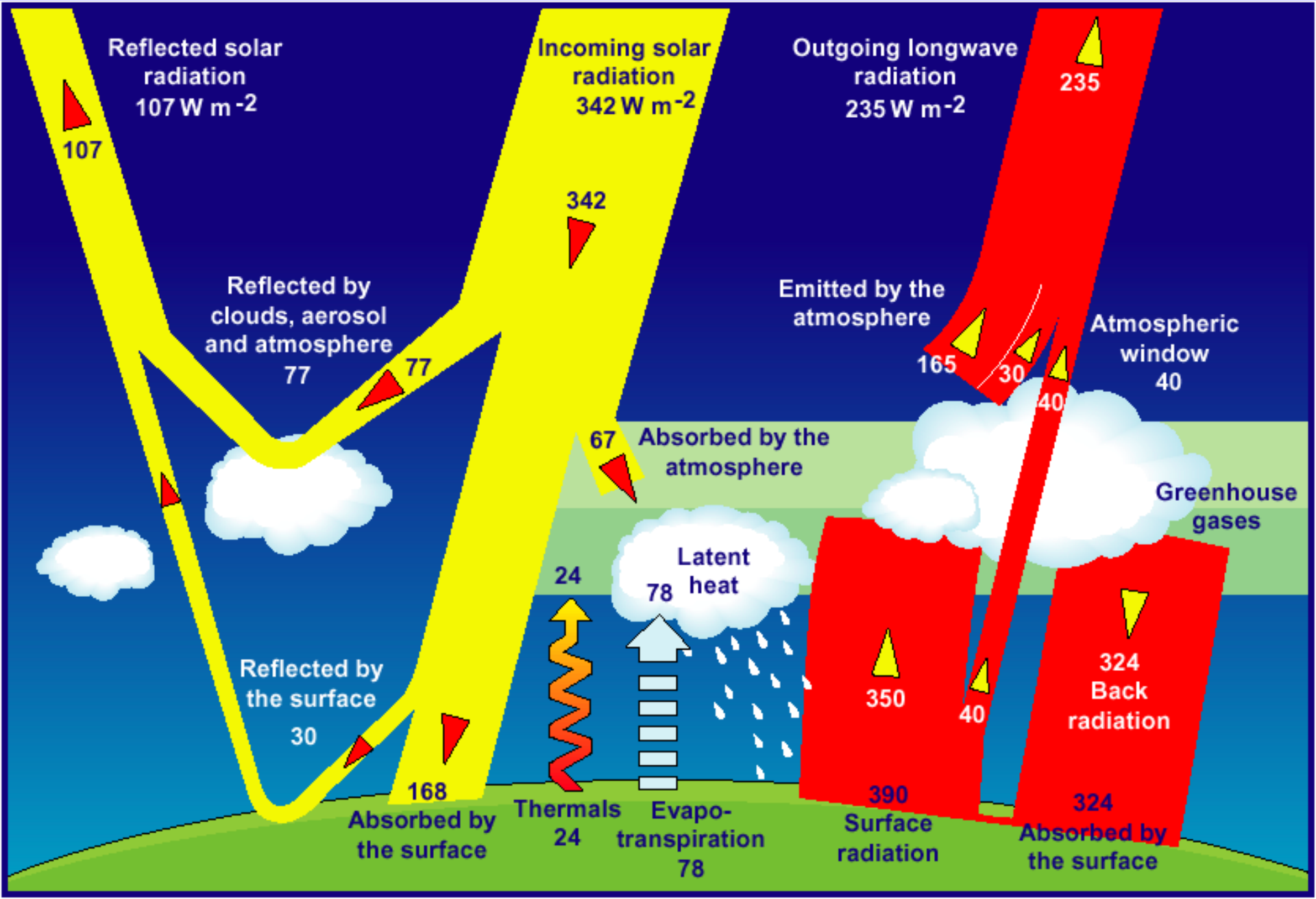

Major Climate System Elements

Carbon Cycle

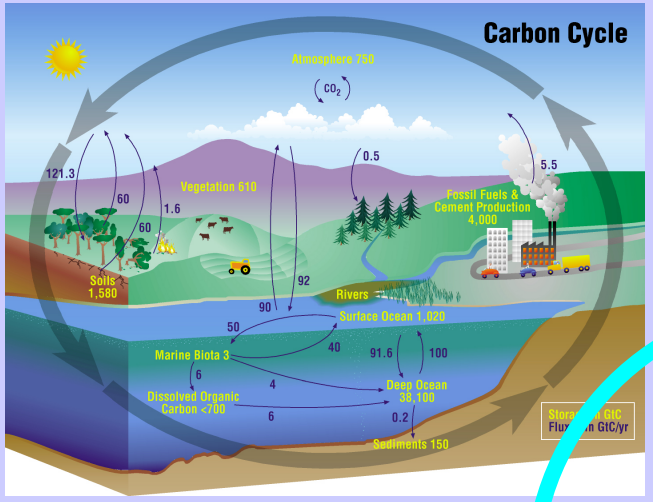

Water & Energy Cycle

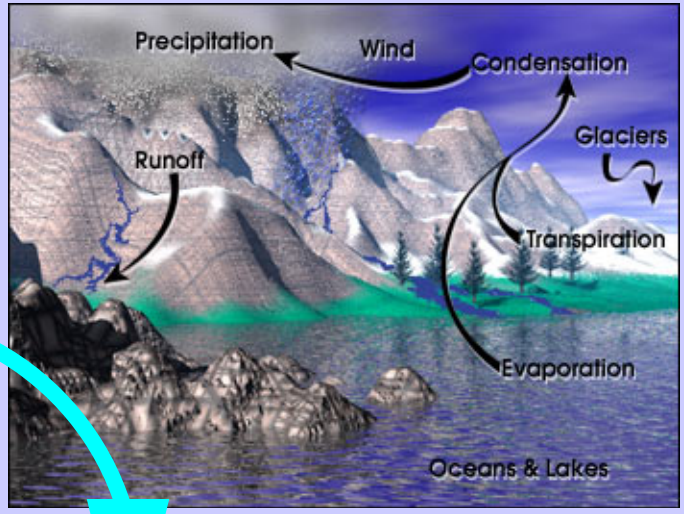

Coupled Chaotic Nonlinear

Atmospheric Chemistry

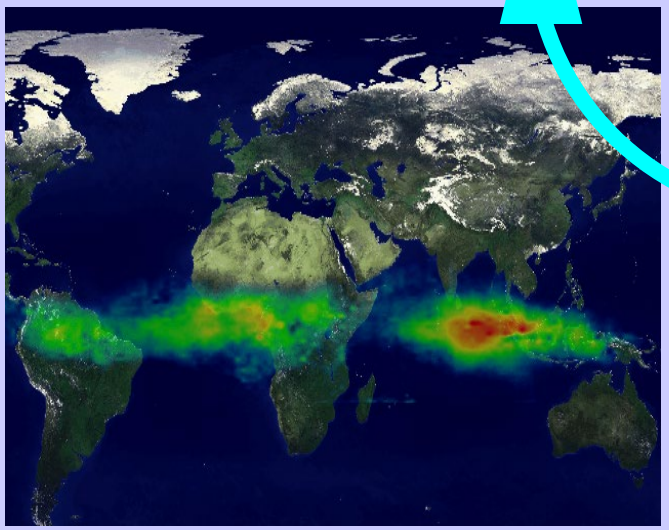

Atmosphere and Ocean Dynamics

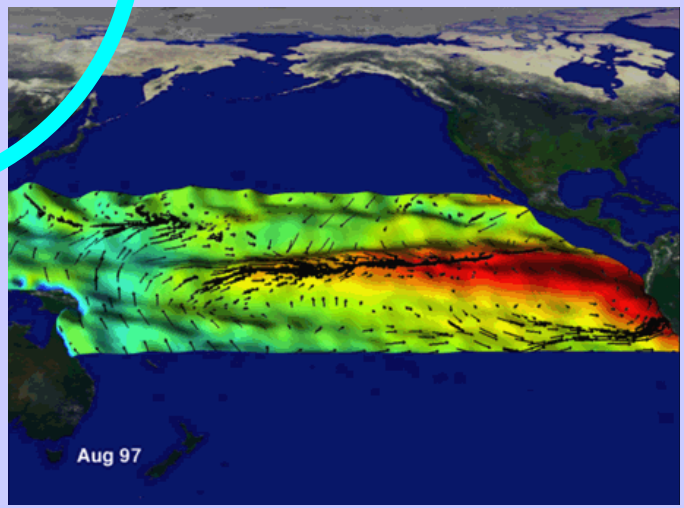

What global surface temperature change has occurred so far?

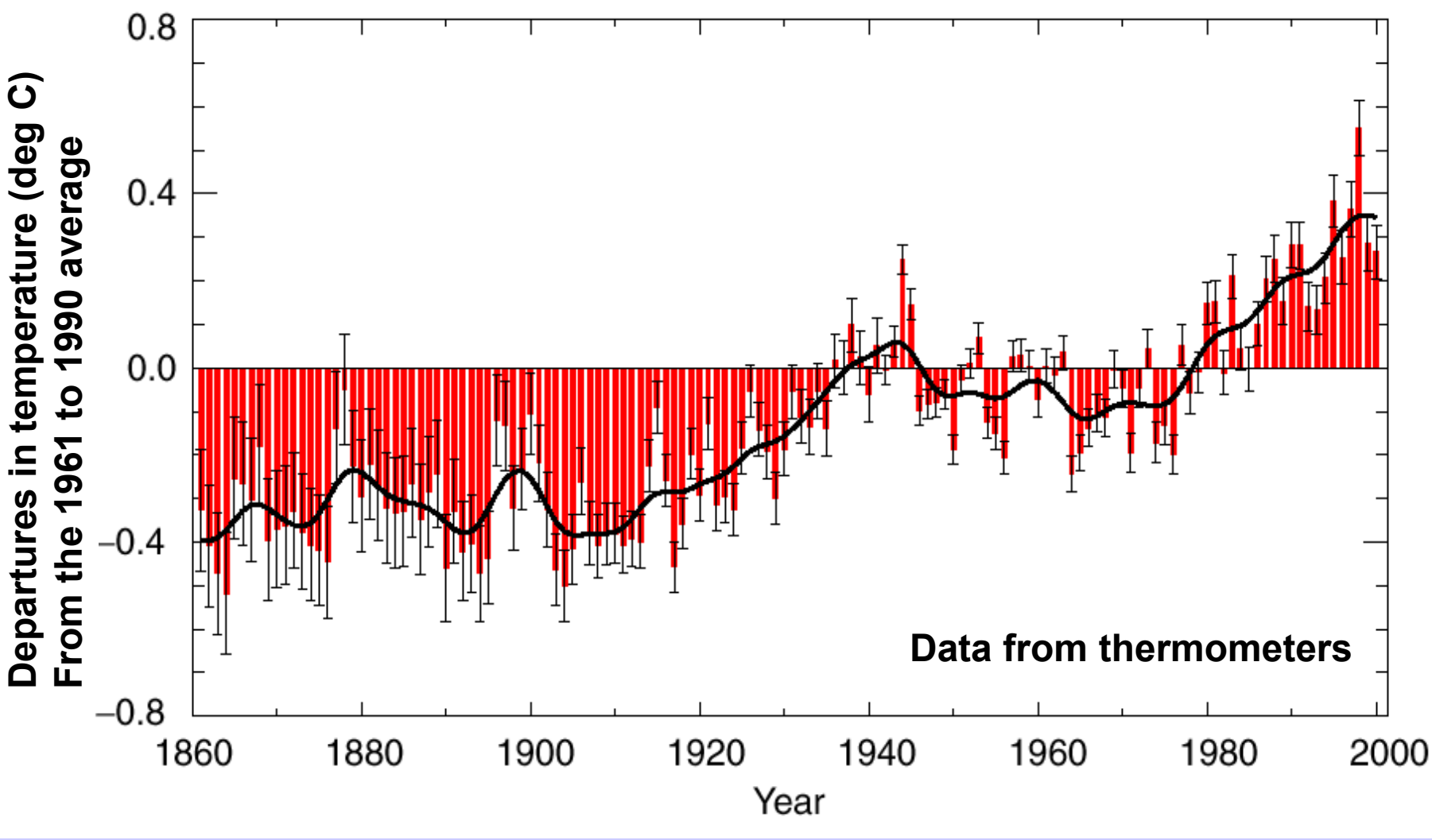

IPCC 2001

Human Influence on Climate

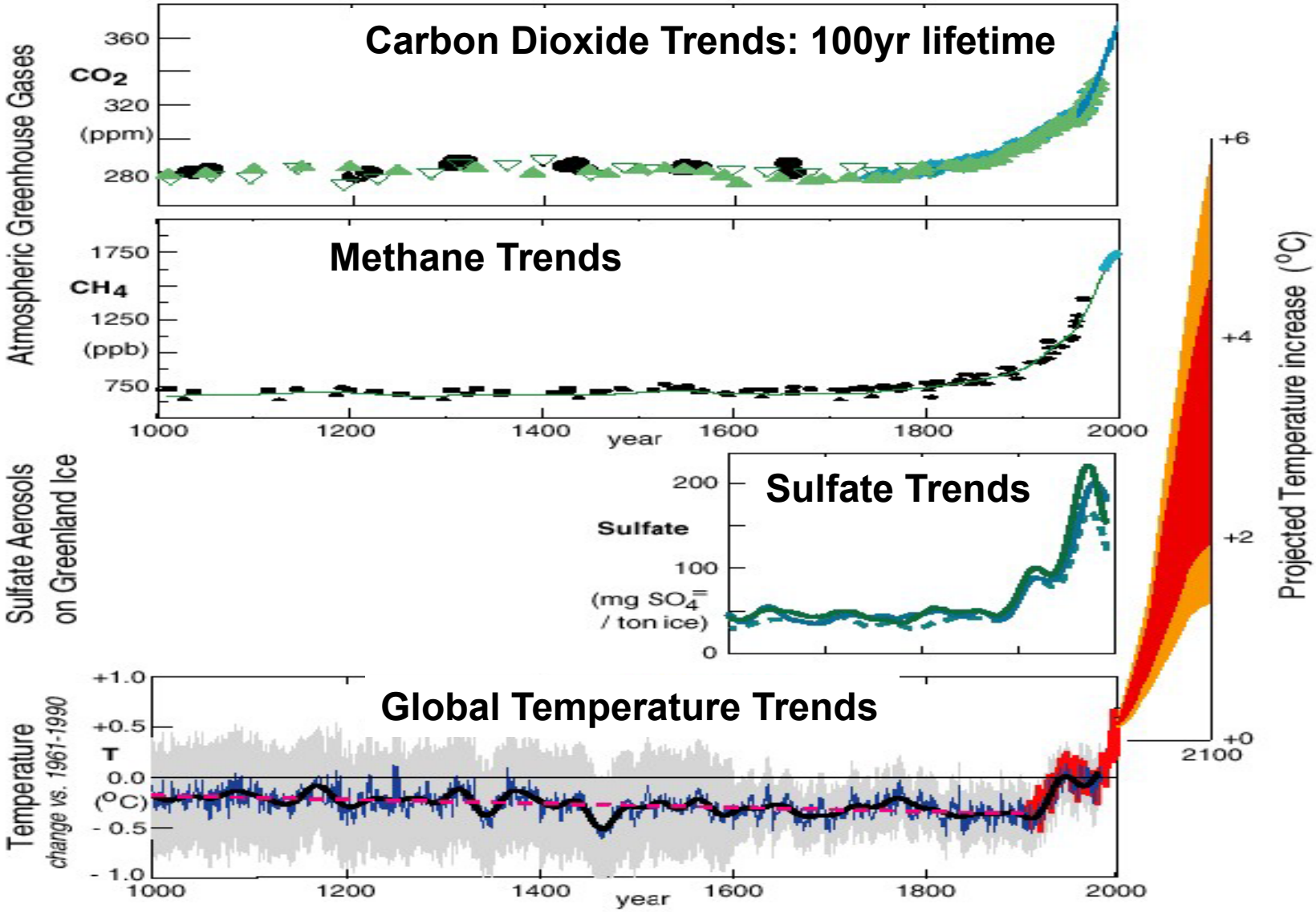

From M. Prather University of California at Irvine

Striving for the Sustainable Society

"A place where humans and their use of the environment are in balance with nature"

"living in harmony with the environment and having resilience to natural hazards"